JOURNAL OF THE AERONAUTICAL SCIENCES

VOLUME 13 JUNE, 1946 NUMBER 6

The Combination of Dynamical Systems

THOMAS G. SOFRIN*

United Aircraft Corporation

SUMMARY

This paper presents a method whereby the forced vibration characteristics of a system formed by interconnecting a group of subsystems can be predicted in terms of the interconnection constants and properties of such subsystems which are readily and accurately determinable by experiment. These properties are the generalized dynamic admittances—motions of system components due to application of unit oscillating forces. The method was devised to enable selection of a means of connecting two structures together so that excessive vibration due to imposed forces can be prevented, under the conditions that: (1) the structures already exist and cannot be modified; (2) the interconnection constants are the only quantities over which selection can be exercised; (3) the structures are, in general, so complicated that formulation of their equivalent dynamical systems and analysis thereof by conventional methods is impracticable or impossible.

Elementary tensor and matrix algebra comprise the mathematical tools. Application of the theory to aircraft power-plant installation problems is discussed, but extensions to other problems and fields are possible.

INTRODUCTION

THE BEHAVIOR of a vibrating continuous system can be specified with sufficient accuracy by the equations applicable to a multiple degree-of-freedom lumped parameter system. Attention is restricted herein to systems excited by sinusoidal forces of identical frequency for which the differential equations admit the solution:

$$[Q_i] = [\rho_{ij}][q_j] \tag{1}$$

Here Q and q are generalized complex forces and displacements, respectively. *The term "impedance matrix" will be applied to* $[\rho_{ij}]$ *whose typical element is given by*

$$\rho_{ij} = c_{ij} - a_{ij}\omega^2 + jb_{ij}\omega \tag{2}$$

Solving for the displacements:

$$[q_i] = [\rho_{ij}]^{-1}[Q_j] = [Y_{ij}][Q_j] \tag{3}$$

Received January 16, 1946.

* Installation Engineering, Pratt & Whitney Aircraft Division.

$[Y_{ij}]$ *is called the admittance matrix. Values of its elements, which are functions of frequency, can be found experimentally by applying a unit oscillating force* Q_j *to each coordinate* q_j *and measuring the resulting amplitudes and phases of the coordinates* q_i. *Thus the ratios* q_i/Q_j *are the admittances, classified as direct or cross according as* $i = j$ *and* $i \neq j$. $\theta_{ij}(= arg\, Y_{ij})$ is the phase angle by which q_i leads Q_j. Resonances of the system are indicated by maxima of the Y_{ij}'s. Further properties of admittances per se are well known and will not be discussed here.[1, 2]

In practical studies of complicated systems requiring a large number of coordinates for their specification, interest is usually limited to a reasonable fraction of the total coordinates. For such cases, admittance methods become exceptionally attractive, permitting an arbitrary number of displacements to be found in terms of the known applied group of forces when the appropriate admittances have been experimentally determined.

The purpose of this paper is to reveal the characteristics of the system formed by combining a group of subsystems whose admittance properties are known. This is the problem imposed, for example, when a machine, the operation of which produces oscillating forces, is to be attached to a complex structure. Criteria relating to the mounting of engines in aircraft are particularly sought, and obviously no loss of generality will ensue if illustrations from this field are used.

CLASSIFICATION OF DYNAMICAL SYSTEMS

Since the development and application of the following theory depend to a large extent upon recognition of the type of system under consideration, some space will be devoted to a discussion of various characteristic systems and the explicit qualitative form of their impedance matrices.

Eqs. (1), (2), and (3) are to be interpreted hereafter as follows: the displacements or configuration of a set

of n rigid bodies will be given by n simultaneous values of q_i, where each q_i is a compound coordinate, or a set of six absolute displacements of the body i referred to a rectangular coordinate system, the origin of which is located at the equilibrium position of the center of gravity of body i. The n coordinate systems are established so that their corresponding axes are parallel and have positive extensions in the same directions. A typical system is illustrated in Fig. 1, for which $q_1 = \{x_1, y_1, z_1, \varphi_1, \psi_1, \theta_1\}$ and $q_2 = \{x_2, y_2, z_2, \varphi_2, \psi_2, \theta_2\}$.

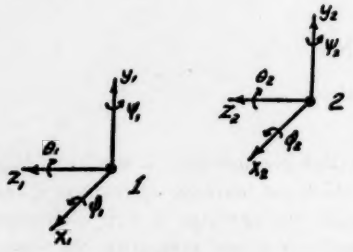

FIG. 1.

Dynamical systems requiring more than one coordinate for the specification of each body will be called "compound." The quantities q, ρ, and Q are then compound tensors. Systems in which the bodies are constrained to move in one and the same direction only or in which the interconnections are such as to decouple some one mode from the others are to be called "simple," and q, ρ, and Q are then ordinary tensors with scalar elements.

Both simple and compound systems are subject to one of two classifications, depending on the manner in which the various bodies are joined. If each body except the first and last is elastically connected with only two others, the combination is called a "chain system." If there are more interconnections, no special identification will be assigned. The form of the impedance tensor reveals at a glance the classifications described.

Table 1 contains an illustration of each classification and a qualitative or schematic representation of the appropriate impedance tensor. Blank elements denote zero values, and, for the coordinate system chosen, only diagonal elements of the diagonal tensors have the form $\rho_{ii} = c_{ii} - a_{ii}\omega^2 + jb_{ii}\omega$. The other nonzero elements are $\rho_{ij} = c_{ij} + jb_{ij}\omega$. Dashpots contributing b terms are not shown on the diagrams. Absence of certain elements of the diagonal tensors in the compound systems illustrated indicates decoupling of the corresponding coordinates due to symmetrical spring configurations. It is helpful to recall that in each case the dynamic tensor is the sum of the stiffness tensor c, $j\omega$ times the damping tensor, and $-\omega^2$ times the inertia tensor.

TABLE 1

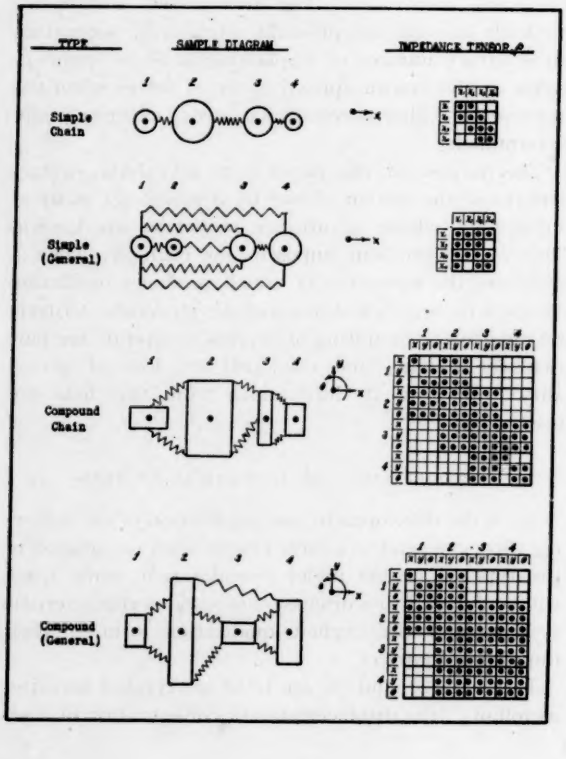

For the chosen coordinate system there is only static coupling, and the elements of the stiffness tensor can be found from $\partial^2 V/\partial q_i \partial q_j$, where V is the potential energy. Similarly, the dissipation function F enables the elements of the damping tensor to be calculated by $\partial^2 F/\partial \dot{q}_i \partial \dot{q}_j$.

Investigation of the dynamic characteristics of the configuration formed by connecting together two subsystems (in terms of the known subsystem properties and the manner of interconnection) can now begin. It will be found that a development applicable to compound systems, involving the use of tensor principles, introduces mathematical advantages of generality and unity which overbalance the physical complexities. In fact, certain properties of simple systems which cannot be revealed by matrix methods are easily found as a special case from the general treatment and will be given later.

ADMITTANCES OF COMBINED COMPOUND SYSTEMS

In the following presentation, compound tensors are expressed mainly in matrix notation, identifying subscripts being employed to prevent ambiguous assignment of indices. Frequent use is made of direct notation, but in no case does a subscript denote covariant properties—that is, true index notation is not used.[3]

Consider two systems, S_1 and S_2, with compound impedance tensors:

$$\left.\begin{aligned}\rho_1 &= \begin{bmatrix}\rho_{11}\rho_{12}\cdots\rho_{1n}\\ \rho_{21}\rho_{22}\cdots\rho_{2n}\\ \cdots\\ \rho_{n1}\rho_{n2}\cdots\rho_{nn}\end{bmatrix}\\ \rho_2 &= \begin{bmatrix}\rho_{(n+1)(n+1)}\ \rho_{(n+1)(n+2)}\cdots\rho_{(n+1)(n+p)}\\ \rho_{(n+2)(n+1)}\ \rho_{(n+2)(n+2)}\cdots\rho_{(n+2)(n+p)}\\ \cdots\\ \rho_{(n+p)(n+1)}\ \rho_{(n+p)(n+2)}\cdots\rho_{(n+p)(n+p)}\end{bmatrix}\end{aligned}\right\} \quad (4)$$

A typical element of ρ_1 or ρ_2 hereafter will be understood to have the form:

	x	y	z	ϕ	ψ	θ
x	ρ_{xx}	ρ_{xy}	·	·	·	$\rho_{x\theta}$
y	ρ_{yx}	ρ_{yy}	·	·	·	$\rho_{y\theta}$
z	·	·	·	·	·	·
ϕ	·	·	·	·	·	·
ψ	·	·	·	·	·	·
θ	$\rho_{\theta x}$	$\rho_{\theta y}$	·	·	·	$\rho_{\theta\theta}$

The complex elements thereof are given by Eq. (2). If the systems are connected in an arbitrary way, the combined impedance tensor, ρ^*, will have elements that are not, in general, simple functions of the original subsystem parameters. However, let them be connected by means of a known arrangement of springs and dashpots between the nth body of S_1 and the $(n+1)$ body of S_2. Introducing compound coordinates q_α and q_β, the connecting spring-dashpot impedance tensor, ρ_{12}, can be specified:

$\rho_{12} =$

	q_α	q_β
q_α	K	L
q_β	L_t	K'

(5)

The collection of systems S_1 and S_2 and the connecting elements can be represented by the tensor, ρ, before the interconnection is made.

$$\rho = \begin{bmatrix}\rho_1 & & \\ & \begin{matrix}K & L\\ L_t & K'\end{matrix} & \\ & & \rho_2\end{bmatrix} \quad (6)$$

Interconnection is now made by merging the coordinate q_α with q_n and q_β with q_{n+1} and is defined by the equations

$$q = Tq^*$$

where q^* are the new coordinates, and T is the singular transformation tensor.

$\mathbf{T} =$

q \ q^*	1	2	n	$n+1$	$n+2$	$n+p$
1	I					
2		I				
n			I			
α			I			
β				I		
$n+1$				I		
$n+2$					I	
$n+p$						I

(7)

The impedance of the combined system is found from

$$\rho^* = T_t \rho T$$

In expanded form:

$$\rho^* = \left[\begin{array}{ccc|ccc} \rho_{11} & \cdots & \rho_{1n} & 0 & \cdots & 0\\ \cdots & \cdots & \cdots & \cdots & \cdots & \cdots\\ \rho_{n1} & \cdots & \rho_{nn}+K & L & \cdots & 0\\ \hline 0 & \cdots & L_t & \rho_{(n+1)(n+1)}+K' & \cdots & \rho_{(n+1)(n+p)}\\ \cdots & \cdots & \cdots & \cdots & \cdots & \cdots\\ 0 & \cdots & 0 & \rho_{(n+p)(n+1)} & \cdots & \rho_{(n+p)(n+p)} \end{array}\right] \quad (8)$$

In practice, the systems S_1 and S_2 are too complicated to permit determination of reasonable values of the impedance elements. The representation of complicated continuous structures, such as aircraft fuselages and wings, by a sufficiently large number of concentrated masses, in order to study the behavior of various small components, is often an unsatisfactory compromise between accuracy and effort in which the parameters cannot but be uncertainly selected. However, any element of the admittance tensor, the reciprocal of the system impedance, can be found experimentally with great accuracy and little effort.

The mathematical problem, then, is to find the combined system admittance tensor, Y^*, in terms of the known tensors Y_1, Y_2, K, K', and L. The fact that *all* the elements of Y_1 and Y_2 need not be known creates no difficulty.

If a square matrix, α, and its reciprocal, β, be partitioned according to the scheme:

$$\alpha = \left[\begin{array}{c:c}\alpha_{11} & \alpha_{12}\\ \hdashline \alpha_{21} & \alpha_{22}\end{array}\right] \quad \text{and} \quad \alpha^{-1} = \beta = \left[\begin{array}{c:c}\beta_{11} & \beta_{12}\\ \hdashline \beta_{21} & \beta_{22}\end{array}\right]$$

it can be shown[4,5] that the elements of β are given by the alternative forms

$$\left.\begin{aligned}
\beta_{11} &= \alpha_{11}^{-1} + \alpha_{11}^{-1}\cdot\alpha_{12}\cdot(\alpha_{22} - \alpha_{21}\cdot\alpha_{11}^{-1}\cdot\alpha_{12})^{-1}\cdot\alpha_{21}\cdot\alpha_{11}^{-1} = (\alpha_{11} - \alpha_{12}\cdot\alpha_{22}^{-1}\cdot\alpha_{21})^{-1}\\
\beta_{12} &= -\alpha_{11}^{-1}\cdot\alpha_{12}(\alpha_{22} - \alpha_{21}\cdot\alpha_{11}^{-1}\cdot\alpha_{12})^{-1} = -(\alpha_{11} - \alpha_{12}\cdot\alpha_{22}^{-1}\alpha_{21})^{-1}\cdot\alpha_{12}\cdot\alpha_{22}^{-1}\\
\beta_{21} &= -(\alpha_{22} - \alpha_{21}\cdot\alpha_{11}^{-1}\cdot\alpha_{12})^{-1}\cdot\alpha_{21}\cdot\alpha_{11}^{-1} = -\alpha_{22}^{-1}\cdot\alpha_{21}\cdot(\alpha_{11} - \alpha_{12}\cdot\alpha_{22}^{-1}\cdot\alpha_{21})^{-1}\\
\beta_{22} &= (\alpha_{22} - \alpha_{21}\cdot\alpha_{11}^{-1}\cdot\alpha_{12})^{-1} = \alpha_{22}^{-1} + \alpha_{22}^{-1}\cdot\alpha_{21}\cdot(\alpha_{11} - \alpha_{12}\cdot\alpha_{22}^{-1}\cdot\alpha_{21})^{-1}\cdot\alpha_{12}\cdot\alpha_{22}^{-1}
\end{aligned}\right\} \quad (9)$$

Eqs. (9) will be employed to find Y^*, and it is seen that a method must be devised for evaluating α_{11}^{-1} and α_{22}^{-1}. Now α_{11} can be considered the sum of ρ_1 and a tensor J, where J has n^2 tensor elements, the (n,n)th of which is K, and the others are null tensors. The reciprocal of $\rho_1 \equiv Y_1$ contains known tensor elements, and it is required to find α_{11}^{-1} in terms of these and J. Thus $\alpha_{11}^{-1} = (\rho_1 + J)^{-1}$. Now perform the operations:

$$\begin{aligned}
\rho_1\alpha_{11}^{-1} &= \rho_1(\rho_1 + J)^{-1}\\
\alpha_{11}\rho_1^{-1} &= (\rho_1 + J)\rho_1^{-1} = (I + J\rho_1^{-1})
\end{aligned}$$

where I is the unit tensor.

$$\rho_1^{-1} = \alpha_{11}^{-1}(I + J\rho_1^{-1})$$

hence,

$$\alpha_{11}^{-1} = \rho_1^{-1}(I + J\rho_1^{-1})^{-1} \equiv Y_1(I + JY_1)^{-1} \quad (10)$$

Clearly Eq. (10) may be applied to α_{22}^{-1} and other reciprocations with obvious change of symbols. To illustrate the method of reciprocation and, in particular, the scheme of partitioning to be used, the calculation of α_{11}^{-1} is given in detail. Let Y_1 be expressed in partitioned form:

$$Y_1 = \left[\begin{array}{c|c} Y_{1aa} & Y_{1an} \\ \hline Y_{1na} & Y_{1nn} \end{array}\right]$$

According to the subscript scheme, Y_1 has been partitioned between the $(n-1)$ and nth compound indices. It is clear that Y_{1aa} is a compound square tensor of $(n-1)^2$ elements and that Y_{1an} and Y_{1na} are column and row tensors, respectively. By partitioning the tensor J between the same indices as Y_1, the product JY_1 can be calculated with facility, since three of the J subtensors are null. As an example of the concise notation, Y_1 is given in expanded form:

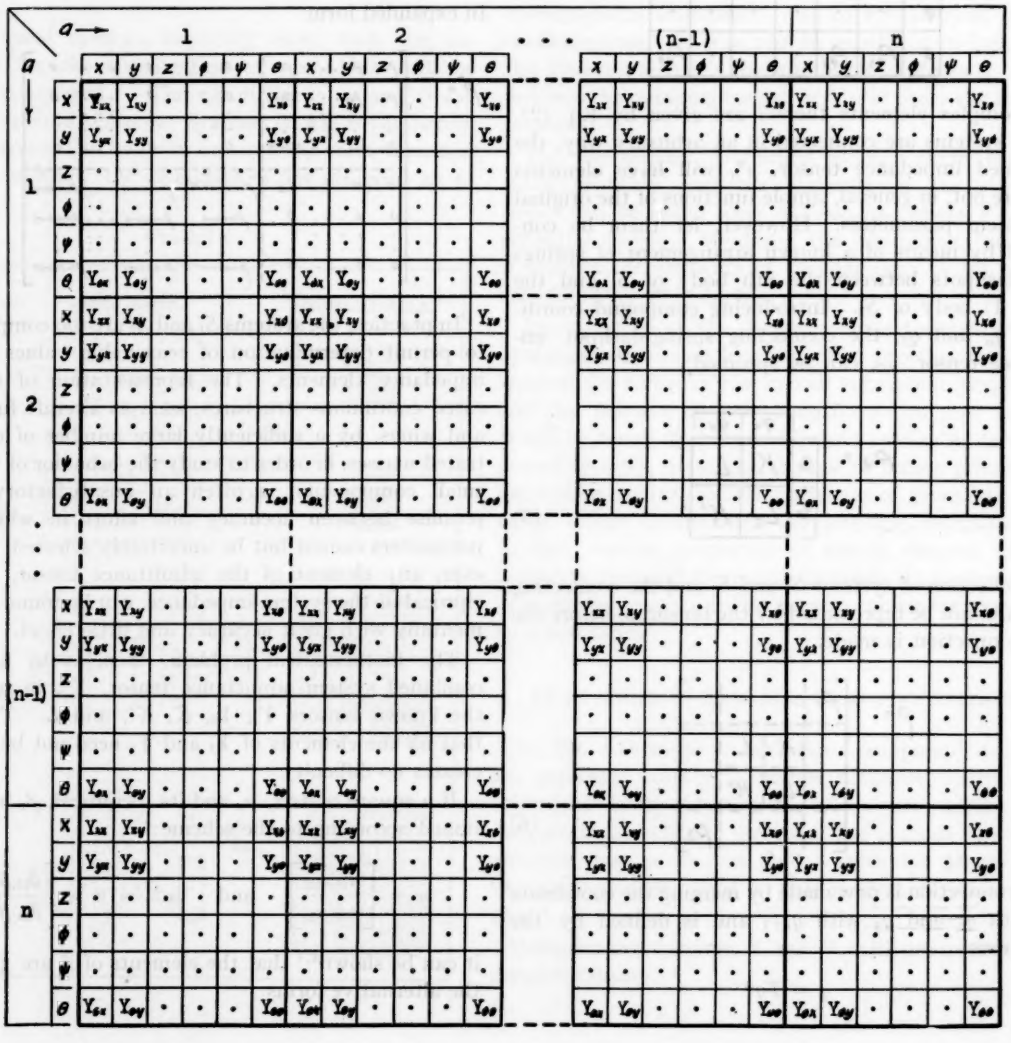

Let J be similarly partitioned. Then

$$JY_1 = \left[\begin{array}{c|c} 0 & 0 \\ \hline 0 & K \end{array}\right]\left[\begin{array}{c|c} Y_{1aa} & Y_{1an} \\ \hline Y_{1na} & Y_{1nn} \end{array}\right] = \left[\begin{array}{c|c} 0 & 0 \\ \hline KY_{1na} & KY_{1nn} \end{array}\right]$$

$$I + JY_1 = \left[\begin{array}{c|c} I & 0 \\ \hline KY_{1na} & I + KY_{1nn} \end{array}\right]$$

$(I + JY_1)^{-1}$ may conveniently be found by means of Eqs. (9). Omitting intermediate steps,

$$(I+JY_1)^{-1} = \left[\begin{array}{c|c} I & 0 \\ \hline -(I+KY_{1nn})^{-1}KY_{1na} & (I+KY_{1nn})^{-1} \end{array}\right]$$

Hence

$$\alpha_{11}{}^{-1} = Y_1(I + JY_1)^{-1} =$$

$$\left[\begin{array}{c|c} Y_{1aa} - Y_{1an}(I+KY_{1nn})^{-1}KY_{1na} & Y_{1an}(I+KY_{1nn})^{-1} \\ \hline Y_{1na} - Y_{1nn}(I+KY_{1nn})^{-1}KY_{1na} & Y_{1nn}(I+KY_{1nn})^{-1} \end{array}\right] \tag{11}$$

The advantages of finding the inverse of a tensor by means of submatrix reciprocation when some of the compound elements are unit or null tensors are shown by the relatively simple form of $\alpha_{11}{}^{-1}$ given by Eq. (11).

It will be convenient to abbreviate this equation to read

$$\alpha_{11}{}^{-1} = \left[\begin{array}{c|c} \alpha_{11aa}{}^{-1} & \alpha_{11an}{}^{-1} \\ \hline \alpha_{11na}{}^{-1} & \alpha_{11nn}{}^{-1} \end{array}\right] \tag{11a}$$

Finally, ρ^* can be expressed:

$$\rho^* = \left[\begin{array}{c|c} \alpha_{11} & \alpha_{12} \\ \hline \alpha_{21} & \alpha_{22} \end{array}\right] = \left[\begin{array}{cc|cc} \alpha_{11aa} & \alpha_{11an} & 0 & 0 \\ \alpha_{11na} & \alpha_{11nn} & \mathrm{L} & 0 \\ \hline 0 & L_l & \alpha_{22(n+1)(n+1)} & \alpha_{22(n+1)b} \\ 0 & 0 & \alpha_{22b(n+1)} & \alpha_{22bb} \end{array}\right] \tag{12}$$

Caution should be exercised to interpret $\alpha_{11aa}{}^{-1}$, for example, as the (a,a)th compound element of $\alpha_{11}{}^{-1}$ and *not* as the reciprocal of α_{11aa}. Steps in the calculation of $\rho^{*-1}(= Y^*)$ from Eqs. (9) are of interest and are presented below.

$$\alpha_{11}{}^{-1}\alpha_{12} = \left[\begin{array}{c|c} \alpha_{11aa}{}^{-1} & \alpha_{11an}{}^{-1} \\ \hline \alpha_{11na}{}^{-1} & \alpha_{11nn}{}^{-1} \end{array}\right]\left[\begin{array}{c|c} 0 & 0 \\ \hline L & 0 \end{array}\right] = \left[\begin{array}{c|c} \alpha_{11an}{}^{-1}L & 0 \\ \hline \alpha_{11nn}{}^{-1}L & 0 \end{array}\right] \tag{13}$$

$$\alpha_{21}\alpha_{11}{}^{-1} = \left[\begin{array}{c|c} 0 & L_l \\ \hline 0 & 0 \end{array}\right]\left[\begin{array}{c|c} \alpha_{11aa}{}^{-1} & \alpha_{11an}{}^{-1} \\ \hline \alpha_{11na}{}^{-1} & \alpha_{11nn}{}^{-1} \end{array}\right] = \left[\begin{array}{c|c} L_l\alpha_{11na}{}^{-1} & L_l\alpha_{11nn}{}^{-1} \\ \hline 0 & 0 \end{array}\right] \tag{14}$$

$$\alpha_{21}\alpha_{11}{}^{-1}\alpha_{12} = \left[\begin{array}{c|c} L_l\alpha_{11na}{}^{-1} & L_l\alpha_{11nn}{}^{-1} \\ \hline 0 & 0 \end{array}\right]\left[\begin{array}{c|c} 0 & 0 \\ \hline L & 0 \end{array}\right] = \left[\begin{array}{c|c} L_l\alpha_{11nn}{}^{-1}L & 0 \\ \hline 0 & 0 \end{array}\right] \tag{15}$$

Let

$$C = \alpha_{22} - \alpha_{21}\alpha_{11}{}^{-1}\alpha_{12} \tag{16}$$

Then

$$C = \left[\begin{array}{c|c} \alpha_{22(n+1)(n+1)} - L_l\alpha_{11nn}{}^{-1}L & \alpha_{22(n+1)b} \\ \hline \alpha_{22b(n+1)} & \alpha_{22bb} \end{array}\right] \tag{17}$$

C^{-1} may be found similarly from Eq. (10).

$$C^{-1} = (\rho_2 + H)^{-1} = \rho_2{}^{-1}(I + H\rho_2{}^{-1})^{-1} \equiv Y_2(I + HY_2)^{-1}.$$

where H is the tensor difference between C and ρ_2.

Expanding in terms of partitioned values:

$$HY_2 = \left[\begin{array}{c|c} K' - L_l\alpha_{11nn}{}^{-1}L & 0 \\ \hline 0 & 0 \end{array}\right]\left[\begin{array}{c|c} Y_{2(n+1)(n+1)} & Y_{2(n+1)b} \\ \hline Y_{2b(n+1)} & Y_{2bb} \end{array}\right] =$$

$$\left[\begin{array}{c|c} (K' - L_l\alpha_{11nn}{}^{-1}L)Y_{2(n+1)(n+1)} & (K' - L_l\alpha_{11nn}{}^{-1}L)Y_{2(n+1)b} \\ \hline 0 & 0 \end{array}\right]$$

$$I + HY_2 = \left[\begin{array}{c|c} I + (K' - L_l\alpha_{11nn}{}^{-1}L)Y_{2(n+1)(n+1)} & (K' - L_l\alpha_{11nn}{}^{-1}L)Y_{2(n+1)b} \\ \hline 0 & I \end{array}\right]$$

$$(I + HY_2)^{-1} =$$

$$\left[\begin{array}{c|c} [I + (K' - L_l\alpha_{11nn}{}^{-1}L)Y_{2(n+1)(n+1)}]^{-1} & -[I + (K' - L_l\alpha_{11nn}{}^{-1}L)Y_{2(n+1)(n+1)}]^{-1}(K' - L_l\alpha_{11nn}{}^{-1}L)Y_{2(n+1)b} \\ \hline 0 & I \end{array}\right]$$

and

$$C^{-1} = \left[\begin{array}{c|c} Y_{2(n+1)(n+1)}[I + (K' - L_l\alpha_{11nn}{}^{-1}L)Y_{2(n+1)(n+1)}]^{-1} & - \\ \hline Y_{2b(n+1)}[I + (K' - L_l\alpha_{11nn}{}^{-1}L)Y_{2(n+1)(n+1)}]^{-1} & - \end{array}\right.$$

$$\left.\begin{array}{c|c} Y_{2(n+1)(n+1)}[I + (K' - L_l\alpha_{11nn}{}^{-1}L)Y_{2(n+1)(n+1)}]^{-1}(K' - L_l\alpha_{11nn}{}^{-1}L)Y_{2(n+1)b} + Y_{2(n+1)b} \\ \hline Y_{2b(n+1)}[I + (K' - L_l\alpha_{11nn}{}^{-1}L)Y_{2(n+1)(n+1)}]^{-1}(K' - L_l\alpha_{11nn}{}^{-1}L)Y_{2(n+1)b} + Y_{2bb} \end{array}\right] \tag{18}$$

Omitting further intermediate steps, the admittance tensor, $\rho^{*-1} = Y^*$ of the combined system can now be expressed. The compound tensor elements are expressed in the simpler alternative forms of Eqs. (9) and are partitioned according to the scheme:

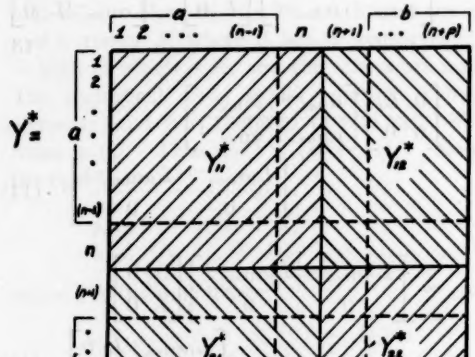

(19)

The elements are as follows:

$$Y^*_{aa} = \begin{bmatrix} Y_{aa} - Y_{an}E(K - L\alpha^{-1}_{22(n+1)(n+1)}L_t)Y_{na} & Y_{an}E \\ Y_{na} - Y_{nn}E(K - L\alpha^{-1}_{22(n+1)(n+1)}L_t)Y_{na} & Y_{nn}E \end{bmatrix} = \begin{bmatrix} Y^*_{aa} & Y^*_{ab} \\ Y^*_{ba} & Y^*_{bb} \end{bmatrix} \quad (19a)$$

$$Y^*_{ab} = \begin{bmatrix} -Y_{an}EL\alpha^{-1}_{22(n+1)(n+1)} & -Y_{an}EL\alpha^{-1}_{22(n+1)b} \\ -Y_{nn}EL\alpha^{-1}_{22(n+1)(n+1)} & -Y_{nn}EL\alpha^{-1}_{22(n+1)b} \end{bmatrix} = \begin{bmatrix} Y^*_{aa} & Y^*_{ab} \\ Y^*_{ba} & Y^*_{bb} \end{bmatrix} \quad (19b)$$

$$Y^*_{ba} = \begin{bmatrix} -Y_{2(n+1)(n+1)}D\,L_t\alpha^{-1}_{11nn} & -Y_{2(n+1)(n+1)}DL_t\alpha^{-1}_{11na} \\ -Y_{2b(n+1)}DL_t\alpha^{-1}_{11nn} & -Y_{2bna}DL_t\alpha^{-1}_{11na} \end{bmatrix} = \begin{bmatrix} Y^*_{ba} & Y^*_{aa} \\ Y^*_{bb} & Y^*_{ba} \end{bmatrix} \quad (19c)$$

$$Y^*_{bb} = \begin{bmatrix} Y_{2(n+1)(n+1)}D & Y_{2(n+1)b} - Y_{2(n+1)(n+1)}D(K - L\alpha^{-1}_{11nn}L)Y_{2(n+1)b} \\ Y_{2b(n+1)}D & Y_{2bb} - Y_{2b(n+1)}D(K - L\alpha^{-1}_{11nn}L)Y_{2(n+1)b} \end{bmatrix} = \begin{bmatrix} Y^*_{ba} & Y^*_{aa} \\ Y^*_{bb} & Y^*_{ba} \end{bmatrix} \quad (19d)$$

where

$$D = [I + (K' - L_t\alpha_{11nn}{}^{-1}L)Y_{2(n+1)(n+1)}]^{-1} \quad (20)$$

$$E = [I + (K - L\alpha_{22(n+1)(n+1)}{}^{-1}L_t)Y_{1nn}]^{-1} \quad (21)$$

For convenience, the elements of $\alpha_{22}{}^{-1}$, omitted in the discussion, together with a repetition of $\alpha_{11}{}^{-1}$, are given below.

$$\alpha_{11aa}{}^{-1} = Y_{1aa} - Y_{1an}(I + KY_{1nn})^{-1}KY_{1na} \quad (22a)$$

$$\alpha_{11an}{}^{-1} = Y_{1an}(I + KY_{1nn})^{-1} \quad (22b)$$

$$\alpha_{11na}{}^{-1} = Y_{1na} - Y_{1nn}(I + KY_{1nn})^{-1}KY_{1na} \quad (22c)$$

$$\alpha_{11nn}{}^{-1} = Y_{1nn}(I + KY_{1nn})^{-1} \quad (22d)$$

$$\alpha_{22(n+1)(n+1)}{}^{-1} = Y_{2(n+1)(n+1)}(I + K'Y_{2(n+1)(n+1)})^{-1} \quad (23a)$$

$$\alpha_{22(n+1)b}{}^{-1} = Y_{2(n+1)b} - Y_{2(n+1)(n+1)}(I + K'Y_{2(n+1)(n+1)})^{-1}K'Y_{2(n+1)b} \quad (23b)$$

$$\alpha_{22b(n+1)}{}^{-1} = Y_{2b(n+1)}(I + K'Y_{2(n+1)(n+1)})^{-1} \quad (23c)$$

$$\alpha_{22bb}{}^{-1} = Y_{2bb} - Y_{2b(n+1)}(I + K'Y_{2(n+1)(n+1)})^{-1}K'Y_{2(n+1)b} \quad (23d)$$

Examination of Eqs. (19) through (23) discloses that calculation of the Y^* elements is not so formidable as it might first appear. For example, to compute a typical element, $Y^*_{12a_ib_j}$, of Y^*_{12ab}, knowledge of K, K', and L and the four original admittance tensors, Y_{1nn}, $Y_{2(n+1)(n+1)}$, Y_{1a_in}, and $Y_{2(n+1)b_j}$ is sufficient. Table 2 summarizes the requirements.

TABLE 2
Missing Elements are Supplied by Conditions of Symmetry

Element	Area	Original Elements Required
$Y^*_{11a_ia_j}$	Y^*_{11aa}	Y_{1nn} , $Y_{1(n-1)(n-1)}$, $Y_{1a_ia_j}$, Y_{1a_in} , Y_{1na_j}
$Y^*_{11a_in}$	Y^*_{11an}	" , " , Y_{1a_in}
Y^*_{11na}	Y^*_{11an}	" , "
$Y^*_{12a_i(n+1)}$	$Y^*_{12a(n+1)}$	" , " , Y_{1a_in}
$Y^*_{12a_ib_j}$	Y^*_{12ab}	" , " , Y_{1a_in} , $Y_{2(n+1)b_j}$
$Y^*_{12n(n+1)}$	$Y^*_{12n(n+1)}$	" , "
$Y^*_{12nb_j}$	Y^*_{12nb}	" , " , $Y_{2(n+1)b_j}$
$Y^*_{22(n+1)(n+1)}$	$Y^*_{22(n+1)(n+1)}$	" , "
$Y^*_{22(n+1)b_j}$	$Y^*_{22(n+1)b}$	" , " , $Y_{2(n+1)b_j}$
$Y^*_{22b_ib_j}$	Y^*_{22bb}	" , " , $Y_{2b_ib_j}$, $Y_{2b_i(n+1)}$, $Y_{2(n+1)b_j}$

APPLICATION OF THE THEORY

Two structures, in which the degree of complexity prevents determination of their parameters, are to be connected in a known way. It is desired to predict the vibration response of various elements in the combined structure because of action of known forces imposed at selected points. Development of the theory shows that experimental determination of the original admittances provides sufficient information to solve the problem and that no intrinsic structural details are needed.

The treatment supposed that interconnection was made between one body of each structure, but this was a restriction employed for convenience only. Actually, a number of interconnections among bodies may be made and the resulting system analyzed, although the computations are considerably more involved. This more general case will be discussed presently, but now applications in which various simplifications demonstrate the flexibility and simplicity of the method can be considered.

Vibration Isolation of Power-Plant Installations—General

In aircraft, where the mass of the power plant is a substantial part of the airplane mass and where the air frame certainly does not act as a rigid body, conventional methods of calculating the desirable suspension flexibilities often lead to ineffective isolation of the power-plant exciting forces. Usually, the vibration engineer must accept the air-frame and power-plant dynamic properties as they stand and restrict

his attention to means of connecting the two components. The method of analysis presented herein permits an indication of the complete airplane vibration characteristics; for, by applying calibrated excitation to the engine mount structure and determining the response of various fuselage components, the air-frame admittances, in the range of engine-propeller excitation frequencies, may be found. These, together with the power-plant admittances and selected values of suspension stiffness, enable the fuselage vibration to be predicted for known power-plant exciting forces. A final value of suspension stiffness may be chosen on the basis of the predicted overall performance. It should be noted that the equivalent viscous effect of structural and still air damping is implicitly taken into account; advanced instrumentation allows accurate determination of the amplitudes and phases of the admittances.

Some Features of Vibration Isolation

(a) In most applications, interest is centered on components of the structure to which the exciting system is appended. Accordingly, if S_1 is the original structure, the only significant part of Y^* is the area Y^*_{12} of Eq. (19).

(b) Frequently, the appended system consists of a few known elements, in which case the quantities $Y_{2(n+1)(n+1)}$ and $Y_{2(n+1)b}$ may be computed with greater facility than by experimental determination.

(c) Cases where the added system is merely a rigid body prove especially easy. Only $Y^*_{12a(n+1)}$ and $Y^*_{12n(n+1)}$ are required, which in turn demand experimental values of Y_{1an} and Y_{1nn}; $Y_{2(n+1)(n+1)}$ is simply the diagonal tensor $-(1/\omega^2)[m_{ij}]^{-1}$. Applications of this type are the installation of heavy machinery in buildings and ships and installation of aircraft engines, neglecting the effect of propeller-blade flexibility. If the propeller be considered as a rigid inertia, the effect of its rotation on the calculated engine admittances can be found. However, since the effect of spin is to couple the yaw and pitch coordinates, this calculation becomes rather lengthy.

(d) An interesting application of power-plant vibration isolation is one in which the vibration characteristics of the nonrotating propeller are included. The admittance tensor at the engine center of gravity may be found from experimental values of propeller admittances and calculated engine admittances, somewhat as discussed above. This total power-plant admittance is then used in conjunction with the air-frame admittances to provide the final result. It should be mentioned that the effect of rotation on the nonrotating propeller admittance has as yet not been derived.

(e) Often, specification of the system does not require 6th order compound coordinates because of structural symmetry. When only two or three individual coordinates are needed to define each body, the simplification of calculation procedures is apparent.

(f) A further reduction of effort accrues when the forces are simple or are compounded of only two or three simple forces. These conditions are by far more common in engineering applications than the general case.

Additional Considerations

It has been mentioned that the interconnection between two subsystems was restricted to the chain type in the interest of clarity. The method may be extended to include a seemingly hopeless combination formed by connecting r bodies of S_1 with s bodies of S_2.

Assign identifying subscripts to the coordinates in such sequence that the impedance tensor, ρ^*, may be written

$$\rho^* = \left[\begin{array}{cc:cc} \rho_{1aa} & \rho_{1ar} & 0 & 0 \\ \rho_{1ra} & \rho_{1rr} + K_{rr} & L_{rs} & 0 \\ \hdashline 0 & L_{sr} & \rho_{2ss} + K'_{ss} & \rho_{2sb} \\ 0 & 0 & \rho_{2bs} & \rho_{2bb} \end{array}\right] \tag{24}$$

Clearly, a similar analysis can now be applied with further partitioning made between the indices $(n - r)$ and $(n - r + 1)$, and $(n + s)$ and $(n + s + 1)$. Eqs. (19) through (23) then give the components of Y^*, where the subtensors Y^*_{11nn} and $Y^*_{22(n+1)(n+1)}$ change from unit order to r and s and the others are suitably revised.

The schematic solution may be written $Y^* =$

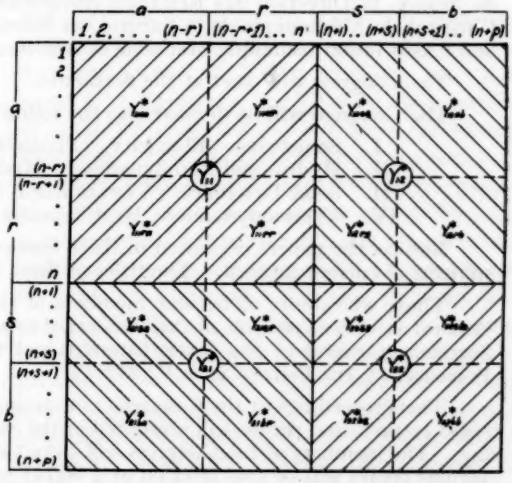

(25)

A study of the vibration characteristics of multi-engined aircraft installations is particularly susceptible to analysis by this more general method. Ordinarily the air-frame system would be combined with the first power plant by means of Eq. (19) to produce the first modification. This process would demand reoperation

with Eq. (19) on the first modification and the second power plant, and so on, until all power plants had been "installed." Eq. (25), however, gives the complete airplane admittance in one operation. The calculations involved are practicable since the interconnection tensors K, K', L_{sr}, and L_{rs} are diagonal.

Evaluation of the interconnection tensors for both chain and general connections may usually be facilitated by a change to relative coordinates and use of the transformation tensor.[6, 7] The inconvenience of operating with complex admittance tensors may be avoided by replacing them by tensors with twice their number of rows and columns containing only real quantities.[8]

REFERENCES

[1] von Kármán, Th., and Biot, M. A., *Mathematical Methods in Engineering*, 1st Ed., pp. 370–378; McGraw-Hill Book Company, Inc., 1940.

[2] Biot, M. A., *Coupled Oscillations of Aircraft Engine-Propeller Systems*, Journal of the Aeronautical Sciences, Vol. 7, No. 9, pp. 376–382, July, 1940.

[3] Kron, Gabriel, *Tensor Analysis of Networks*, pp. 7–13; John Wiley & Sons, Inc., 1939.

[4] Frazer, R. A., Duncan, W. J., and Collar, A. R., *Elementary Matrices*, pp. 112–113; Cambridge University Press, London, 1938.

[5] Kron, Gabriel, *op. cit.*, pp. 257–258.

[6] Kron, Gabriel, *op. cit.*, pp. 92–116.

[7] Concordia, C., *The Use of Tensors in Mechanical Engineering Problems*, General Electric Revue, July, 1936.

[8] Kron, Gabriel, *op. cit.*, pp. 541–542.

Sixth International Congress for Applied Mechanics

At a meeting initiated by Dr. J. C. Hunsaker and Dr. Th. von Kármán, acting as joint secretaries of the Fifth International Congress for Applied Mechanics, a committee was formed for the organization of the Sixth Congress. In line with the decision reached at Cambridge in 1938, it is proposed that the Sixth International Congress for Applied Mechanics be held in Paris, from September 22 to September 29, 1946.

The invitations to the Congress are extended on behalf of l'Académie des Sciences de l'Institut de France, la Direction des Relations culturelles, le Centre national de la Recherche scientifique, l'Institut de Méchanique de la Faculté des Sciences de Paris, la Société française des Mécaniciens, and l'Association technique Maritime et Aéronautique.

The Congress will meet at the Sorbonne.

The Congress will be divided into the following Sections:

I. Structures. Elasticity. Plasticity.
II. Hydro- and Aerodynamics. Hydraulics.
III. Solid Dynamics. Vibration and Sound. Friction and Lubrication.
IV. Thermodynamics. Heat Transfer. Combustion. Fundamentals of Nuclear Energy.

Besides the papers presented in these Sections, a number of General Lectures will be given on subjects of current interest. The titles of these Lectures will be made known in a later notice.

Those who desire to become members of the Congress are requested to inform the Secretary General as soon as possible of their intention to attend. Communications are to be addressed to the Secretary General of the Sixth International Congress for Applied Mechanics, Institut Henri-Poincaré, 11, rue Pierre-Curie, PARIS (V°).

The Proceedings of the Congress, containing the minutes of the sessions, the texts of the General Lectures, and the papers presented in the Sections, will be published with the least possible delay. The members of the Congress will have the right to buy these volumes by subscription. The surplus copies will be sold later on at a higher price.

The payment of an inscription fee of 300 francs is required from the members of the Congress; this fee can be paid immediately or not later than on the opening day of the Congress. Ladies accompanying members will not be required to pay such fee, except those who wish to address the meetings or to submit papers.

Vortex Frequency and Flow Pattern in the Wake of Two Parallel Cylinders at Varied Spacing Normal to an Air Stream*

HERMAN M. SPIVACK
National Bureau of Standards

ABSTRACT

The frequency of vortex formations in the flow about a pair of parallel cylinders, at various separations, is investigated with the hot wire anemometer. A résumé of the literature on vortex frequencies is given with a view to relate the studies of obstacles of diverse shapes to the present case. The law of dynamical similitude is developed for individual solids, for the efflux through a rectangular orifice, for secondary eddies, and for the two-cylinder system.

When two cylinders are separated by a gap just smaller than the diameter, instability occurs. At larger gaps the cylinders behave like independent bodies. As the gap is decreased, the main sequence of frequencies (probably generated on the outer sides of the cylinders) changes from a value corresponding to a single cylinder, of diameter d, to a value associated with a solid body of breadth equal $2d$ (at zero gap). A minimum frequency is reached at $G/d = 1/11$, where G is the gap distance. For gaps smaller than the critical, a formula is given to represent the main sequence:

$$fd/U = 0.09 + \{[(G/d) - 1/6]/[(G/d) + 2]\}^2$$

where f is the frequency and U is the velocity.

The picture is complicated by vortexes generated within the gap. At spacings less than one-half diameter, a low gap frequency is found. Between one-half and one diameter a high gap frequency is present, decreasing to the independent cylinder value at the critical spacing $G/d = 1$. In addition, doubled frequencies of the main sequence are also found, generally on the centerline of the wake, attributed to overlapping vortexes from the external sides of the cylinders.

For all values of the gap, the dimensionless parameter fd/U is shown to be independent of Reynolds numbers greater than 15,000. Below this value, fd/U rises at first and then drops sharply, the maximum apparently depending on the gap.

The velocity distribution in the wake was obtained by traversing with a pitot static tube. In a plane four diameters downstream from the center of the system, it was found that the wakes of both cylinders are mixed for gaps below the critical and separate for larger gaps. At G/d less than about one-half, the central pressure drop is great enough to cause the flow to reverse.

INTRODUCTION

THE FORMATION OF VORTEXES in the flow downstream from obstacles immersed in moving fluids is of interest in fluid dynamics and acoustics and has been the subject of numerous investigations.

Received December 6, 1945.

* A thesis on this topic has been submitted to the Graduate School of the Catholic University of America in partial fulfillment of the requirements for the degree of Master of Science.

Early Investigations

Mallock,[1] in 1907, was apparently the first to explain that the aeolian tones investigated by Strouhal, Rayleigh, and others were the result of vortexes being shed alternately in the wake of cylindrical wires subjected to an air current. In 1908, Bénard[2] published the results of an extended experimental investigation of alternating vortexes.

Stability of the Vortex Street

In a remarkable investigation, von Kármán[3] has derived the criterion for the stability of the two rows of vortexes forming a two-dimensional street and has also indicated the relationship between the resistance of immersed objects and the vortexes associated with the flow. The stable type of vortex formation is an asymmetrical pattern that is referred to in the literature as the von Kármán or Bénard vortexes. In this case the vortexes are detached alternately from each side of an obstacle, and the centers of the successive eddies maintain a constant separation.

Under ideal conditions, if the distance between the centers of the vortex rows is h and the vortexes in each row are spaced a distance l, the spacing ratio h/l has the constant value 0.281 for stability. In the experiments of von Kármán and Rubach[4] made on cylinders in water, photographic methods gave the values 0.305 and 0.280. Tyler obtained 0.308 for cylinders. In the Fage and Johansen experiments[5] with a flat plate in the wind tunnel, this ratio is found to change from 0.250 at a downstream distance of five times the plate width, to 0.52 at a downstream distance of 20 times the width of the plate (the channel width was 14 times the plate width). Change in the spacing ratio is accompanied by a diffusion of vorticity, and it is problematical that vortexes, as such, can be said to exist far downstream. The actual arrangement of the vortexes can be considerably affected by external conditions, such as the proximity of the walls of a channel, the viscosity of the fluid, and the turbulence of the stream. Rosenhead[6] has shown that the presence of channel walls causes h/l to increase downstream. An analysis by Hooker[7] attributes the downstream variation in the spacing ratio principally to the viscosity of the fluid, while Dryden and Heald[8] have found that changing the

turbulence in the stream modifies the vortex configuration.

Frequency of Vortex Formation

The frequency at which two-dimensional cylindrical vortexes are shed is a linear function of the velocity over the entire range of the stable formation except at Reynolds numbers below 1,000. Otherwise, it has been demonstrated[9, 10] that the linear range holds up to Reynolds numbers of 5×10^5. Expressing the frequency in the form of the dimensionless parameter fd/U, for a circular cylinder, von Kármán[4] obtained 0.207 and 0.198; Relf and Simmons,[9] 0.18 to 0.20; Blenk, Fuchs, and Liebers,[11] 0.207. Tyler[12] found somewhat lower values. In the plane of symmetry behind an immersed body it is possible to measure the effect of vortexes from each row overlapping to produce a double frequency.

Edge Tones

The presence of alternating vortexes may be noted for an entirely different flow condition. This was shown, for example, by Benton[13] in the study of edge tones produced when a thin plate is attacked by a jet of air. The jet issuing from a narrow rectangular aperture enters a body of still air with no contraction. The vortexes generated yield for the ratio h/l values ranging from 0.35 to 0.276, depending upon the width of the slit. These values are established indirectly and their determination involves acoustic considerations. Earlier investigators have examined various acoustical aspects of this problem. Carriere[14] has obtained interesting photographs of such vortexes.

Secondary Vortexes

A brief reference to the so-called secondary vortexes as distinguished from alternating vortexes may be desirable. These are sometimes produced at the borders of wakes of semiplanes (i.e., a sharp-edged plate extending into the fluid from one of the boundaries) placed in a current. Such secondary vortexes have also been observed with cylinders,[15] in which case they begin at a Reynolds number of about 1,250 and also tend to reach a limiting upper frequency and may become coincident with the principal vortex formation. They are of relatively small dimensions and high frequency. The most extended study of this subject was undertaken by Crausse, whose results are included in an informative discussion by Camichel and Escande.[16] Photographs have also been taken by Prandtl[17] of the formation of secondary vortexes.

The Present Problem

While numerous investigations have been conducted upon individual obstacles having continuous surfaces and diverse shapes, few studies have been made of the vortex pattern associated with more complex forms. The extension of the study of alternating vortexes may naturally lead to multiple cylinders, the simplest arrangement being the case of a pair of cylinders separated by various distances. This case, however, is not the simplest for a theoretical study. Various theoretical problems may find their guidance in the actual observation of vortexes. In this paper the principal study will be of the frequencies appearing in the wake of two cylinders, dependence of the frequency on velocity, and the effect of the separation of the cylinders.

Symbols

- b = total cross-stream breadth of an obstacle
- d = diameter of a cylinder ($^{11}/_{8}$ in.)
- f = frequency, cycles per sec.
- G = gap between, or separation of, the adjacent walls of the cylinders
- R = Reynolds number (Ud/ν)
- S = Strouhal number (fd/U)
- u = local velocity in the x-direction at any point in the flow, ft. per sec.
- Δu = fluctuations of the mean velocity
- U = free stream velocity
- x = coordinate direction parallel to the wind stream
- y = coordinate direction normal to the wind stream
- ν = kinematic viscosity

Laws of Dynamical Similitude for Vortex Frequencies

Similarity Law for Cylinders

It was observed by Strouhal[18] that the frequency of the sound emitted by a wire of diameter d, moving in air at a velocity U, obeys, within limitations, the relation

$$S = fd/U \tag{1}$$

where S is constant. Bénard[2] referred to the quantity S as the Strouhal number. Lord Rayleigh[19] examined the data of Strouhal and, assuming negligible compressibility of the air, derived the expression for alternating vortexes:

$$S = 0.195[1 - (20.1/R)] \tag{2}$$

where R is the Reynolds number Ud/ν. This is the law of dynamical similitude for the vortexes leaving the cylinder and is in good agreement with the formula obtained in an investigation by Tyler:[12]

$$S = 0.198[1 - (19.7/R)] \tag{3}$$

These formulas are valid at low Reynolds number down to the point where the eddies that are formed do not detach from the cylinder, so that the Kármán trail no longer exists. Thom[20] finds this limit to be about $R = 30$, and Camichel[16] gives the value $R = 48$. The physical significance of this criterion is that for flow at lower Reynolds numbers the eddies that are formed do not detach from the cylinder, and any disturbances are damped out.

The Strouhal number has been shown to be constant for the range $R = 10^3$ to $R = 5 \times 10^5$. This is approx-

imately the range in which the drag of a cylinder has a constant value. Different investigations are in fair agreement regarding the numerical magnitude of S for a cylinder. Dryden and Heald[8] obtained 0.19; Camichel[16] and his collaborators, 0.20; Relf and Simmons,[9] from 0.18 to 0.20. Measurements made with a single cylinder in connection with the present investigation yielded 0.207, which is the value given by Blenk, Fuchs, and Liebers.[11]

Similarity Law for Prismatic Solids

For prismatic solids the dynamical similitude law is, of course, similarly expressed as for the cylinder. Taking b as the breadth of an object whose length traverses a two-dimensional flow, the Strouhal number is given by fb/U and the Reynolds number by bU/ν. There also appears to be a range of R for prismatic solids wherein S has a constant value. Camichel[16] gives the following: for a rectangular body with depth three times the breadth, $S = 0.156$; for a square rod, $S = 0.130$; for a rectangular block terminating in an equilateral wedge, $S = 0.235$; for a wedge tapering downstream, with the base three times the depth, 0.255.

With flat plates fb/U is nearly constant for angles of incidence exceeding 30°. Fage and Johansen[5] obtained an average value of 0.148; von Kármán,[3] 0.144; Tyler,[12] 0.158; and Blenk, Fuchs, and Liebers,[11] 0.180. For airfoils, Tyler found the value 0.15, whereas Blenk, Fuchs, and Liebers found 0.21. For the shapes of a wedge, an ogive, and an extended ogive, respectively, the values 0.238, 0.271, and 0.254 are given by Fage and Johansen,[21] who are of the opinion that the frequency and spacing ratio depend upon the lateral spacing of the vortex sheets leaving the body and, to a lesser extent, upon the form of the body. The relation of S to R shows marked difference for solids of various shapes, but the values obtained for similar shapes by different investigators show the order of dispersion to be almost as marked.

Similarity Law for Jets

Under certain conditions, vortexes are formed in the efflux from an orifice. For the vortexes associated with the flow in jets, dynamical similitude for the vortex frequency may be expressed in the form:

$$fd/U = \mathrm{F}_1(Ud/\nu) \tag{4}$$

where F_1 is a functional symbol, d is the width of the jet, and U is the velocity of efflux. In the experiments of Benton,[13] when the edge plate is close to the slit, no tone is obtained. However, when the edge is moved to a greater distance a_0, a note suddenly appears. For the determination of a_0, Benton gives the dynamical similitude law:

$$(a_0/d)^2 = 1.50 + (B\nu/Ud) \tag{5}$$

where B is a constant approximately 2,000. In view of Konig's formula

$$f = U/2a_0 \tag{6}$$

where f is the frequency of edge tone, Benton's equation may be modified to yield a result conforming with Eq. (4). Putting $S = fd/U$, Konig's formula becomes

$$S = d/2a_0 \tag{7}$$

and, when this is introduced in Benton's equation, Eq. (5), the new form is

$$1/4S^2 = 1.50 + (B\nu/Ud) \tag{8}$$

This relationship may be depended upon to give satisfactory results for small Reynolds number. The curve giving the relation between S and Reynolds number may be obtained from the data in Fig. 5 of Benton's paper. This curve as derived from the original data is given in Fig. 2. The value of constant S obtained by this indirect means is approximately 0.32, but it must be remembered that the data are for low Reynolds numbers.

Similarity Law for Secondary Vortexes

The secondary vortexes have been best observed when they arise from a semiplane. The law of dynamical similarity for the frequency of the secondary vortexes takes on a different form in this case. Consider a point at a distance X from the edge of a semiplane and located within the same plane as the latter. The velocity at X will be U, and, since the dimensions of the boundaries may be said to have no effect on the flow, the Reynolds number will be referred to the distance X. The similarity law will then be given in the form:

$$U/\sqrt{f\nu} = F_2(XU/\nu) \tag{9}$$

Camichel's[16] analysis of the experiments of Crausse and Baubiac gives (at $X = 6$) approximately

$$U/\sqrt{f\nu} = 28 \tag{10}$$

For the secondary vortexes in the wake of a cylinder the appropriate law should be of the form

$$U/\sqrt{f\nu} = F_3(dU/\nu) \tag{11}$$

where d is the diameter of the cylinder.

Dynamical Similarity for Two Cylinders

Depicting the Flow.—The vortexes formed behind two parallel cylinders may assume a configuration that is not readily susceptible of an analysis. In the absence of precise information regarding the structure of the wake, we may conceive of a particular arrangement of the vortexes. The data obtained by observations may then be examined in the light of such conception. One vortex street may be set up at the external sides of the two cylinders corresponding to a flow about a solid body

with the same overall dimensions. Another type of street may be set up about each cylinder, corresponding to the conventional flow about an individual cylinder. A third type of vortex formation corresponding to flow through a narrow rectangular orifice may also be envisioned. Complication of the flow patterns may be caused by interaction of the various vortex streets and by secondary vortexes. For simplicity of treatment, we may restrict ourselves to just two types of vortex flows, internal and external. The frequency of the alternating vortexes generated at the external borders of the two cylinder system must now be expressed by

$$fd/U = F_4(Ud/\nu, G/d) \tag{12}$$

where F_4 is a functional symbol. The diameter, d, of each cylinder, and G, the gap distance between them, are the only geometrical quantities governing the flow. When G exceeds a certain critical value to be considered later, the frequencies become practically independent of the gap. The frequency of the vortexes generated at the internal boundaries of the cylinders—that is, at the gap—are likewise expressed by a form

$$fd/U = F_5(Ud/\nu, G/d) \tag{13}$$

Here again, when G exceeds the same critical value mentioned above, the frequency becomes independent of G. For separations of the cylinders greater than the critical gap, Eqs. (12) and (13) become identical. As the size of the gap is changed, marked differences must occur in flow through the gap. Such changes may be discontinuous and reflect on the manner in which the vortexes are formed. Visual or photographic observation could serve to resolve this problem, but in the absence of such information we may further contemplate the details of the internal flow.

Internal Vortex Picture

When the gap is zero the system behaves as a single solid of breadth equal $2d$. Since there is no flow through the internal boundaries, the vortexes are generated only on the external sides. It may be possible, however, for a stationary vortex pair to be set up in the downstream cavity formed by the cylinders, and, when the outer vortexes are detached, the stationary pair may oscillate or be dislodged. Proceeding to the case of a small gap, a stable jet may be issued with a parabolic velocity distribution. Being laminar, the jet may widen downstream and become bifurcated upon encountering the principal flow in the wake. The separating branches of the jet would be endowed with vorticity of opposing sign, forming two cylindrical eddies. As the gap is further increased in size, the jet may issue in a cone of uniform velocity between two vortex sheets which may unfold into an asymmetrical vortex street. In this state the mechanism of formation of the inner and outer vortexes differs but little. The difference, if it exists, would be in the effective

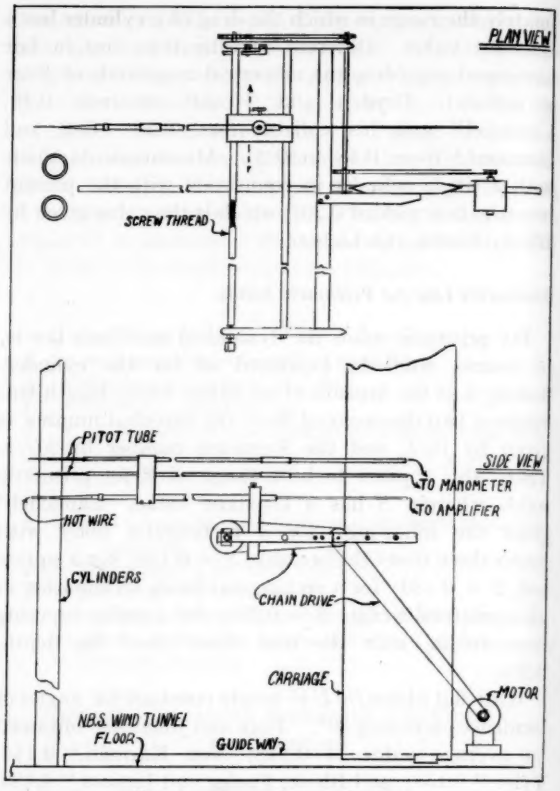

FIG. 1. Traversing mechanism.

circulation of the inner and the outer eddies. As a result of the conditions of flow for various gap values, the law given in Eq. (13) may show various discontinuities. The secondary vortexes may, of course, be present in any of the cases discussed above, but, since they may become confluent with the more prominent vortexes and thus indistinguishable, no further statement can be made at present.

EXPERIMENTAL SETUP

The study was conducted in the $4^1/_2$-ft. wind tunnel of the National Bureau of Standards. The cylinders used were of commercial brass tubing $1^3/_8$ in. in diameter, $^1/_{16}$-in. wall thickness, mounted to extend completely across the $4^1/_2$-ft. working section of the wind tunnel. The setting of the gap between the cylinders was held to within 0.04 in. in the plane of the measurements and to closer tolerance for the smaller spacings.* The cylinders were rigidly clamped to steel angles at the walls of the tunnel and did not vibrate perceptibly for any of the speeds encountered. The flow in the empty working section is of low turbulence (see footnote on page 299) and an examination with threads disclosed it

* A slight bend in one of the cylinders (0.04 in. in $4^1/_2$ ft.) was neglected as having no measurable effect, since random interchange of the cylinders throughout the investigation did not give rise to any attributable discrepancies.

TABLE 1
Frequencies of Vortexes Downstream from Two Parallel Cylinders. Velocity = 40 Ft. per Sec.

Gap, In.	G/d	Main Sequence Frequencies — Coupled	Main Sequence Frequencies — Uncoupled	Doubled Frequencies	Gap Frequencies	Other Frequencies
0	0	35.4		71		
1/32	0.023	36.1		72		
1/16	0.045	36		70		
3/32	0.068	33		66		
1/8	0.091	30.6				
2/8	0.182	31.7				15.5
3/8	0.273	34		68	17	20–22
4/8	0.364	34				
5/8	0.455	35.7		70	16, 114	16, 22
6/8	0.545	39.5				
7/8	0.636	42		80	115	
8/8	0.727	46.6		90	110–116	70, 80, 90
9/8	0.818	50		100	100	
10/8	0.909	58	74			16, 25, 84, 90
11/8	1.000		73–77	150		36, 93
12/8	1.091		72			
13/8	1.182		72	142		
33/16	1.500		74			
22/8	2.000		71	140		
33/8	3.000		73.5	142		
44/8	4.000		73	146		
55/8	5.000		73	145		
Single cylinder			72	144		

to be as uniform as visual observation will reveal. An absence of frequencies capable of interfering with the cylinder measurements, in the flow in the empty tunnel, was also indicated by an exploration with the hot wire.

Measurements were made of the velocity pressure distribution across the wake at several stations downstream from the cylinder system. To accomplish this, the flow was traversed with a pitot static tube, using the traversing apparatus shown in Fig. 1, especially constructed for the purpose. The accuracy of such measurements was within 2 per cent. Frequency measurements were made in similar explorations of the flow with the National Bureau of Standards Hot Wire Anemometer,[22] with which the velocity distribution was also checked in a few cases. Readings were taken in a plane parallel to the windstream approximately midway between the ends of the cylinders. Thus, wall interference and end effects were reduced to a minimum. The hot wire mount was kept to small dimensions and the carriage of the traversing apparatus was, in every case, held at no less than 15 diameters downstream from the point at which the readings were being taken in order to minimize interference between the carriage and the cylinders. Vibration of the hot wire mount, Fig. 1, was not easily eliminated because of the narrow depth cantilever, unsupported for about 20 in. However, vibration was not detected in the direction normal to the two-dimensional plane of flow, and it is in this plane that the wire is most sensitive. An oscillation did appear at a very low frequency (about 3 cycles) at a wind speed of 40 ft. per sec., and, since it occurred in the direction parallel to the longitudinal axes of the hot wire and of the cylinder system, it is believed to be of minor importance.

To obtain the frequency with which a hot wire (platinum, 0.0003 in. in diameter, 0.2 in. long, heated by a current from 50 to 100 milliamp.) was periodically cooled when subjected to an eddying flow, the output of the hot wire anemometer was impressed on the horizontal plates of an oscilloscope. The output of a variable frequency oscillator (Hewlett Packard) was impressed on the vertical plates and tuned until the screen of the oscilloscope showed a simple closed figure. The preferred figure is a circle, representing a 1:1 correspondence of the frequency picked up in the stream to the calibrating frequency. By tuning to Lissajou figures of multiples, a check on the frequency is obtained. Fage and Johansen[5] indicate that relatively steady readings could be obtained in the region outside the wake. However, with practice, the observer was able to recognize frequencies present in all but the most turbulent sections of the wake. Extraneous frequencies generated in line voltages, amplifying circuits, and other pickup could be reduced to negligible proportions by reducing the oscilloscope amplification and increasing the heating current to the hot wire. Thus the hot wire pickup was generally made overwhelmingly predominant on the screen. The error of the frequency measurements was within 2 per cent at all speeds, except in the critical region (see "Results of Frequency Measurements" below) where it may be double this value.

RESULTS OF FREQUENCY MEASUREMENTS

Classification of the Frequencies

In exploring the flow behind and between the cylinders, a number of different frequencies were obtained for the same air speed and cylinder spacing. Usually these frequencies occurred at different positions in the field of flow, but different frequencies were also found simultaneously in the same place. Figs. 6 to 15 show

the positions at which the measurements were made for the various gaps and the precise distribution of the frequencies found at an air speed of 40 ft. per sec.

The observed values are collected in Table 1. These are classified as follows: The frequencies measured in the general domain of the cylinder wakes are referred to as the "main sequence." When the flow about one cylinder has an effect on the flow about the other, as at small separations, the main sequence will be said to consist of "coupled frequencies." When the cylinders are separated by a larger gap, where the flow about one does not appear to influence the frequency at the other, the main sequence will be called "uncoupled frequencies."

Another group of frequencies, these measured distinctly in the vicinity of the gap, are listed under "gap frequencies." Miscellaneous frequencies that could not readily be classified were also recorded, and these are listed as "other frequencies." Corresponding to the main sequence is a group that registered frequency values twice as high as the latter; these are given as "doubled frequencies."

Doubled Frequencies Explained

The existence of the doubled frequencies can be explained as follows: When the vortexes detached from a cylinder in a von Kármán train have developed to the magnitude at which they reach or overlap the centerline of flow, each side of the street will contribute equally to the measurement at that point and effect a frequency twice as high as that obtained in the general flow (as given in the "Introduction"). Reference 5 also reports such observations. In the case of the cylinders touching, the double frequency is, in fact, found on the centerline and can be explained by the overlap of the outer sides of the vortex street. This is also true for gaps of $^1/_{32}$ and $^3/_{32}$ in., as in Figs. 6 and 7. For gaps of $^{13}/_8$, $^{33}/_8$, $^{44}/_8$, and $^{55}/_8$ in. (Figs. 10, 13, 14, and 15), the doubled frequencies occur only at the centerlines of the individual cylinders, as in the case of a single cylinder. At the intermediate gaps no simple statement can be made. Whether the doubled frequencies, which are in such cases more widely distributed over the field, owe their origin to an overlap of the vortex formation from the two cylinders, cannot be said with certainty.

Main Sequence of Frequencies

A graphic representation of the data of Table 1 is given in Fig. 3. Disregarding the curve corresponding to the doubled frequencies, it is seen that the observations taken at values of G less than $^{11}/_8$ in. distribute themselves in three distinct groups. All the frequencies at gaps larger than $^{11}/_8$ in. appear to fall on a line of constant ordinate, indicating that the flow about the cylinders is uncoupled, and each cylinder generates vortexes of like nature. For the ordinate having the value $f = 72$ cycles per sec., the cylinder diameter $^{11}/_8$ in., and the velocity of air 40 ft. per sec., the corresponding Strouhal number is $fd/U = 0.207$.

If the assumption is made that the main sequence is due to vortexes formed in an external street (and this assumption is not unfounded), a satisfactory explanation of the phenomena may be arrived at. When the cylinders are touching, there is only one dominant frequency and it must be external. For this case

$$f(2d/U) = 2fd/U = 0.21$$

and the frequency of the vortexes is about 36 cycles per sec. As the gap is enlarged, the frequency of the external vortexes changes from the initial value of 36 to a final value of approximately 72. The flow modification at the external borders is a continuous process up to a gap of $^{10}/_8$ in., where an unstable distribution seems to produce several prominent frequencies. Thus, the lower branch of the two curves that join at $G = {}^{11}/_8$ in. represents the variation of the external frequencies as a function of gap distance. This is the main sequence curve for the coupled frequencies and exhibits a minimum at $G = {}^1/_8$ in., rising in an approximate parabola as it approaches $G = {}^{10}/_8$ in. in one direction and more sharply toward $G = {}^1/_{32}$ in. where the frequency is slightly higher than at $G = 0$.

Vortexes at Small Gaps

The decrease in frequency from $G = 0$ to $G = {}^1/_8$ in. may be explained by considering the flow through the gap of closely spaced cylinders as of a nature to delay the separation of the vortexes at the external borders. Since the boundary layer separates from the surface of a cylinder in the form of a vortex sheet, which at Reynolds number encountered in this investigation is in the form of a discreet vortex, a definite quantity of fluid must be available at each air speed to maintain this periodic detachment. If a leak of the fluid in the boundary layer occurs (i.e., at very small spacing) the process of vortex formation at the external sides may be retarded. Prandtl[17] has shown that removal of fluid from the boundary layer can delay or prevent separation.

Vortexes in the Gap

Returning to the remaining groups of frequencies, the highest branch, descending as it approaches the critical value, was tabulated as a gap frequency because it was recorded with some intensity in the gap. A peculiarity of this descending branch is that the frequencies are also noted in the general wake of the two cylinders. This could mean that the vortexes from an internal jet produce periodic pressure variations that cause velocity fluctuations. Another possibility suggested by the scattering of the readings is that these vortexes are unstable and meander under the action of the external pressures. That these internal vortexes are not quite similar to the edge-tone vortexes dis-

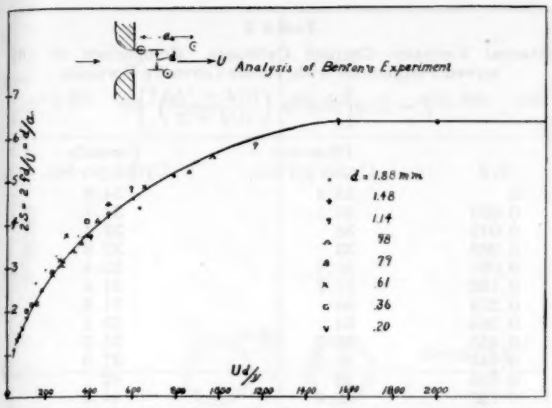

FIG. 2. Vortexes in the jet from a rectangular orifice.

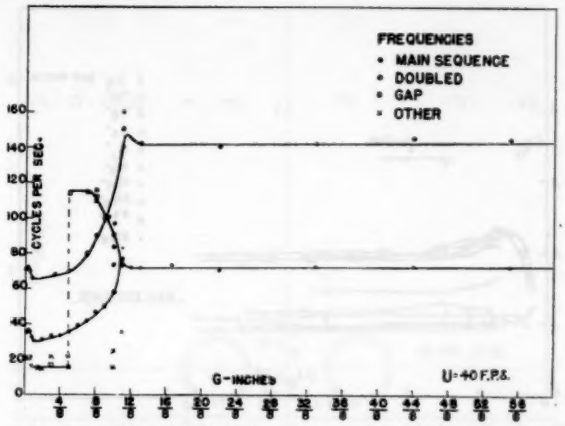

FIG. 3. Vortex frequencies found at varied spacings of two cylinders of $^{11}/_{8}$-in. diameter.

cussed above results from a consideration of gap dimensions and measured frequency. A connection is suggested, however, if the constant value of $2S$, shown in Fig. 2, is considered to be too high for the orifice that is formed by two adjacent cylinders in an airstream. For a gap of $^{8}/_{8}$ in., for example, Fig. 2 yields a frequency of about 140, whereas 113 was observed, but the discrepancy becomes progressively greater at smaller gaps. This example, however, assumes a linear extrapolation for Reynolds numbers from 2,000 to 28,000.

Since it is believed that extraneous vibrations, as of the cylinders and apparatus, do not enter into the picture, the distinctness and separation of the two branches of the gap frequencies suggest two possibilities. First, there may be two modes of vortex formation at the borders of the internal jet, or, second, as the gap distance is increased two distinct régimes are established, depending upon the cylinder separation. As may be seen from Fig. 3, none of the high gap frequencies were obtained below $G = {}^{5}/_{8}$ in., which indicates that the flow does not support these frequencies at the smaller gaps or that they are too weak to be detected. On the other hand, none of the low gap frequencies were observed at gaps larger than $^{5}/_{8}$ in., which supports the idea of a discontinuity at that point.

Other Frequencies

The low gap frequencies indicated by the squares of Fig. 3 may be contrasted with a number of other readings, of the same order of magnitude, which could not be obtained distinctly. These readings, tabulated as "other frequencies," are shown by x's in Fig. 3. They were not sharply defined but spread over a band of several cycles and were found rather close to the cylinder at gaps above, as well as below, $^{5}/_{8}$ in. Since such readings were also obtained with a single cylinder (and were absent with both cylinders removed), this may be the limiting value of the secondary vortexes mentioned by Courregelongue.[15] The lack of such data for cylinders, however, prevents the making of conclusive statements.

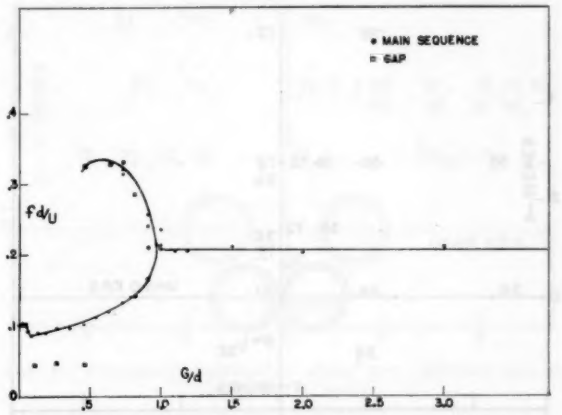

FIG. 4. Strouhal number as a function of separation of two cylinders (for air speeds from 20 to 140 ft. per sec. with $^{11}/_{8}$-in. diameter cylinders).

DEPENDENCE OF FREQUENCY ON REYNOLDS NUMBER

The pertinent data of Fig. 3 are reproduced in Fig. 4 in the form of dimensionless parameters. This representation is for a Reynolds number of 28×10^{3}, taking the kinematic viscosity of air as 16×10^{-5} ft.^{2} per sec. It is desirable to examine the data to determine whether or not there is any observable effect when the Reynolds number of the flow is varied. In particular, it is important to know whether the critical value of G/d depends upon the Reynolds number. To determine this point the values of the Strouhal number for values of the Reynolds number from 5,000 to 93,000 were superimposed on Fig. 4. The result was that all the values above R about 15,000 fell within a few per cent of each other and were indistinguishable on the curve and, hence, omitted.

At $R = 12{,}000$ the curve was about 10 per cent higher, and at $R = 5{,}000$ the curve was about 10 per cent lower than the mass of measurements at greater values of R, for all gaps. This indicated that a scale effect exists for the lower velocities.

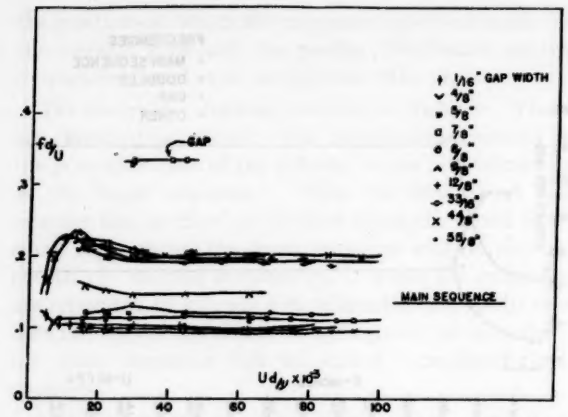

FIG. 5. Strouhal number as a function of Reynolds number for varied spacing of two cylinders.

TABLE 2

External Vortexes—Coupled Cylinders. Comparison of Observed Frequencies with Values Given by Formula

$$f = U/d\left[0.09 + \left(\frac{G/d - 1/5}{G/d + 2}\right)^2\right]$$

G/d	Observed Cycles per Sec.	Formula Cycles per Sec.
0	35.4	34.9
0.023	36.1	34.1
0.045	36	33.4
0.068	33	32.8
0.091	30.6	32.4
0.182	31.7	31.4
0.273	34	31.8
0.364	34	33.1
0.455	35.7	35.2
0.545	39.5	37.8
0.636	42	42
0.727	46.6	44.5
0.818	50	48.2
0.909	58 (16–90)	52.1

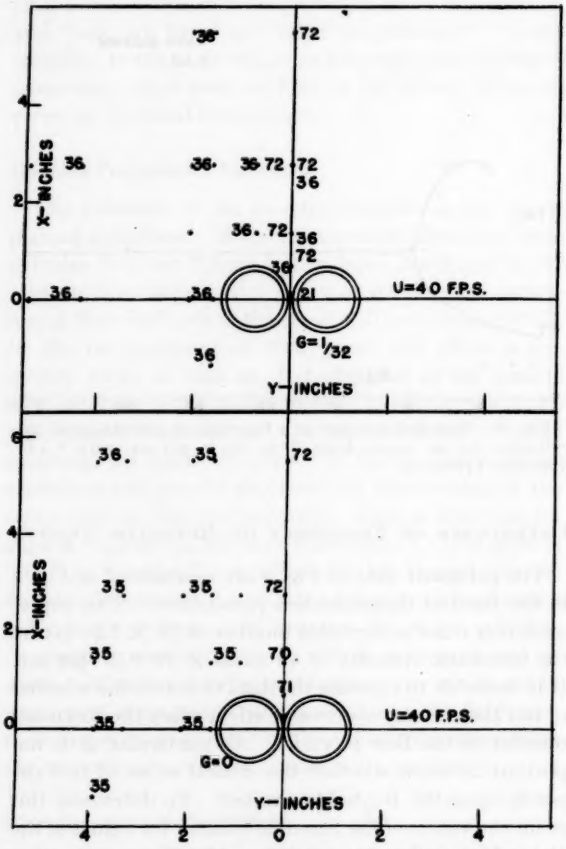

FIG. 6. Frequency distribution about two cylinders, touching and separated by 1/32 in.

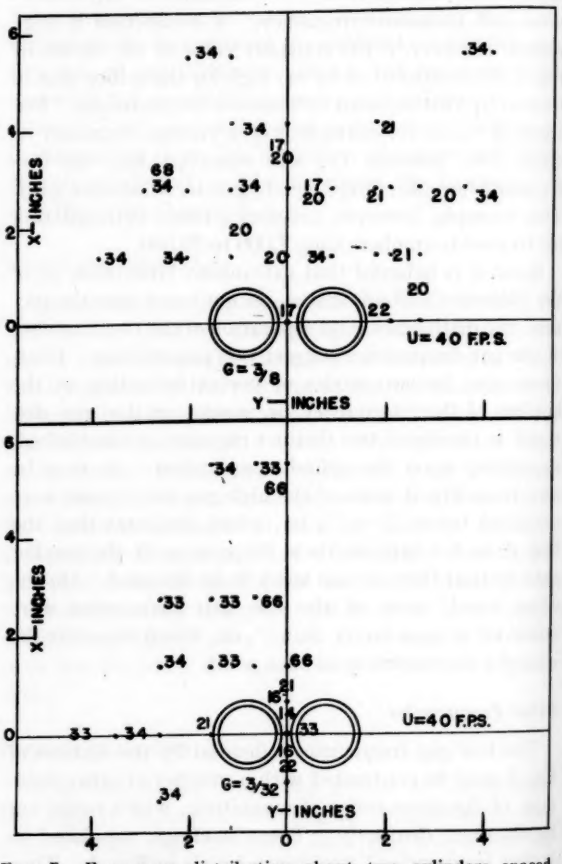

FIG. 7. Frequency distribution about two cylinders spaced 3/32 and 3/8 in. apart.

Linear Behavior of Strouhal Number

To examine this condition further, Fig. 5 has been prepared, where the data relate principally to the main sequence of external vortex frequencies. As indicated in the "Introduction," the limits of the stable vortex formation is also the region of constant fd/U for a given body.

For this condition to be fulfilled the frequency must be a linear function of the velocity of the airstream. Such behavior of the frequency is shown for all cylinder spacings in Fig. 5, where, for $R > 15{,}000$, the lines drawn through the observed points are practically parallel to the ordinate axis. But as shown by the curves corresponding to gaps of 44/8, 33/16, 7/8, and 1/16

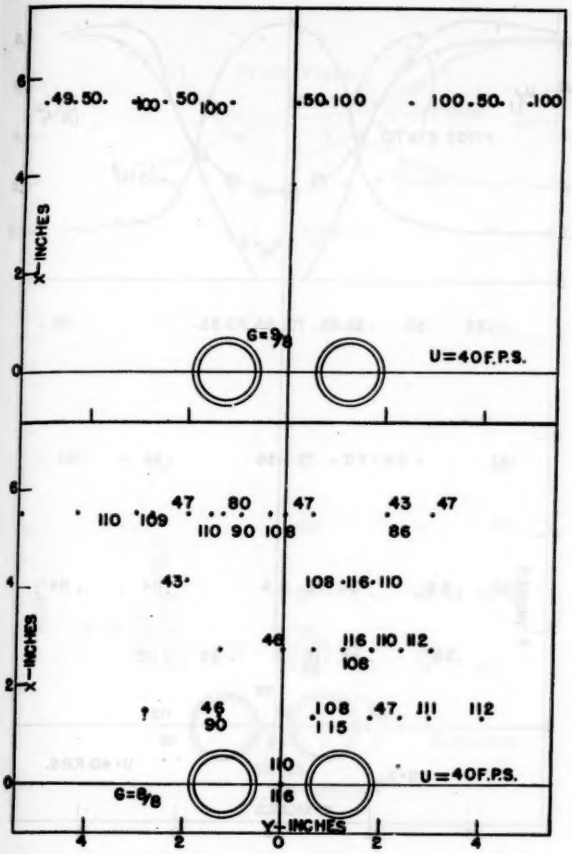

FIG. 8. Frequency distribution about two cylinders spaced $^{8}/_{8}$ and $^{9}/_{8}$ in. apart.

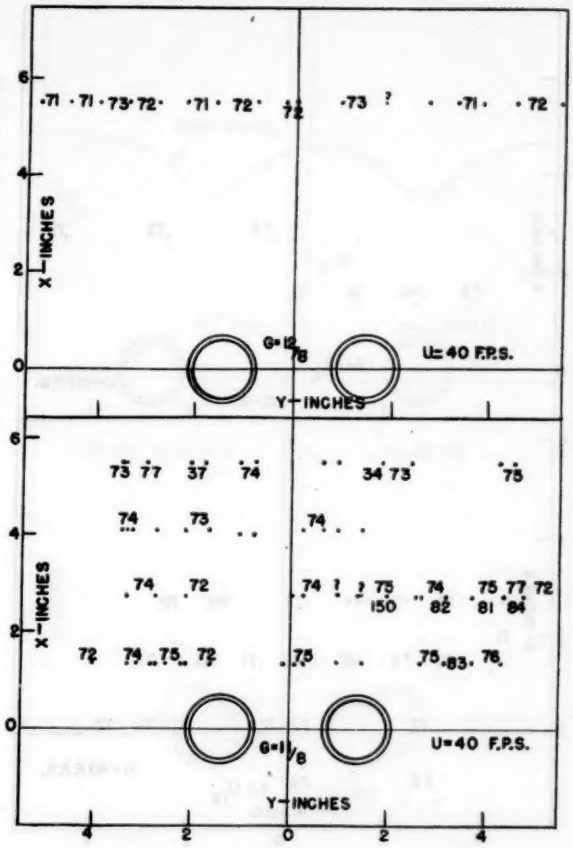

FIG. 9. Frequency distribution about two cylinders spaced $^{11}/_{8}$ and $^{12}/_{8}$ in. apart.

in. for the Reynolds numbers below 15,000, the Strouhal number rises and then drops sharply toward the low end. While sharp definition of the lowest frequencies is difficult, it nevertheless appears that a transition in the flow has occurred. This agrees with the discussion of the preceding paragraph. The departure occurs within the usually stable range for a single cylinder. In this respect, it may be deduced that the two-cylinder system is an anomalous case.

An Empirical Formula for the Frequency

When the two cylinders are far removed from each other (uncoupled), one will produce a vortex street as if the other were absent and the Strouhal number may be expressed by fd/U for either. On the other hand, as the gap approaches zero, the limiting frequency of the total system must approach a value for which S is given by $f(2d/U)$. For the intermediate case, between these two limiting conditions of the external vortex formation, a law of the form

$$fd/U = F_4(G/d) \qquad (14)$$

may be used to express the frequency parameter. This is in accord with Eq. (12) above, since S has been shown to be largely independent of Ud/ν. To express this lower branch of the main sequence curve of Fig. 4, the following empirical formula is given:

$$fd/U = 0.09 + \{[(G/d) - {}^{1}/_{6}]/[(G/d) + 2]\}^{2} \qquad (15)$$

Eq. (15) is valid for gap parameters less than the critical value, and the accuracy with which it approximates the observations is shown in Table 2.

VELOCITY MEASUREMENTS

Velocity pressure measurements were made for the several cylinder spacings with the pitot static tube shown in Fig. 1. Readings were taken in a plane normal to the flow mainly four diameters downstream from the center of the system. In this plane ($x/d = 4$), the pitot static tube was generally out of the region of severe pressure changes, stagnation, or reversal of flow behind the cylinders. The dynamic pressures were obtainable, therefore, without error caused by directional flow around the pressure tubes.

Figs. 11 to 15 show the results of such measurements. In Fig. 16 u/U_0 is plotted for several spacings both smaller and larger than the critical value of $G/d = {}^{10}/_{11}$.

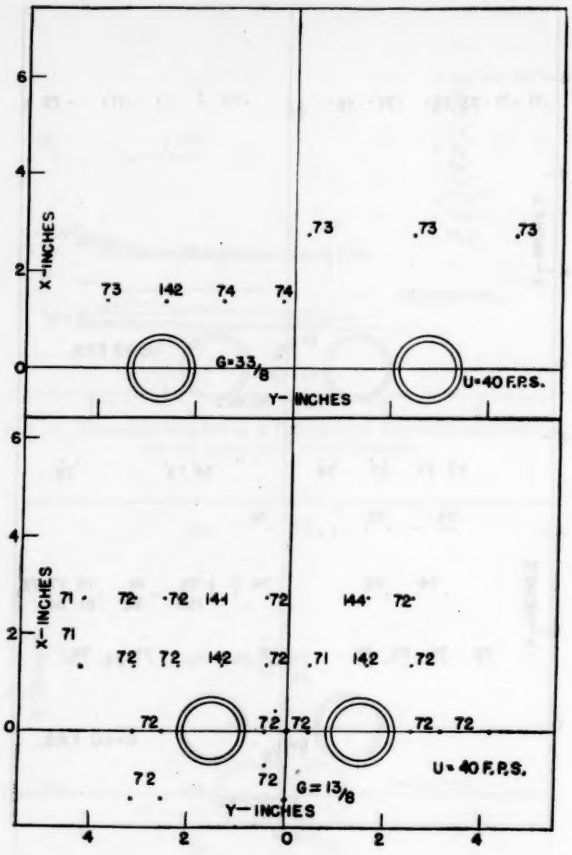

FIG. 10. Frequency distribution about two cylinders spaced $^{13}/_{8}$ and $^{33}/_{8}$ in. apart.

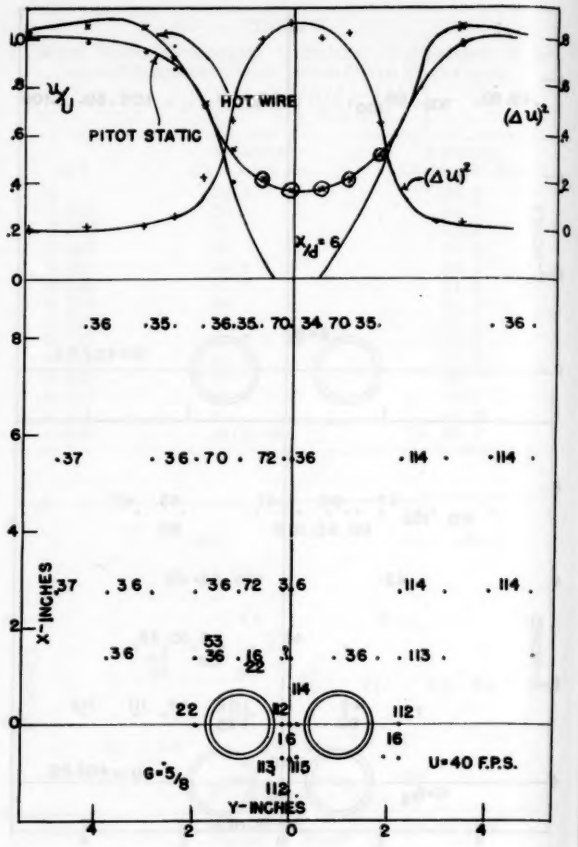

FIG. 11. Velocity and frequency distributions about two cylinders spaced $^{5}/_{8}$ in. apart.

At $x/d = 4$ the wakes behind the cylinders are definitely separate for gaps greater than the critical. At smaller gaps the wakes have definitely merged to exhibit pressure distributions like those at a greater distance downstream from a single continuous obstacle. Such behavior is significant in supporting the frequency observations above and below the critical gap value.

At $G/d = {}^{44}/_{11}$ the velocity along the central axis of flow has reached the free stream velocity in the plane $x = 4d$. It is natural, therefore, to suppose that the flow from each cylinder is here, independent of the other. At $G/d = {}^{22}/_{11}$ the central velocity does not quite reach the free stream value so that slight coupling is assumed. The central pressure has dropped still farther at $G/d = {}^{12}/_{11}$, although mixing of the wakes has not yet occurred. At $G/d = {}^{9}/_{11}$ a single wake pattern exists with minimum pressure at the axis of symmetry. While single wake patterns are expected below $G/d = {}^{10}/_{11}$, the central pressure region is flat at $^{9}/_{11}$ but becomes steep immediately at smaller gaps until, as at $^{4}/_{11}$, the flow has reversed direction and cannot be measured precisely with the pitot static tube. Mixing of the wakes from each cylinder occurs earlier for smaller spacings, but for measurements made directly behind the system individual wakes were detected at all but the smallest gaps. At $G/d = {}^{3}/_{11}$ the wakes were found to mix between one and two diameters downstream. The positions shown in Figs. 6 to 15 are the approximate limits beyond which mixing or excessively weak signal prohibited reading of the frequencies. The outer boundaries of the wake can be discerned for all gaps by pressure measurements, at least as far downstream as $x/d = 8$, although mixing has obviously obliterated the initial vortex frequencies (see Fig. 99, reference 23).

In the wake of a single cylinder, reversal of flow is characterized by stationary vortexes attached to the rear of the body.[3] At a single cylinder, the dead space (the region of reversal of flow) is wedge-shaped, with the base of the wedge at the cylinder and the vertex about $2d$ downstream. For two cylinders close together ($G < d$) but not touching, there are two such dead space wedges, even for a gap $^{1}/_{16}d$, one for each cylinder. But the vertexes are about $1d$ downstream, so that—e.g., for $x = {}^{1}/_{2}d$—the width of each dead space is smaller than in the case of the single cylinder.

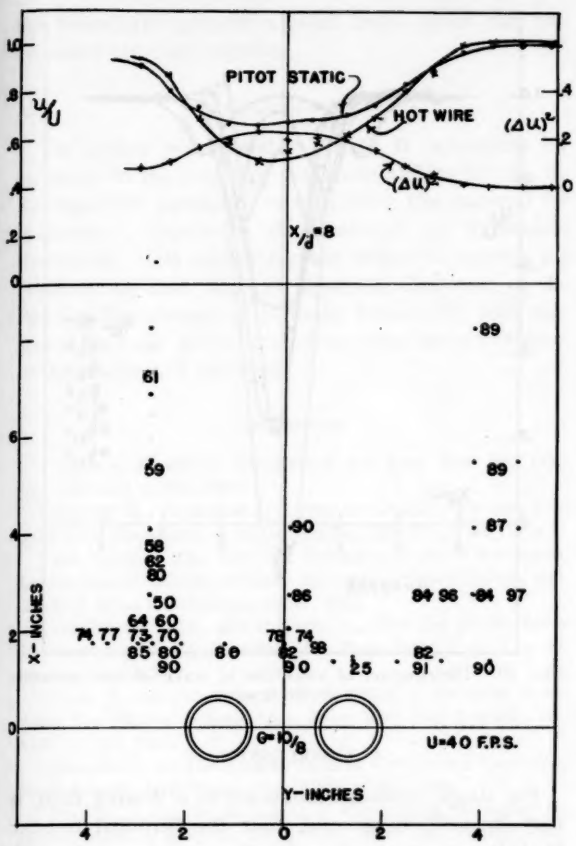

FIG. 12. Velocity and frequency distributions about two cylinders spaced $^{10}/_{8}$ in. apart.

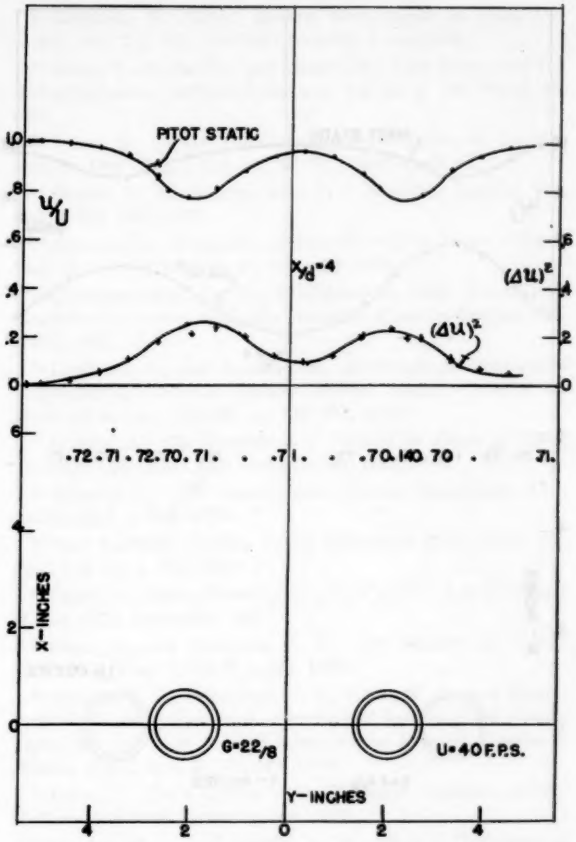

FIG. 13. Velocity and frequency distributions about two cylinders spaced $^{22}/_{8}$ in. apart.

At the downstream half of each cylinder up to a distance of 0.25 in., the hot wire exploration shows a high degree of turbulence, which seemed to be more noticeable than for single cylinders.

Measurements of the mean speeds were obtained in traverse of the wake with the hot wire anemometer. Resulting readings were substantially as obtained with the pitot static tube for a few spacings observed, as in Figs. 6 to 15. As applied, the single hot wire is not sensitive to directional changes in the x-y plane so that only the magnitude of the mean speed and not the velocity is disclosed. When the single hot wire is used in coordination with the pitot static tube, reversal of flow, as well as the magnitude, may be detected. The circled values (in the upper portion of Fig. 11) of the speed measured with the hot wire are shown to be in a negative direction by the pitot static tube measurements.

Vorticity

The N.B.S. Hot Wire Anemometer circuit is equipped to indicate the value (squared) of the fluctuations about the mean speed. This arrangement has been used[22] to determine the intensity of the turbulent fluctuations in the airstream. While quantitative results can be obtained by the procedure outlined in reference 24, Table IX, the circuit is admirably suited to furnish a direct qualitative indication of the vorticity distribution in the wake. The magnitude of the fluctuations is a function of the vortex strength at the point that readings are being taken, and the square of the velocity fluctuations has the dimensions of vortex strength per unit area.

In a von Kármán vortex street, the fluctuations have definite frequencies. In the free stream the existing vorticity appears as "isotropic turbulence,"[25] in which discreet vortex frequencies cannot be detected but a more or less continuous spectrum of eddy frequencies of much smaller scale and intensity than the von Kármán vortexes exists. This requires the wake of upstream obstacles to be thoroughly mixed and diffused before reaching the point in question.* (For details see reference 26.) Upstream from the two cylinders or far to one side—i.e., in the free stream—the von Kármán vorticity is not of measurable proportions. It becomes

* In the N.B.S. $4^1/_2$ ft. wind tunnel working section the turbulence at 40 ft. per sec. is of the order of $100(u'^2 + v'^2 + w'^2)/3U = 0.02$ per cent.

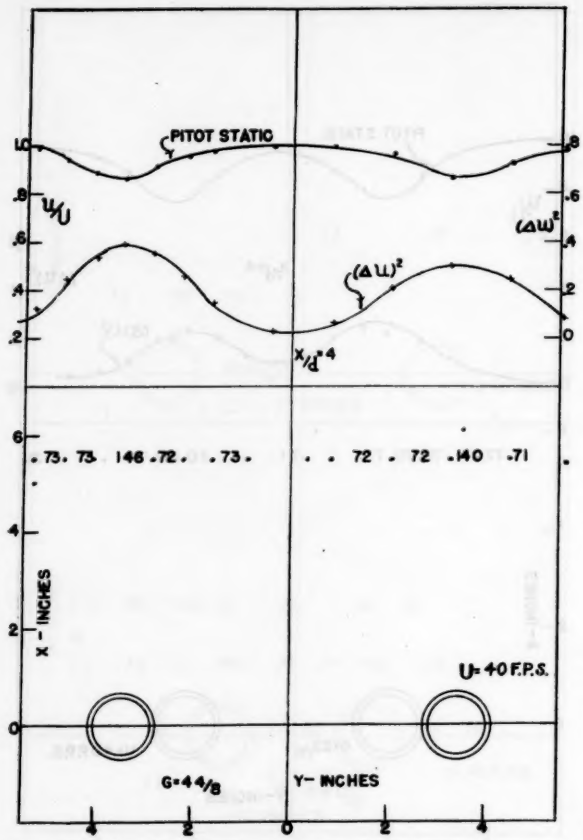

FIG. 14. Velocity and frequency distributions about two cylinders spaced $4^{4}/_{8}$ in. apart.

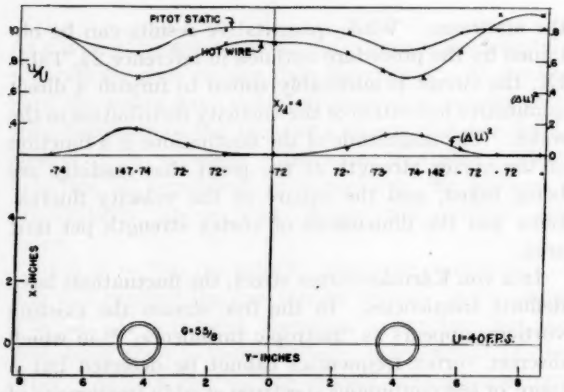

FIG. 15. Velocity and frequency distributions about two cylinders spaced $5^{5}/_{8}$ in. apart.

measurable as the wake is approached. The fluctuations increase as the wake is entered, rising violently at the center of the wake whether the latter is formed by two individual streets or by a single coupled pattern. This is illustrated in the upper portions of Figs. 11, 12, 13, 14, and 15, where $(\Delta u)^2$ is plotted to an arbitrary scale dependent on the dimensions of the wire, the heating current, and the velocity.

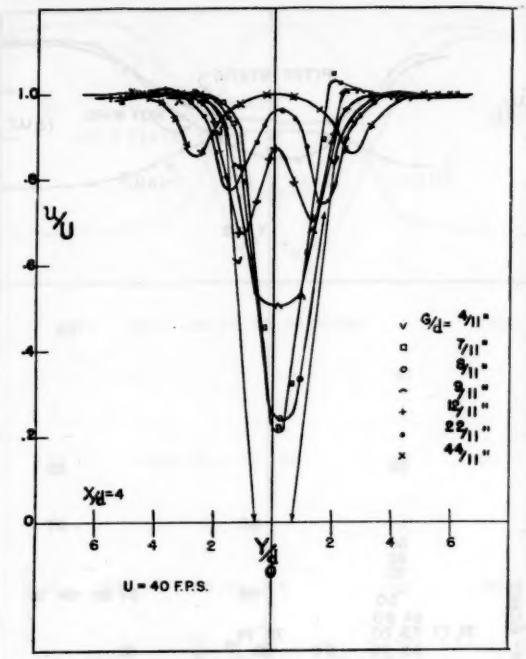

FIG. 16. Distribution of velocities in wake of two cylinders at varied spacing.

CONCLUSIONS

For single obstacles immersed in a flowing fluid, it may be said, in general, that the Strouhal number fb/U is a constant, where b is the cross-stream breadth and independent of the Reynolds number for the turbulent flow régime. The same statement may be applied to the case of two cylinders, except that the constant value fd/U changes for $(G/d) < 1$. For Reynolds numbers, Ud/ν, less than 15,000, a nonlinear relation between frequency and velocity indicates a transition in the state of flow. $G/d = 1$ is the critical spacing above which the cylinders behave independently. At smaller values of the gap, individual von Kármán vortex streets are not detached from each cylinder; instead, a coupled vortex street is formed by the overall system along with certain internal vortexes that depend upon the gap. The internal vortexes are probably generated in vortex sheets bordering a jet that emanates from the orifice formed by the adjacent sides of the two cylinders.

A discontinuity may be said to exist in the internal vortexes at $G/d = {}^{5}/_{11}$, below which a low frequency, and above which a high frequency, is found. The frequencies of the coupled external vortex street are given approximately by

$$fd/U = 0.09 + \{[(G/d) - {}^{1}/_{5}]/[(G/d) + 2]\}^{2}$$

This formula holds up to $G/d = {}^{10}/_{11}$ where the frequench exhibits an instability. A minimum frequency at $G/d = {}^{1}/_{11}$ is explained by delay of separation of vortexes, caused by a condition analogous to a leak in

the boundary layer at a solid body, when the two cylinders are close together.

Acknowledgment

The author is indebted to Dr. G. B. Schubauer for guidance in the hot wire technique and to Dr. G. H. Keulegan for assistance in organizing the material for publication, especially the material on dynamical similitude. The author further wishes to express his gratitude to Prof. Karl F. Herzfeld, Chairman of the Physics Department of Catholic University, who suggested the topic, for his unstinting attention and interest in the progress of the work.

References

[1] Mallock, A., *On the Resistance of Air*, Proc. Roy. Soc. London, Vol. A79, p. 262, 1907.

[2] Bénard, H., *Formation de Centres de Giration a l'arriere d'un Obstacle en Mouvement*, Comptes Rendus, Vol. 147, p. 839, 1908.

[3] von Kármán, Th., *Uber den Mechanismus des Widerstandes, den ein bewegter Korper in einen Flussigkeit erfahrt*, Nachr. Kgl. Gesell. d. Wiss. z. Gottingen, p. 547, 1912.

[4] von Kármán, Th., and Rubach, H., *Uber den Mechanismus des Flussigkeits und Luftwiderstandes*, Phys. Zeits., Vol. 13, p. 49, January 15, 1912.

[5] Fage, A., and Johansen, F. C., *The Flow of Air about an Inclined Flat Plate of Infinite Span*, Proc. Roy. Soc. London, Vol. A116, p. 170, 1927.

[6] Rosenhead, L., *The Karman Street of Vortices in a Channel of Finite Breadth*, Phil. Trans., Vol. A228, p. 275, 1929.

[7] Hooker, S. G., *On the Action of Viscosity in Increasing the Spacing Ratio of a Vortex Street*, Proc. Roy. Soc. London, Vol. A154, p. 67, 1936.

[8] Dryden, H. L., and Heald, R. H., *Investigation of Turbulence in Wind Tunnels by a Study of the Flow about Cylinders*, N.A.C.A. T.R. No. 231, 1925.

[9] Relf, E. F., and Simmons, L. F. G., *The Frequency of the Eddies Generated by the Motion of Circular Cylinders Through a Fluid*, Phil. Mag. 7, p. 509, 1925.

[10] Goldstein, S., Editor, *Modern Developments in Fluid Dynamics*, Vol. 2, p. 557; Oxford University Press, 1938.

[11] Blenk, J., Fuchs, D., and Liebers, F., *Uber Messungen von Wirbelfrequenzen*, Luftfahrtforschung, Bd. 12, p. 38, March 28, 1935.

[12] Tyler, E., *Vortex Formation behind Obstacles of Various Sections*, Phil. Mag. 7, Vol. 11, No. 72, p. 849, April, 1931.

[13] Benton, W. E., *On Edge Tones*, Proc. Phys. Soc. London, Vol. A38, p. 109, 1925–1926.

[14] Carriere, Z., *Phenomenes a l'Embrochure d'un Tuyau d'Orgue*, Jour. de Phys. et Rad., p. 57, February, 1925.

[15] Courregelongue, J., *Sur l'Existence de Deux Familles de Tourbillons a l'arriere de Solides Immerges*, Comptes Rendus, 189, p. 972, 1929.

[16] Camichel, O., and Escande, E., *Similitude Hydraulique et Techniques des Modeles Reduits*, Public. Scient. e. Tech. du Ministere de l'Air, No. 127, pp. 249–285, 1938.

[17] Prandtl, L., *The Generation of Vortices in Fluids of Small Viscosity*, Jour. Roy. Aero. Soc., Vol. 31, 1927.

[18] Strouhal, V., *Ueber eine besondere Art der Tonerregung*, Ann. der Physik 5, p. 215, 1878.

[19] Lord Rayleigh, *Aeolian Tones*, Cambridge Univ. Press, Sci. Pap., Vol. VI, p. 313, 1920.

[20] Thom, A., *Eddies Behind an Circular Cylinder*, A.R.C., R. and M. No. 1373, December, 1930.

[21] Fage, A., and Johansen, F. C., *The Structure of Vortex Sheets*, Phil. Mag. 7, Vol. 5, p. 417, 1928.

[22] Dryden, H. L., Schubauer, G. B., Mock, W. C., and Skramstad, H. K., *Measurement of Intensity and Scale of Wind Tunnel Turbulence and Their Relation to the Critical Reynolds Number of Spheres*, N.A.C.A. T.R. No. 581, 1937.

[23] Rouse, H., *Fluid Mechanics for Hydraulic Engineers*, p. 220; McGraw-Hill Book Company, Inc., 1938.

[24] Dryden, H. L., and Kuethe, A. M., *Effect of Turbulence in Wind Tunnel Measurements*, N.A.C.A. T. R. No. 342.

[25] Dryden, H. L., *Experimental Techniques for Studying Turbulent Airflow*, Journal of the Aeronautical Sciences, Vol. 3, p. 173, March, 1936.

[26] Dryden, H. L., *Turbulence, Companion of Reynolds Number*, Journal of the Aeronautical Sciences, Vol. 1, p. 68, April 1, 1934.

Notes on the Design of Pressurized Cabin Aircraft*

DANIEL O. DOMMASCH†
Civil Aeronautics Administration

ABSTRACT

If the possibility of a variation of load factor with altitude is admitted, then the cabin portion of a pressurized aircraft is subjected to two sets of loads, both of which vary with altitude. The first set of loads is composed of the loads due to the flight load factors; the second set, of all the loads imposed by internal pressure in the cabin.

In the section of this paper titled "Variation of Load Factor with Altitude" it is shown that the flight load factors will probably decrease with altitude. Since pressure loads will increase with altitude, it follows that various structural components in the cabin region will be critically loaded at what may be designated as the *critical structural altitude* (i.e., since the structural members are loaded by one set of loads decreasing with altitude and another increasing with altitude, there must exist some altitude at which the state of stress in a particular member becomes critical. It is, of course, possible that this altitude will be sea level or possibly the aircraft absolute ceiling). In general, the critical altitude will be different for each structural component.

Of the conclusions reached in this paper, there is one of particular interest because it represents a departure from accepted practice. This conclusion is:

In general, it is not possible to assume that diametral pressure loads are carried by hoop tension in the skin unless a careful investigation proves that there is no other structure capable of carrying these loads (this holds for fuselages of any cross section).

VARIATION OF LOAD FACTOR WITH ALTITUDE

THERE ARE TWO TYPES of flight loadings to which an aircraft structure may be subjected. These are (1) maneuvering loads and (2) gust loads. To determine a true picture of the variation with altitude of either of these loading types is beyond the scope of this paper, and unnecessary as far as the following discussions are concerned. The only fact that it is desired to establish is that the magnitude of both these loading types probably will decrease in some fashion with altitude.

Maneuvering Loads

Since maneuvering load factors are in general arbitrarily assigned, it is difficult to state exactly how they will vary with altitude. It is known, however, that the higher up an airplane flies, the less maneuverable it becomes. This follows from the fact that the maneuverability of an aircraft is largely dependent on the effectiveness of its control surfaces which, in turn, is dependent in part on the air density (which decreases with altitude). To make this point clearer, it is only necessary to imagine a projectile flying in some manner through space with only conventional tail surfaces available for control. It is obvious, since the air density would be zero, that the projectile would be uncontrollable (that is, unmaneuverable).

On the basis of the above,

$$n_m = f(\rho) = f(h)$$

where

n_m = maneuver load factor
$f(\rho)$ = function of air density
$f(h)$ = function of altitude

Since there are many other factors that influence the value of the maneuver load factor, it should be recognized that the only point brought out above is the dependence of the maneuver load factor on altitude.

It now remains to demonstrate that the gust load factor also varies in some fashion with altitude.

Gust Loads

In discussing gust loads for pressurized cabin aircraft, it is necessary to keep in mind that the primary purpose of pressurization is to permit the airplane to avoid turbulent air conditions, such as those encountered in thunderstorms, fronts, and the like (i.e., over the weather flight).

It is known that extremely severe gusts are encountered even at the base of the stratosphere in thunderstorm cloud formations. However, it is not logical to assume that pressurized cabin aircraft will fly through this type of disturbance when these aircraft are specifically designed to avoid this type of flight.

Working on the sensible assumption that pressurized aircraft will avoid turbulent air conditions at all times except during take-offs and landings, and recalling that, except during storm conditions, gusts are associated with ground discontinuities (mountains, lake, shore, etc.), it is readily seen that the magnitude of gusts which a pressurized airplane may be expected to encounter will decrease in some fashion with altitude and become negligible in the stratosphere.[1]

On the basis of the above, it appears that the gust velocity that should be used to design pressure cabin

Received January 3, 1946.

* From a thesis submitted to the Graduate Division of the College of Engineering in partial fulfillment of the requirements for the degree of Master of Aeronautical Engineering at New York University. The opinions expressed in this paper are those of the author and are not necessarily those of the C.A.A.

† Aeronautical Engineer. Now with Bell Aircraft Corporation.

aircraft is a function of altitude and decreases with increased altitude.

The accepted formula[2] for gust load factor increment is:

$$\Delta n_g = (\rho/2)KUV(dC_L/d\alpha)/(W/S)$$

where

Δn_g	= gust load factor increment
ρ	= air density
K	= a factor depending on wing loading
U	= gust velocity
V	= true air speed
$dC_L/d\alpha$	= lift slope
W/S	= wing loading

In the above formula, ρ, U, and V may vary with altitude. It follows, therefore, that $\Delta n_g = f(h)$; furthermore, Δn_g is apparently a decreasing function of h, which eventually becomes zero.

An Arbitrary Altitude Load Factor Reduction Formula

In order to permit numerical results to be presented in the next section, the following arbitrary formula for load factor variation with altitude is assumed.

$$n_h = 1 + \beta \Delta n_0 \tag{1}$$

where Δn_0 = load factor increment at sea level and

$$\left.\begin{aligned} \beta &= 1 - \frac{0.6942h}{35{,}332};\ 0 \le h \le 35{,}332' \\ \beta &= 0.3058;\ h > 35{,}332' \end{aligned}\right\} \tag{2}*$$

Terminology

P_r	= internal pressure running load (lbs. per in.)
ϑ, φ	= angles
X_m, X_p, X_v	= unknown bending moment, axial load, and shear load, respectively
p	= pressure
p_0	= pressure at sea level
x, y, z	= rectangular coordinates
a, b	= sides of plate
t	= thickness
ν	= Poisson's ratio
u, v, w	= components of displacements
W	= running load at section
E	= Young's modulus
σ_i, σ_b	= normal stresses due to inertia or flight load
$\sigma_n, \sigma_p, \sigma_l$	= stresses due to pressure
$\sigma_t, \sigma_{t_1}, \sigma_{t_2}, \sigma_{t_3}$	= total stress
j	= $\sqrt{EI/P_a}$
I	= moment of inertia
P_a	= axial load in beam column or frame
L	= beam length
M	= moment
A_s, A_f	= area stringer, area frame cross section
r	= frame radius
P_1	= concentrated inertia load on frame

* Up to the base of the stratosphere, β as given by this equation is merely a linear approximation of the density ratio ρ/ρ_0; above 35,332 ft. β was assumed to be constant.

Determination of Critical Structural Altitude and Discussion of Stress Analysis Problems Peculiar to the Design of Pressurized Cabins

Hoop Tension and Membrane Tension Stresses in Skin

Although in earlier works[3] on the topic of this paper, hoop tension in the skin was considered as the major factor resisting radial pressure due to pressurization, it is not possible to tacitly assume that this is always the case. Consider the following argument pertaining to a fuselage of circular section.

(a) For hoop tension to exist in the skin the skin must be continuous.

(b) If hoop tension in the skin is to be of importance, internal framework must have less resistance to radial and circumferential, deformation than the skin.

(c) Since the skin of the modern metal monocoque fuselage is composed of numerous small panels riveted to each other and to the internal framework and, since in the cabin or pressurized portion of the fuselage the skin is of necessity cut by windows, doorways, and escape hatches, the skin may not be considered perfectly continuous. As a consequence, condition (a) above is violated to some degree. It follows that the skin may be incapable of carrying hoop tension loads.

(d) In the cabin portion of a fuselage large concentrated loads are applied to the structure (wing reactions, landing gear reactions, seat loads, cargo loads, and the like). These loads require the use of strong, rigid bulkheads and heavy stringers. Additional heavy frames are required in many instances to prevent buckling of the skin since the greatest fuselage bending moments occur at the cabin portion.

Before assuming that the skin (in hoop tension), rather than the internal framework, carries the internal pressure loads, an elastic analysis should be made which proves that the skin is less elastic than its supporting structure.

Although the skin may not be capable of carrying diametral pressure loads in hoop tension, it will in any event serve as a means of transmitting the pressure loads to the internal structure. Since the skin thickness will generally be small in comparison to the edge dimensions of the panel considered, membrane theory may be used in the analysis of the skin.

If one assumes that the boundary conditions provided by the riveted attachments of the skin to the internal framework may be approximated by considering the skin panel to be simply supported along the edges but restrained at the edges from moving in the plane of the skin, then the development presented on pages 345 and 346 of reference 4 may be extended to panels of rectangular shape.†

The results of such an extension for a Poisson's ratio of $\nu = 0.3$ (Timoshenko chose 0.25) for aluminum are

† It is interesting to note that there is an arithmetical error in Timoshenko's work on page 346.[4] In Eq. (204), for w_0 the numerical constant should be 0.817 rather than 0.802.

TABLE 1*

σ_x at $y = b/2, x = 0,a$; σ_y at $x = a/2, y = 0,b$ for $\nu = 0.3$

σ_x and σ_y vs. a/b

a/b	$\sigma_x/(a^2p^2E/t^2)$	$\sigma_y/(a^2p^2E/t^2)$
1/3	0.575	0.258
1/2	0.585	0.339
2/3	0.560	0.400
3/4	0.542	0.427
1	0.460	0.460

* Curves of $\sigma_x/(a^2p^2E/t^2)$ and $\sigma_y/(a^2p^2E/t^2)$ are plotted in Fig. 1.

summarized in Table 1 and presented graphically in Fig. 1.

The stresses σ_x and σ_y, as given in the table and in the figure, are the stresses at the midpoints of the panel sides, since the calculations made indicated that the stresses attained their maximum values at these points.

In applying either Table 1 or Fig. 1, it should be noted that the origin of coordinates is at a corner of the plate whereas in reference 4 the origin was taken as the center of the plate; hence the dimension a of this paper is twice as large as a in reference 4.

Effects of Pressurization on the Ability of a Skin Panel to Carry Shear or Compression

In the event that a panel buckles under either shear or compression, the buckled pattern is generally in the form of a number of waves that require both inward and outward displacement of the panel. (This is also true in the case where the pattern involves more than one panel.) Internal pressure retards the formation of the inward buckles and aids the formation of outward buckles. On this basis it might be assumed that internal pressure would leave the buckling load unaltered, since the amount of additional energy required to produce the inward buckles appears to be offset by the smaller amount of energy required to produce outward buckles.

A theoretical investigation of the problem is beyond the scope of this paper; however, the limited amount of test data available to date seems to indicate that the buckling load is not reduced by internal pressure.

On the basis of the above and the fact that the discussions in "Variation of Load Factor with Altitude" indicate that compression and shear loadings will probably decrease with increased altitude (and, consequently, with increased internal pressure), it may be stated that the critical altitude for panels subject to shear and compression will probably be sea level. It should be noted when considering compressive stresses in the skin produced by the flight loads that the membrane tension stresses due to pressurization will be relieving stresses.

Extending the above discussion, it may be concluded that internal pressure has the net effect of increasing the effective width of the skin under compression.

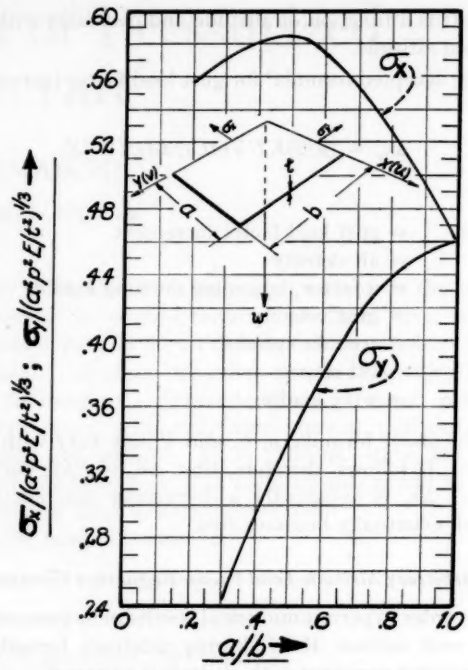

FIG. 1. Membrane tension stresses at the midpoints of the panel sides. The direction of the stress is shown in the small inset figure.

Effects of Pressurization on the Ability of a Skin Panel to Carry Tensile Loads

The foregoing discussion deals with two of the three types of stresses to which the skin is subject in performing its structural functions (i.e., shear and compression stresses). In the discussion of these two types of stress, the conclusion was reached that the critical structural altitude for a panel loaded by either type was probably at sea level. This statement was permissible, since loads causing compression or shear decrease in proportion to the load factor (which should decrease with altitude) and therefore are greatest at sea level. It will be shown below that this statement does not apply to skin panels under tensile loads.

Tensile loads in the skin of an airplane fuselage are imposed, in general, by external or inertia loads that vary with the load factors, and therefore with altitude. The skin of a pressurized cabin is loaded also by membrane tension stresses, and longitudinal stresses caused by its action as a carry-through between the fore and aft pressure-sealing bulkheads. As a consequence, the skin is loaded by one set of loads increasing with altitude and another set decreasing with altitude. The critical structural altitude of a typical skin panel is determined below.

On the basis of Eq. (1) the stresses due to inertia or external loads are given as follows.

$$\sigma_i = K_i(1 + \Delta n\beta) \qquad (3)$$

where K_i = stress at sea level/$(1 + \Delta n)$.

From Table 1, the stresses due to normal pressure are

$$\sigma_n = K_n(p)^{2/3} \tag{4}$$

where K_n for a square plate would be

$$K_n = 0.46(a^2E/t^2)^{1/3} \tag{5}$$

For longitudinal stresses:

$$\sigma_l = K_l(p) \tag{6}$$

where K_l = the cross-sectional area of the cabin at a point considered divided by the total area of the skin and the stringers at the cross section and σ_t = total stress = $\sigma_t + \sigma_n + \sigma_l$.

$$\sigma_t = K_t(1 + \Delta n\beta) + K_n(p)^{2/3} + K_l(p) \tag{7}$$

To simplify calculations it is assumed that p (the internal pressure) increases linearly with altitude, between $h = 0$ and $h = 35{,}332$ ft. The error introduced by this assumption is in the order of 25 per cent at 17,000 ft., but this error, as is shown later, does not affect the calculation of the critical structural altitude.

The linear variation of p is expressed below (assuming sea-level pressure is maintained in the cabin).

$$p = 11.289h/35{,}332;\ 0 \leq h \leq 35{,}332 \tag{8}$$

In terms of Eq. (8), Eq. (7) may be written

$$\sigma_t = K_t\left(1 + \Delta n - \frac{0.6942h\,\Delta n}{35{,}332}\right) + K_n\left(\frac{11.280h}{35{,}332}\right)^{2/3} + K_l\left(\frac{11.280h}{35{,}332}\right)$$

For σ_t maximum, $\partial\sigma_t/\partial h = 0$; whence

$$h = \left(\frac{311K_n}{1.962\,\Delta nK_t - 31.95K_l}\right)^3;\ 0 \leq h \leq 35{,}332 \tag{9}$$

From examination of Eq. (9), it is seen that if $(1.962\,\Delta nK_t - 31.95K_l)$ is negative, then the critical altitude is at sea level. Furthermore, if this equation yields a value of h greater than 35,332, which is beyond the domain of applicability of the equation, it is apparent that the critical altitude will be the absolute ceiling of the aircraft.

For purposes of illustration the critical altitude h will be calculated for a typical skin panel. Values for Δn, K_t, K_l, and K_n are determined below.

Take $\Delta n = 3.061$. K_t is assumed to be 8,000 lbs. per sq.in.

To determine K_n, assume that $a = 10$ in., $E = 10^7$ lbs. per sq.in., $t = 0.064$ in. Then for a square panel

$$K_n = 0.46\left(\frac{10^2 \times 10^7}{0.064^2}\right)^{1/3} = 2{,}875\ (\text{lbs. per sq.in.})^{1/3}$$

For the determination of K_l, a circular fuselage 12 ft. in diameter is assumed having a skin thickness of 0.064 in. The area of the skin and stringers is assumed equal to twice the area of the skin.

$$K_l = [\pi(72)^2]/[\pi 2(144)(0.064)] = 281.5$$

Substituting the above values of Δn, K_t, K_l, and K_n into Eq. (9), it is found that $h = 12{,}200$ ft.

To evaluate the error introduced by the assumption of a linear pressure variation, the variation of total stress (σ_t) with altitude is determined from Eq. (7) using the true pressure variation, and the results plotted in Fig. 2. From examination of this figure it is seen that the critical structural altitude is 12,200 ft., which checks the results obtained from Eq. (9).

It will be noted from examination of Fig. 2 that there is little variation in σ_t between $\sigma_{t_{min}}$ and $\sigma_{t_{max}}$. This is the result of the choice of K_t, K_n, and K_l, and does not indicate that the variation of σ_t with altitude is small in all cases.

In the calculation of σ_t vs. h, no ultimate factor of safety was assumed, since a true picture of stress variation was desired. At this point it is of interest to note that when dealing with a structure possessing a non-linear load-stress relationship, it is desirable to base all margins of safety on the ratio of allowable yield stress to limit stress rather than the ratio of allowable ultimate stress to ultimate stress.

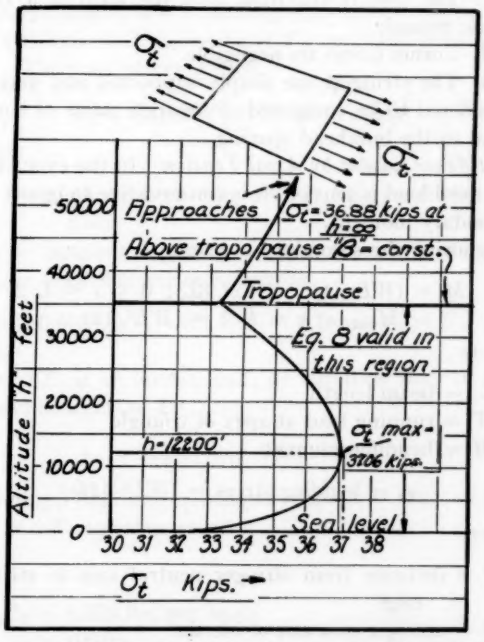

FIG. 2. Variation of total tension stress in skin panel with altitude. Note that the maximum stress intensity occurs at 12,200 ft.

Effects of Internal Pressure on the Load-Carrying Ability of the Longitudinal Stiffeners

In general, the functions of longitudinal stiffeners result in the stiffeners being in a state of either pure tension or pure compression, if no internal pressure exists. In addition to the pure tensile or compressive stresses that normally exist, bending stresses due to lateral

loads are induced in the stiffeners when buckling of the skin, bulkheads, or of the stringers themselves occurs.

To resist these lateral buckling loads and also to resist tendencies toward premature general instability failure, stiffeners are designed to have a large amount of flexural rigidity in comparison to the skin or plating. As a consequence of this, stringers function as beams under lateral load.

Lateral loads on stiffeners or stringers are generally ignored in analysis; however, in designing stringers for a pressurized cabin, it is impossible to ignore lateral loading, since lateral loads are built up in direct proportion to the internal pressure. The effects of lateral pressure loading of the stringers due to internal pressure will now be considered.

Distribution of Pressure Load on Stringer—In order to facilitate computations, the following simplifying assumptions are made regarding pressure load distribution on the stringers.

(1) The total normal plate load is divided equally between the four boundaries: i.e., if the panels on both sides of the stringers are the same size, then each panel causes a load $abp/4 + abp/4 = abp/2$, where a and b are the plate edge dimensions.

(2) The load distribution is in the form of a symmetric triangle.

(3) Corner forces are negligible.

(4) The stringers are simply supported and may be considered to be composed of separate parts of length equal to the bulkhead spacing.

Stiffener Loaded by Axial Tension—In the event that the axial load is tension, it is conservative to ignore the secondary moment.

Ignoring the secondary moment

$$M = (WLx/4) - (Wx^3/3L);\ 0 \leq x \leq L/2$$
$$M_{max.} \text{ at } x = L/2 = (WL^2/12)$$

where

L = beam length
W = running load at apex of triangle
M = bending moment

$$\sigma_b = \text{bending stress} = (WL^2/12I)c$$

where

c = distance from stringer neutral axis to stringer edge
I = stringer moment of inertia

In addition to the bending load due to normal pressure, the stiffener is subject to the same axial tension loads as the skin, namely:

$$\sigma_i = K_i(1 + \Delta n\beta) \text{ and } \sigma_i = K_i(p)$$

hence

$$\sigma_{t_1} = \sigma_b + \sigma_i + \sigma_i = \frac{WL^2c}{12I} + K_i(1 + \Delta n\beta) + K_i(p)$$

From "Distribution of Pressure Load on Stringer," $WL/2 = abp/2$ or $W = abp/L$; whence

$$\sigma_{t_1} = K_b(p) + K_i(1 + \Delta n\beta) + K_i(p) \qquad (10)$$

where $K_b = abLc/12I$.

A plot of σ_{t_1} vs. h (considering true pressure variation) is presented in Fig. 3 using the following values for the constants involved.

K_i = 8,000 lbs. per sq.in.
Δn = 3.061
K_i = 281.5
$a = b = L$ = 10 in.
I/c = 1/3
K_b = 250

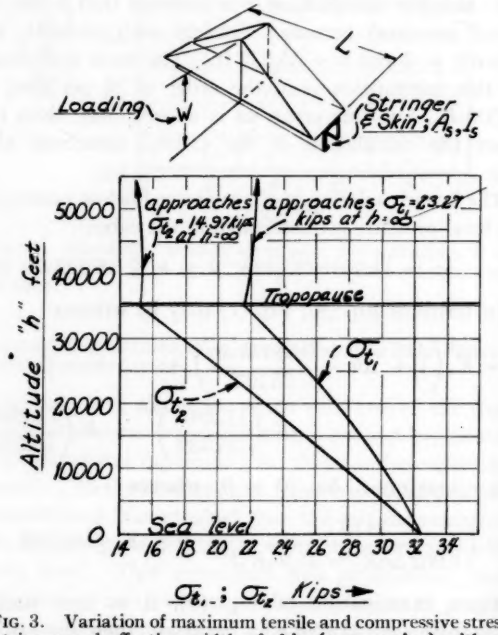

FIG. 3. Variation of maximum tensile and compressive stresses in stringer and effective width of skin (compression) with altitude.

Fig. 3 indicates that the maximum stringer stress occurs at sea level. This result should not be interpreted to mean that all stringers subject to tension are critical at sea level, inasmuch as a different choice of constants could lead to a critical altitude either at the aircraft ceiling or, in special cases, at some intermediate altitude.

Stiffener Loaded by Axial Compression—It can be shown that the maximum moment for a simply supported beam under axial load and subjected to a symmetric triangular loading occurs at the center of the beam and has the value

$$M = -(2Wj^3/L)(\tan L/2j) + Wj^2 \qquad (11)$$

where W and L are defined above and

$j^2 = EI/P_a$
P_a = axial load

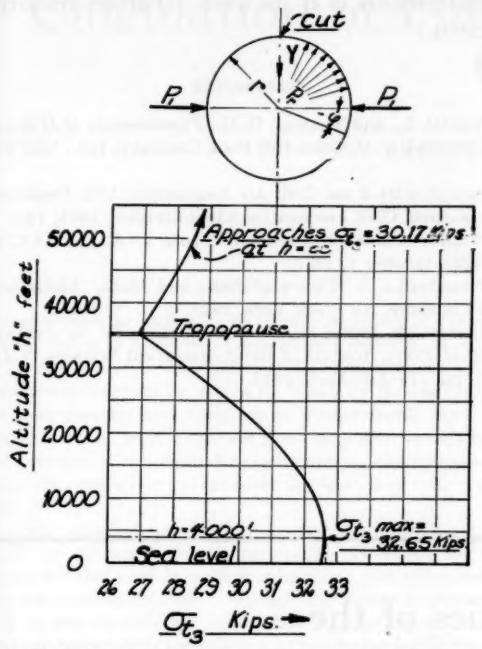

FIG. 4. Variation of maximum tensile stress in the circular bulkhead (shown at the top of the figure) with altitude.

The axial load P_a acting in a stringer under compression is the difference of the compression stress σ_i and the tension stress σ_l, multiplied by the area of the stringer and its associated effective width of skin, i.e.:

$$P_a = (\sigma_i - \sigma_l)A_s$$

where A_s = area of stringer and effective width of skin. Substituting the equations for σ_i and σ_l:

$$P_a = [K_t(1 + \Delta n\beta) - K(p)]A_s$$

The curve of σ_{t_2} vs. h is plotted in Fig. 3 for the values of K_t, Δn, K_l, A_s, W, L, I/c, a, and b assumed below:

K_t = 8,000 lbs. per sq.in.
Δn = 3.061
K_l = 281.5
A_s = 0.60 sq.in.
I = 1/3
c = 1
$W = abp/L = 10p$
$j^2 = EI/P_a = 10^7/3P_a$

From examination of Fig. 3, it is seen that the critical altitude is sea level as in the case of σ_{t_1}. As in the previous case, the conclusion should not be drawn that the critical altitude will always be sea level.

Effects of Internal Pressure on the Load-Carrying Ability of Bulkheads Loaded in the Plane of the Bulkhead

The analysis presented in preceding sections has shown that a critical structural altitude (which may be sea level or any other altitude up to and including the aircraft's absolute ceiling) exists for both stringers and skin. It is possible to generalize and state that a critical altitude exists for any structural component subjected to the simultaneous action of a variable internal pressure and variable flight or inertia loads. The proof of this statement is of an intuitive nature and, consequently, the statement may be considered axiomatic.

A method of determining the critical structural altitude of a typical bulkhead is now considered. The bulkhead to be analyzed is shown in Fig. 4.

Using the method of analysis of reference 5 it can be shown that for the problem of Fig. 4:

$$X_p' = p_r r$$

where

X_p' = axial tension at cut due to internal pressure
p_r = running load due to internal pressure
r = radius of ring (ring is circular)

$$\left.\begin{aligned} X_m &= 0.1901P_1 r \\ X_p &= 0.5000P_1 \\ X_v &= 0 \end{aligned}\right\} \text{internal loads at cut due to } P_1$$

Making the assumption that the ring is critical in bending and that shear stresses may be ignored, the critical stresses occur at $\varphi = 0$ (see Fig. 4 for φ).

At this point, $M_{max.} = 0.6901P_1 r$ and axial tension = $p_r r$. The total stress is then:

$$\sigma_{t_3} = (0.6901P_1 rc/I_f) + (P_r r/A_f) \qquad (12)$$

where

c = distance from the neutral axis to outermost fiber
I_f = moment of inertia of frame cross section
A_f = area of frame cross section

Letting $0.6901rc/I_f = K_t$, $r/A_f = K_p$, and $\sigma_{t_3} = K_t P_1 + K_p p_r$.

Since P_1 is an inertia load, its variation may be expressed in terms of Eq. (1):

$$\sigma_{t_3} = K_t P_0(1 + \Delta n\beta) + K_p p_r \qquad (13)$$

Assuming a bulkhead spacing of 10 in., $p_r = 10p$; where p is the differential pressure.

Let

$K_t P_0$ = 8,000 lbs. per sq.in.
K_p = 100/in.
Δn = 3.061

then

$$\sigma_{t_3} = 8{,}000(1 + 3.061\beta) + 100p, \qquad (14)$$

To illustrate the variation of σ_{t_3} with altitude, values of σ_{t_3} have been calculated at various altitudes and the results plotted in Fig. 4. From examination of this figure, it is seen that σ_{t_3} has a maximum value of 32,650 lbs. per sq.in. at 4,000 ft.

Conclusions

(1) The load factor that an airplane may be expected to develop is apparently a function of altitude. However, an equation expressing the exact variation cannot be derived without considerably more study.

(2) Under the influence of a varying load factor there exists a critical structural altitude for each structural component of the pressurized portion of the airplane.

(3) In general, it is not possible to tacitly assume that diametral pressure loads are resisted by hoop tension in the skin.

(4) On the basis of available information it appears that the critical structural altitude for skin subject to shear or compression and the simultaneous action of internal pressure is at sea level. (Further research is indicated.)

References

[1] Prandtl, L., and Tietjens, O. G., *Fundamentals of Hydro and Aero-Mechanics;* McGraw-Hill Book Company, Inc., New York, 1934.

[2] Part 03 or 04 of the Civil Air Regulations, U.S. Department of Commerce, Civil Aeronautics Administration, 1944, 1945.

[3] *Pressure Cabin Investigations—Phase I,* A.C.I.C.-A.C.T.R. No. 4220, October 1, 1937.

[4] Timoshenko, S., *Theory of Plates and Shells;* McGraw-Hill Book Company, Inc., New York, 1940.

[5] Dommasch, Daniel O., *General Equations for the Analysis of Elliptical Rings,* Journal of the Aeronautical Sciences, Vol. 10, No. 4, pp. 119–126, April, 1943.

Library Facilities of the
Institute of the Aeronautical Sciences

To serve Institute members and others in the aeronautical industry, the Institute of the Aeronautical Sciences offers the facilities of:

The W. A. M. Burden Library
2 East 64th Street
New York 21, N.Y.

The facilities of this library are available for reference study at the Institute.

The Paul Kollsman Lending Library
2 East 64th Street
New York 21, N.Y.

This library loans books without charge to members and others in the United States over eighteen years of age. Full information will be sent on request.

The Pacific Aeronautical Library
6715 Hollywood Boulevard
Hollywood 28, Calif.

This is a service and reference library for West Coast organizations. Full information as to its facilities will be sent on request.

Calculation of Flow of Air and Diatomic Gases

CHESTER W. SMITH*

General Electric Company

ABSTRACT

Measurement of airflow is frequently required in connection with aeronautical projects. Conventional practice, as exemplified by the *A.S.M.E. Test Code for Flow Measurement*, provides two different formulas (or sets of formulas) for the calculation of flow from pressure and temperature measurements made with standard nozzles, orifices, and the like, the proper formula for use in any particular case depending upon whether the pressure ratio across the restriction is greater or less than the critical value.

In most cases of aeronautical interest the formula for subcritical (or restricted) flow is applicable. However, the exact formula for this case is quite cumbersome, and often requires much laborious calculation. Without sacrifice of exactness, the much simpler formula for critical flow may be generalized and used in all cases merely by including a "restriction factor" that is a function of pressure ratio only, and so may be tabulated once and for all. This paper proposes such a formula and presents a table of restriction factors applicable to air and other diatomic gases.

SYMBOLS

A	= throat area
C	= discharge coefficient
c_p	= specific heat at constant pressure
c_v	= specific heat at constant volume
g	= acceleration of gravity
k	= ratio of specific heats ($= c_p/c_v$)
K, K'	= constants (Tables 2 and 3)
N	= restriction factor (Table 1)
p	= absolute pressure
Δp_t	= $p_{1t} - p_2$
r	= pressure ratio ($= p_{1t}/p_2$)
γ	= specific weight
R	= gas constant
T	= absolute temperature
v	= specific volume
V	= velocity
w	= gravimetric flow
X	= isentropic (or adiabatic) factor ($= r^{(k-1)/k} - 1$)

Subscripts

0 = at selected standard or reference conditions
1 = at initial, or high-side, conditions
2 = at final, or low-side, conditions
3 = at discharge, or throat, conditions (i.e., just preceding throat area A)
c = corresponding to critical pressure ratio
t = based on total pressure, total temperature

(The subscript t is added to a numerical subscript, as p_{1t}, T_{1t}, v_{1t}. Without the subscript t it is to be understood that pressures and temperatures are static values and that specific volume and specific weight are based on static pressure and temperature.)

Received September 23, 1945.

* Aircraft Gas Turbine Engineering Division.

INTRODUCTION

MEASUREMENT OF AIRFLOW is frequently necessary in connection with tests of aircraft power plants, accessories, and the ducts required in the airplane installation. The usual method of making such measurements is by use of standard nozzles, orifices, venturi meters, or similar restrictions. From the measured pressures and temperatures the flow is calculated by well-known formulas that have been derived in many published papers and textbooks and which are summarized in reference 1. These formulas are also used to calculate the sizes of ducts and openings needed for specified flows and to determine the maximum flow capacity for given conditions.

It is customary to distinguish sharply between different types of flow of a compressible fluid. If the total pressure and temperature just preceding the restriction are constant, the flow per unit area gradually increases as the absolute pressure on the downstream side decreases, until a certain "critical" pressure ratio is reached at which it is a maximum. The flow at this pressure ratio is termed "critical." Further decrease of the downstream pressure does not change the flow, which under this condition is still termed "critical" or sometimes "supercritical." When the downstream pressure is higher than that corresponding to the critical ratio, the flow is a function of this pressure and is termed "subcritical." The words "restricted" and "nonrestricted," or "affected" and "unaffected," or "subsonic" and "supersonic" are often used instead of "subcritical" and "critical," respectively.

The exact formula for subcritical flow is quite cumbersome, and approximations have been proposed by different writers.[2, 3] However, for any group of gases having approximately the same ratio of specific heats or isentropic exponent, it is possible, by tabulation of a certain function called the "restriction factor" (perhaps "subcritical flow factor" would be a better name, but "restriction factor" is the term originally applied and now generally adopted), to use without approximation what is essentially the simple formula for critical flow over the entire range of pressure ratios. Such a table (Table 1) is given here for air and diatomic gases, which have approximately the same ratio of specific heats, taken as 1.3947 for reasons explained later in more detail. A similar table could be easily made up for other gases if the need should arise.

TABLE 1

Values of Restriction Factor N for Air and Diatomic Gases

$$w = \frac{KCAp_uN}{\sqrt{T_u}}$$

A = throat area
C = discharge coefficient
K = constant (Table 2)
N = restriction factor
p_u = high-side pressure (total)
p_2 = low-side pressure (static)
T_u = high-side temperature (total)
w = gravimetric flow

To obtain volumetric flow at any specified pressure and temperature, multiply w by the specific volume at that pressure and temperature.

N is based on isentropic exponent
$k = 1.3947$, or $(k - 1)/k = 0.283$

p_u/p_2	0	1	2	3	4	5	6	7	8	9
1.0000	0	0.006540	0.009249	0.01133	0.01308	0.01462	0.01602	0.01730	0.01850	0.01962
1.0001	0.02068	0.02169	0.02265	0.02358	0.02447	0.02532	0.02616	0.02696	0.02774	0.02850
1.0002	0.02924	0.02996	0.03067	0.03136	0.03203	0.03269	0.03334	0.03397	0.03460	0.03521
1.0003	0.03581	0.03640	0.03698	0.03756	0.03812	0.03868	0.03922	0.03977	0.04030	0.04082
1.0004	0.04134	0.04186	0.04236	0.04287	0.04336	0.04385	0.04433	0.04481	0.04529	0.04576
1.0005	0.04622	0.04668	0.04713	0.04758	0.04803	0.04847	0.04891	0.04935	0.04978	0.05020
1.0006	0.05063	0.05105	0.05146	0.05187	0.05228	0.05269	0.05309	0.05349	0.05389	0.05429
1.0007	0.05468	0.05507	0.05545	0.05583	0.05621	0.05659	0.05697	0.05734	0.05771	0.05808
1.0008	0.05845	0.05881	0.05917	0.05953	0.05989	0.06024	0.06059	0.06094	0.06129	0.06164
1.0009	0.06198	0.06233	0.06267	0.06301	0.06334	0.06368	0.06401	0.06435	0.06468	0.06500
1.0010	0.06533	0.06566	0.06598	0.06630	0.06662	0.06694	0.06726	0.06757	0.06789	0.06820
1.0011	0.06851	0.06882	0.06913	0.06944	0.06974	0.07005	0.07035	0.07065	0.07095	0.07125
1.0012	0.07155	0.07185	0.07214	0.07244	0.07273	0.07302	0.07331	0.07360	0.07389	0.07418
1.0013	0.07447	0.07475	0.07503	0.07532	0.07560	0.07588	0.07616	0.07644	0.07672	0.07699
1.0014	0.07727	0.07754	0.07782	0.07809	0.07836	0.07863	0.07890	0.07917	0.07944	0.07971
1.0015	0.07997	0.08024	0.08050	0.08077	0.08103	0.08129	0.08155	0.08181	0.08207	0.08233
1.0016	0.08259	0.08284	0.08310	0.08335	0.08361	0.08386	0.08412	0.08437	0.08462	0.08487
1.0017	0.08512	0.08537	0.08562	0.08586	0.08611	0.08636	0.08660	0.08685	0.08709	0.08734
1.0018	0.08758	0.08782	0.08806	0.08830	0.08854	0.08878	0.08902	0.08926	0.08950	0.08973
1.0019	0.08997	0.09020	0.09044	0.09067	0.09091	0.09114	0.09137	0.09160	0.09184	0.09207
1.0020	0.09230	0.09253	0.09275	0.09298	0.09321	0.09344	0.09366	0.09389	0.09412	0.09434
1.0021	0.09457	0.09479	0.09501	0.09524	0.09546	0.09568	0.09590	0.09612	0.09634	0.09656
1.0022	0.09678	0.09700	0.09722	0.09744	0.09765	0.09787	0.09809	0.09830	0.09852	0.09873
1.0023	0.09895	0.09916	0.09937	0.09959	0.09980	0.1000	0.1002	0.1004	0.1006	0.1009
1.0024	0.1011	0.1013	0.1015	0.1017	0.1019	0.1021	0.1023	0.1025	0.1027	0.1029
1.0025	0.1031	0.1033	0.1035	0.1038	0.1040	0.1042	0.1044	0.1046	0.1048	0.1050
1.0026	0.1052	0.1054	0.1056	0.1058	0.1060	0.1062	0.1064	0.1066	0.1068	0.1070
1.0027	0.1072	0.1074	0.1076	0.1078	0.1079	0.1081	0.1083	0.1085	0.1087	0.1089
1.0028	0.1091	0.1093	0.1095	0.1097	0.1099	0.1101	0.1103	0.1105	0.1107	0.1108
1.0029	0.1110	0.1112	0.1114	0.1116	0.1118	0.1120	0.1122	0.1124	0.1125	0.1127
1.003	0.1129	0.1148	0.1166	0.1184	0.1202	0.1219	0.1236	0.1253	0.1270	0.1286
1.004	0.1303	0.1319	0.1334	0.1350	0.1366	0.1381	0.1396	0.1411	0.1426	0.1440
1.005	0.1455	0.1469	0.1483	0.1497	0.1511	0.1525	0.1539	0.1552	0.1566	0.1579
1.006	0.1592	0.1605	0.1618	0.1631	0.1644	0.1656	0.1669	0.1681	0.1693	0.1706
1.007	0.1718	0.1730	0.1742	0.1754	0.1765	0.1777	0.1789	0.1800	0.1812	0.1823
1.008	0.1835	0.1846	0.1857	0.1868	0.1879	0.1890	0.1901	0.1912	0.1922	0.1933
1.009	0.1944	0.1954	0.1965	0.1975	0.1986	0.1996	0.2006	0.2017	0.2027	0.2037
1.010	0.2047	0.2057	0.2067	0.2077	0.2087	0.2096	0.2106	0.2116	0.2125	0.2135
1.011	0.2145	0.2154	0.2164	0.2173	0.2182	0.2192	0.2201	0.2210	0.2219	0.2228
1.012	0.2238	0.2247	0.2256	0.2265	0.2274	0.2283	0.2291	0.2300	0.2309	0.2318
1.013	0.2327	0.2335	0.2344	0.2353	0.2361	0.2370	0.2378	0.2387	0.2395	0.2404
1.014	0.2412	0.2420	0.2429	0.2437	0.2445	0.2453	0.2462	0.2470	0.2478	0.2486
1.015	0.2494	0.2502	0.2510	0.2518	0.2526	0.2534	0.2542	0.2550	0.2558	0.2565
1.016	0.2573	0.2581	0.2589	0.2596	0.2604	0.2612	0.2619	0.2627	0.2635	0.2642
1.017	0.2650	0.2657	0.2665	0.2672	0.2680	0.2687	0.2694	0.2702	0.2709	0.2716
1.018	0.2724	0.2731	0.2738	0.2745	0.2753	0.2760	0.2767	0.2774	0.2781	0.2788
1.019	0.2795	0.2803	0.2810	0.2817	0.2824	0.2831	0.2838	0.2844	0.2851	0.2858
1.020	0.2865	0.2872	0.2879	0.2886	0.2893	0.2899	0.2906	0.2913	0.2920	0.2926
1.021	0.2933	0.2940	0.2946	0.2953	0.2960	0.2966	0.2973	0.2979	0.2986	0.2992
1.022	0.2999	0.3005	0.3012	0.3018	0.3025	0.3031	0.3038	0.3044	0.3051	0.3057
1.023	0.3063	0.3070	0.3076	0.3082	0.3088	0.3095	0.3101	0.3107	0.3114	0.3120
1.024	0.3126	0.3132	0.3138	0.3144	0.3151	0.3157	0.3163	0.3169	0.3175	0.3181
1.025	0.3187	0.3193	0.3199	0.3205	0.3211	0.3217	0.3223	0.3229	0.3235	0.3241
1.026	0.3247	0.3253	0.3259	0.3265	0.3271	0.3276	0.3282	0.3288	0.3294	0.3300
1.027	0.3305	0.3311	0.3317	0.3323	0.3329	0.3334	0.3340	0.3346	0.3351	0.3357
1.028	0.3363	0.3368	0.3374	0.3380	0.3385	0.3391	0.3397	0.3402	0.3408	0.3413
1.029	0.3419	0.3424	0.3430	0.3435	0.3441	0.3446	0.3452	0.3457	0.3463	0.3468
1.030	0.3474	0.3479	0.3485	0.3490	0.3495	0.3501	0.3506	0.3512	0.3517	0.3522
1.031	0.3528	0.3533	0.3538	0.3544	0.3549	0.3554	0.3559	0.3565	0.3570	0.3575
1.032	0.3580	0.3586	0.3591	0.3596	0.3601	0.3607	0.3612	0.3617	0.3622	0.3627
1.033	0.3632	0.3637	0.3643	0.3648	0.3653	0.3658	0.3663	0.3668	0.3673	0.3678
1.034	0.3683	0.3688	0.3693	0.3698	0.3703	0.3708	0.3713	0.3718	0.3723	0.3728
1.035	0.3733	0.3738	0.3743	0.3748	0.3753	0.3758	0.3763	0.3768	0.3773	0.3778
1.036	0.3782	0.3787	0.3792	0.3797	0.3802	0.3807	0.3812	0.3816	0.3821	0.3826
1.037	0.3831	0.3836	0.3840	0.3845	0.3850	0.3855	0.3859	0.3864	0.3869	0.3874
1.038	0.3878	0.3883	0.3888	0.3892	0.3897	0.3902	0.3906	0.3911	0.3916	0.3920
1.039	0.3925	0.3930	0.3934	0.3939	0.3944	0.3948	0.3953	0.3957	0.3962	0.3967
1.040	0.3971	0.3976	0.3980	0.3985	0.3989	0.3994	0.3998	0.4003	0.4007	0.4012
1.041	0.4016	0.4021	0.4025	0.4030	0.4034	0.4039	0.4043	0.4048	0.4052	0.4057

TABLE 1 (*Continued*)

p_1/p_2	0	1	2	3	4	5	6	7	8	9
1.042	0.4061	0.4065	0.4070	0.4074	0.4079	0.4083	0.4087	0.4092	0.4096	0.4101
1.043	0.4105	0.4109	0.4114	0.4118	0.4122	0.4127	0.4131	0.4135	0.4140	0.4144
1.044	0.4148	0.4153	0.4157	0.4161	0.4165	0.4170	0.4174	0.4178	0.4183	0.4187
1.045	0.4191	0.4195	0.4199	0.4204	0.4208	0.4212	0.4216	0.4221	0.4225	0.4229
1.046	0.4233	0.4237	0.4241	0.4246	0.4250	0.4254	0.4258	0.4262	0.4266	0.4271
1.047	0.4275	0.4279	0.4283	0.4287	0.4291	0.4295	0.4299	0.4303	0.4307	0.4312
1.048	0.4316	0.4320	0.4324	0.4328	0.4332	0.4336	0.4340	0.4344	0.4348	0.4352
1.049	0.4356	0.4360	0.4364	0.4368	0.4372	0.4376	0.4380	0.4384	0.4388	0.4392
1.05	0.4396	0.4435	0.4474	0.4512	0.4550	0.4588	0.4625	0.4661	0.4697	0.4733
1.06	0.4768	0.4803	0.4838	0.4872	0.4905	0.4939	0.4972	0.5004	0.5037	0.5069
1.07	0.5100	0.5131	0.5162	0.5193	0.5224	0.5254	0.5283	0.5313	0.5342	0.5371
1.08	0.5400	0.5428	0.5456	0.5484	0.5512	0.5539	0.5566	0.5593	0.5620	0.5646
1.09	0.5673	0.5699	0.5724	0.5750	0.5775	0.5800	0.5825	0.5850	0.5875	0.5899
1.10	0.5923	0.5947	0.5971	0.5994	0.6017	0.6041	0.6064	0.6086	0.6109	0.6131
1.11	0.6154	0.6176	0.6198	0.6220	0.6241	0.6263	0.6284	0.6305	0.6326	0.6347
1.12	0.6368	0.6388	0.6409	0.6429	0.6449	0.6469	0.6489	0.6508	0.6528	0.6547
1.13	0.6566	0.6586	0.6605	0.6624	0.6642	0.6661	0.6679	0.6698	0.6716	0.6734
1.14	0.6752	0.6770	0.6788	0.6805	0.6823	0.6840	0.6858	0.6875	0.6892	0.6909
1.15	0.6926	0.6942	0.6959	0.6976	0.6992	0.7008	0.7025	0.7041	0.7057	0.7073
1.16	0.7088	0.7104	0.7120	0.7135	0.7151	0.7166	0.7181	0.7197	0.7212	0.7227
1.17	0.7241	0.7256	0.7271	0.7286	0.7300	0.7315	0.7329	0.7343	0.7357	0.7372
1.18	0.7386	0.7399	0.7413	0.7427	0.7441	0.7454	0.7468	0.7481	0.7495	0.7508
1.19	0.7521	0.7534	0.7548	0.7561	0.7573	0.7586	0.7599	0.7612	0.7624	0.7637
1.20	0.7650	0.7662	0.7674	0.7687	0.7699	0.7711	0.7723	0.7735	0.7747	0.7759
1.21	0.7771	0.7783	0.7794	0.7806	0.7817	0.7829	0.7840	0.7852	0.7863	0.7874
1.22	0.7886	0.7897	0.7908	0.7919	0.7930	0.7941	0.7951	0.7962	0.7973	0.7984
1.23	0.7994	0.8005	0.8015	0.8026	0.8036	0.8046	0.8057	0.8067	0.8077	0.8087
1.24	0.8097	0.8107	0.8117	0.8127	0.8137	0.8147	0.8157	0.8166	0.8176	0.8186
1.25	0.8195	0.8205	0.8214	0.8223	0.8233	0.8242	0.8251	0.8261	0.8270	0.8279
1.26	0.8288	0.8297	0.8306	0.8315	0.8324	0.8333	0.8342	0.8350	0.8359	0.8368
1.27	0.8376	0.8385	0.8393	0.8402	0.8410	0.8419	0.8427	0.8436	0.8444	0.8452
1.28	0.8460	0.8468	0.8477	0.8485	0.8493	0.8501	0.8509	0.8517	0.8524	0.8532
1.29	0.8540	0.8548	0.8556	0.8563	0.8571	0.8579	0.8586	0.8594	0.8601	0.8609
1.30	0.8616	0.8623	0.8631	0.8638	0.8645	0.8653	0.8660	0.8667	0.8674	0.8681
1.31	0.8688	0.8696	0.8703	0.8710	0.8716	0.8723	0.8730	0.8737	0.8744	0.8751
1.32	0.8757	0.8764	0.8771	0.8777	0.8784	0.8791	0.8797	0.8804	0.8810	0.8817
1.33	0.8823	0.8829	0.8836	0.8842	0.8849	0.8855	0.8861	0.8867	0.8873	0.8880
1.34	0.8886	0.8892	0.8898	0.8904	0.8910	0.8916	0.8922	0.8928	0.8934	0.8940
1.35	0.8945	0.8951	0.8957	0.8963	0.8968	0.8974	0.8980	0.8985	0.8991	0.8997
1.36	0.9002	0.9008	0.9013	0.9019	0.9024	0.9030	0.9035	0.9041	0.9046	0.9051
1.37	0.9057	0.9062	0.9067	0.9072	0.9078	0.9083	0.9088	0.9093	0.9098	0.9103
1.38	0.9108	0.9113	0.9118	0.9123	0.9128	0.9133	0.9138	0.9143	0.9148	0.9153
1.39	0.9158	0.9162	0.9167	0.9172	0.9177	0.9181	0.9186	0.9191	0.9196	0.9200
1.40	0.9205	0.9209	0.9214	0.9218	0.9223	0.9227	0.9232	0.9236	0.9241	0.9245
1.41	0.9250	0.9254	0.9258	0.9263	0.9267	0.9271	0.9276	0.9280	0.9284	0.9288
1.42	0.9293	0.9297	0.9301	0.9305	0.9309	0.9313	0.9317	0.9321	0.9325	0.9329
1.43	0.9333	0.9337	0.9341	0.9345	0.9349	0.9353	0.9357	0.9361	0.9365	0.9369
1.44	0.9372	0.9376	0.9380	0.9384	0.9387	0.9391	0.9395	0.9399	0.9402	0.9406
1.45	0.9410	0.9413	0.9417	0.9420	0.9424	0.9427	0.9431	0.9434	0.9438	0.9441
1.46	0.9445	0.9448	0.9452	0.9455	0.9459	0.9462	0.9465	0.9469	0.9472	0.9475
1.47	0.9479	0.9482	0.9485	0.9489	0.9492	0.9495	0.9498	0.9501	0.9505	0.9508
1.48	0.9511	0.9514	0.9517	0.9520	0.9523	0.9526	0.9529	0.9533	0.9536	0.9539
1.49	0.9542	0.9545	0.9548	0.9550	0.9553	0.9556	0.9559	0.9562	0.9565	0.9568
1.50	0.9571	0.9574	0.9576	0.9579	0.9582	0.9585	0.9588	0.9590	0.9593	0.9596
1.51	0.9599	0.9601	0.9604	0.9607	0.9609	0.9612	0.9615	0.9617	0.9620	0.9622
1.52	0.9625	0.9628	0.9630	0.9633	0.9635	0.9638	0.9640	0.9643	0.9645	0.9648
1.53	0.9650	0.9653	0.9655	0.9658	0.9660	0.9662	0.9665	0.9667	0.9670	0.9672
1.54	0.9674	0.9677	0.9679	0.9681	0.9683	0.9686	0.9688	0.9690	0.9693	0.9695
1.55	0.9697	0.9699	0.9701	0.9704	0.9706	0.9708	0.9710	0.9712	0.9714	0.9716
1.56	0.9719	0.9721	0.9723	0.9725	0.9727	0.9729	0.9731	0.9733	0.9735	0.9737
1.57	0.9739	0.9741	0.9743	0.9745	0.9747	0.9749	0.9751	0.9753	0.9755	0.9757
1.58	0.9759	0.9760	0.9762	0.9764	0.9766	0.9768	0.9770	0.9772	0.9773	0.9775
1.59	0.9777	0.9779	0.9781	0.9782	0.9784	0.9786	0.9788	0.9789	0.9791	0.9793
1.60	0.9795	0.9796	0.9798	0.9800	0.9801	0.9803	0.9805	0.9806	0.9808	0.9809
1.61	0.9811	0.9813	0.9814	0.9816	0.9817	0.9819	0.9821	0.9822	0.9824	0.9825
1.62	0.9827	0.9828	0.9830	0.9831	0.9833	0.9834	0.9836	0.9837	0.9839	0.9840
1.63	0.9841	0.9843	0.9844	0.9846	0.9847	0.9848	0.9850	0.9851	0.9853	0.9854
1.64	0.9855	0.9857	0.9858	0.9859	0.9861	0.9862	0.9863	0.9865	0.9866	0.9867
1.65	0.9868	0.9870	0.9871	0.9872	0.9873	0.9875	0.9876	0.9877	0.9878	0.9880
1.66	0.9881	0.9882	0.9883	0.9884	0.9885	0.9887	0.9888	0.9889	0.9890	0.9891
1.67	0.9892	0.9893	0.9895	0.9896	0.9897	0.9898	0.9899	0.9900	0.9901	0.9902
1.68	0.9903	0.9904	0.9905	0.9906	0.9907	0.9908	0.9909	0.9910	0.9911	0.9912
1.69	0.9913	0.9914	0.9915	0.9916	0.9917	0.9918	0.9919	0.9920	0.9921	0.9922
1.70	0.9923	0.9924	0.9925	0.9925	0.9926	0.9927	0.9928	0.9929	0.9930	0.9931
1.71	0.9932	0.9932	0.9933	0.9934	0.9935	0.9936	0.9937	0.9937	0.9938	0.9939
1.72	0.9940	0.9940	0.9941	0.9942	0.9943	0.9944	0.9944	0.9945	0.9946	0.9947
1.73	0.9947	0.9948	0.9949	0.9949	0.9950	0.9951	0.9952	0.9952	0.9953	0.9954

(*Continued on page 312*)

TABLE 1 (*Continued*)

p_u/p_2	0	1	2	3	4	5	6	7	8	9
1.74	0.9954	0.9955	0.9956	0.9956	0.9957	0.9957	0.9958	0.9959	0.9959	0.9960
1.75	0.9961	0.9961	0.9962	0.9962	0.9963	0.9964	0.9964	0.9965	0.9965	0.9966
1.76	0.9966	0.9967	0.9968	0.9968	0.9969	0.9969	0.9970	0.9970	0.9971	0.9971
1.77	0.9972	0.9972	0.9973	0.9973	0.9974	0.9974	0.9975	0.9975	0.9976	0.9976
1.78	0.9977	0.9977	0.9978	0.9978	0.9978	0.9979	0.9979	0.9980	0.9980	0.9981
1.79	0.9981	0.9981	0.9982	0.9982	0.9983	0.9983	0.9983	0.9984	0.9984	0.9984
1.80	0.9985	0.9985	0.9985	0.9986	0.9986	0.9986	0.9987	0.9987	0.9987	0.9988
1.81	0.9988	0.9988	0.9989	0.9989	0.9989	0.9990	0.9990	0.9990	0.9990	0.9991
1.82	0.9991	0.9991	0.9992	0.9992	0.9992	0.9992	0.9993	0.9993	0.9993	0.9993
1.83	0.9994	0.9994	0.9994	0.9994	0.9994	0.9995	0.9995	0.9995	0.9995	0.9995
1.84	0.9996	0.9996	0.9996	0.9996	0.9996	0.9996	0.9997	0.9997	0.9997	0.9997
1.85	0.9997	0.9997	0.9998	0.9998	0.9998	0.9998	0.9998	0.9998	0.9998	0.9998
1.86	0.9999	0.9999	0.9999	0.9999	0.9999	0.9999	0.9999	0.9999	0.9999	0.9999
1.87	0.9999	0.9999	1.000	1.000	1.000	1.000	1.000	1.000	1.000	1.000

$N = 1.000$ for all higher pressure ratios.

PROPOSED FORMULA

In place of separate formulas for subcritical and critical flow, it is proposed to substitute the single general formula

$$w = KCAp_{1t}N/\sqrt{T_{1t}}$$

which is merely the formula for critical flow multiplied by N, the tabulated restriction factor. The value of N varies from zero to unity for subcritical flow and is unity for critical flow.

This formula was introduced into the General Electric Company some years ago by the late V. Petrovsky and has been found to be convenient and timesaving for both air and steam calculations. Values of N may be read from curves such as are shown in Fig. 1. These are reasonably satisfactory but have the usual disadvantages attendant upon purely graphical presentation. The formula is used so frequently and the advantages of a table over a chart are so manifest that an accurate table for air and diatomic gases has been prepared, based, for the sake of consistency, on fundamental constants which are essentially those adopted in the A.S.M.E. codes for flow measurement[1] and for the testing of air and gas compressors.[4] These codes have been extensively used in the aeronautical industry, and it appears best to standardize on values already in current use.

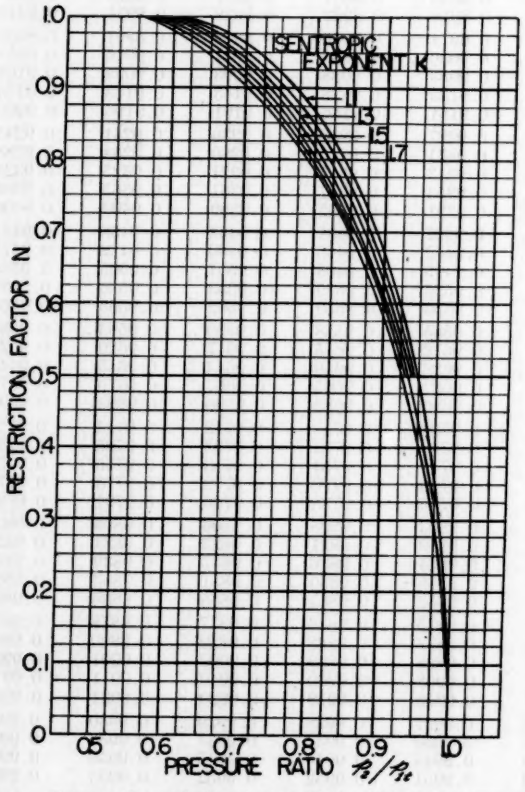

FIG. 1. Values of restriction factor N for different values of isentropic exponent k.

DERIVATION OF FORMULA

The general derivation of the flow formula is well known, and the details will not be emphasized here. The case considered is that of the flow of air or of a diatomic gas through a nozzle or orifice of any kind with a velocity increase corresponding to the pressure drop. The pressure ratio is taken as the high-side *total* pressure divided by the low-side *static* pressure, and this is obviously always greater than unity if there is any flow. The term "high-side" refers to entrance conditions and is somewhat more expressive than the words "inlet" or "initial" frequently used. The use of total pressure and total temperature at this section makes unnecessary the introduction of any approach-velocity correction. The usual assumption as to uniformity of flow over the cross section is made.

The low-side static pressure is the pressure of the region into which the fluid is discharged. For subcritical flow, this is the same as the pressure at area A (or throat), but for critical flow it may be, and usually is, less. Since it is only in the subcritical case that the low-side pressure affects the flow, it is not important in general (at least from the standpoint of flow measurement) to know the actual low-side pressure if it is known definitely that it is below the critical value.

Considering first subcritical flow, the theoretical velocity head acquired in an expansion from inlet to

discharge pressure is equal to the change of enthalpy (otherwise called available energy, isentropic heat drop, or adiabatic heat drop), which is equal to the specific heat at constant pressure multiplied by the isentropic temperature drop.

$$V_3^2/2g = c_p T_{1t} X/(X+1)$$

or

$$V_3 = \sqrt{2gc_p T_{1t} X/(X+1)} \tag{1}$$

The flow per unit of effective area is

$$w/CA = V_3/v_3 \tag{2}$$

Assuming, as usual, an isentropic process (pv^k = constant),

$$v_3 = v_{1t} r^{1/k} = v_{1t}(X+1)^{1/(k-1)} \tag{3}$$

so that

$$\frac{w}{CA} = \sqrt{\frac{2gc_p T_{1t}}{v_{1t}^2} \frac{X}{(X+1)^{(k+1)/(k-1)}}} \tag{4}$$

It is apparent that w/CA is a maximum when the function

$$\phi(X) = X/(X+1)^{(k+1)/(k-1)} \tag{5}$$

is a maximum. Differentiating this expression with respect to X and equating the derivative to zero, the critical value of X is found to be

$$X_c = (k-1)/2 \tag{6}$$

For the critical pressure ratio, then,

$$\frac{w_c}{CA} = \sqrt{\frac{2gc_p T_{1t}}{v_{1t}^2} \frac{X_c}{(X_c+1)^{(k+1)/(k-1)}}} \tag{7}$$

Dividing Eq. (4) by Eq. (7), the formula for the restriction factor is obtained.

$$N = \frac{w}{w_c} = \sqrt{\frac{X}{X_c}\left[\frac{(X_c+1)}{(X+1)}\right]^{(k+1)/(k-1)}} \tag{8}$$

For a constant value of k, this expression is a function of X only. It may therefore be tabulated for different values of r.

The flow for any pressure ratio may then be calculated from the formula

$$\frac{w}{CA} = N\sqrt{\frac{2gc_p T_{1t}}{v_{1t}^2} \frac{X_c}{(X_c+1)^{(k+1)/(k-1)}}} \tag{9}$$

which is reduced to the customary simple form of the critical flow formula by using the relation

$$c_p - c_v = R$$

or

$$c_p[1 - (1/k)] = p_{1t}v_{1t}/T_{1t}$$

so that

$$v_{1t} = (c_p T_{1t}/p_{1t})[(k-1)/k] \tag{10}$$

TABLE 2
Values of K for Use in General Flow Formula

p_{1t}	T_{1t}	A	w	K
Pounds per sq.in. absolute	°F. absolute	sq.in.	lbs. per sec.	0.53033
			lbs. per min.	31.820
			lbs. per hour	1909.2
		sq.ft.	lbs. per sec.	76.368
			lbs. per min.	4582.1
			lbs. per hour	274,920.
	°C. absolute	sq.in.	lbs. per sec.	0.39529
			lbs. per min.	23.717
			lbs. per hour	1423.0
		sq.ft.	lbs. per sec.	56.921
			lbs. per min.	3415.3
			lbs. per hour	204,920.
Inches Hg absolute	°F. absolute	sq.in.	lbs. per sec.	0.26048
			lbs. per min.	15.629
			lbs. per hour	937.74
		sq.ft.	lbs. per sec.	37.510
			lbs. per min.	2250.6
			lbs. per hour	135,030.
	°C. absolute	sq.in.	lbs. per sec.	0.19415
			lbs. per min.	11.649
			lbs. per hour	698.95
		sq.ft.	lbs. per sec.	27.958
			lbs. per min.	1677.5
			lbs. per hour	100,650.
Pounds per sq.ft. absolute	°F. absolute	sq.in.	lbs. per sec.	0.0036829
			lbs. per min.	0.22097
			lbs. per hour	13.258
		sq.ft.	lbs. per sec.	0.53033
			lbs. per min.	31.820
			lbs. per hour	1909.2
	°C. absolute	sq.in.	lbs. per sec.	0.0027450
			lbs. per min.	0.16470
			lbs. per hour	9.8821
		sq.ft.	lbs. per sec.	0.39529
			lbs. per min.	23.717
			lbs. per hour	1423.0

Substituting Eqs. (6) and (10) in Eq. (9), the formula becomes

$$w/CA = Kp_{1t}N/\sqrt{T_{1t}} \tag{11}$$

with

$$K = \left[\frac{k^2}{k-1}\left(\frac{2}{k+1}\right)^{(k+1)/(k-1)}\right]^{1/2}\sqrt{\frac{g}{c_p}} \tag{12}$$

For $k = 1.39470$,

$$K = 1.2855\sqrt{g/c_p}$$

and

$$w/CA = 1.2855\sqrt{(g/c_p)}(p_{1t}N/\sqrt{T_{1t}}) \tag{13}$$

which is the general formula for flow permitting the use of any consistent units.

It is probably desirable to assume some particular system of units and reduce the formula still further in order to eliminate as far as possible the amount of calculation required in routine computations. There is, however, no general agreement on standard units to be used for w, A, p, and T, and Table 2 has been prepared to give the value of K corresponding to all the different combinations of units likely to be used in practice. The working formula for flow for any given values of C, A p_{1t}, T_{1t}, and r then becomes

$$w = KCAp_{1t}N/\sqrt{T_{1t}}$$

with N taken from Table 1 and K from Table 2.

Selection of Basic Constants

The basic physical constants used in preparing the tables are essentially those adopted in A.S.M.E. test codes for measurement of flow and for compressor testing. In particular, the following constant values have been used directly or are implied.

p_0 = 14.70 lbs. per sq.in. absolute
T_0 = 527.6°F. absolute (68°F.)
γ_0 = 0.075 lb. per cu.ft. (exact value by definition)
$(k-1)/k$ = 0.283 (exact value by definition)
k = 1.39470
c_p = 0.242967 B.t.u. per lb. per °F.
g = 32.1740 ft. per sec. per sec.

The "long" values of k and c_p were used in computing the constant K in order to ensure exact consistency with the selected value of $(k-1)/k$, although even here, where the computation needs to be made only once and for all, this is a rather academic proceeding. Normally, these two values would be rounded off to three or four significant figures.

The reasons for selection of these constants are explained in the A.S.M.E. codes and in the references there given. Since it may not be convenient in all cases to consult these references, the reasons will be briefly summarized here.

First, "Normal Air" is defined as air with an average amount of CO_2 and sufficient moisture so that its specific weight at the selected standard conditions—p_0 = 14.70 lbs. per sq.in. absolute and T_0 = 527.6°F. absolute (68°F.)—is exactly γ_0 = 0.075 lb. per cu.ft. These values were selected chiefly because they (or values substantially equal to them) were already being used as standards in allied fields, especially in heating and ventilating engineering.

By combination of the two fundamental thermodynamic relations

$$c_p - c_v = c_p[1 - (1/k)] = R \qquad (14)$$

and

$$pv = RT \qquad (15)$$

the relation connecting c_p, k, and v (or γ) is obtained

$$c_p[1 - (1/k)] = pv/T = p/\gamma T \qquad (16)$$

Investigation of published data on the specific heat of air at temperatures of usual interest (0–200°F.), and containing about the same amount of moisture as Normal Air, led to the selection of 0.243 B.t.u. per lb. per °F. as a reasonable average value. Substituting this in Eq. (16) and using on the right-hand side the values applicable to Normal Air, it was found that

$$(k-1)/k = 1 - (1/k) = 0.28296$$

Since $(k-1)/k$ is a function more commonly used in thermodynamic calculations than k itself and since the value derived from Eq. (16) can be only an average value at best, this figure was rounded off to 0.283, which for the purpose of establishing a consistent set of values for thermodynamic calculations was taken as exact. The corresponding value of c_p then became 0.242967, which would be rounded off to 0.243 for usual calculations but must be retained in full when exact consistency is required. Similarly, the corresponding consistent value of the ratio of specific heats is k = 1.39470.

The ratio $(k-1)/k$ is selected as a basic value because many important thermodynamic formulas, including formulas for the flow of compressible fluids,[5] may be expressed in terms of a certain function

$$(p_1/p_2)^{(k-1)/k} - 1$$

which is sometimes known as "adiabatic factor" but is probably better designated as "isentropic" factor. Tables of this function are now available in various publications, as well as in A.S.M.E. codes. It has been extensively used in the aeronautical industry, usually being denoted by the symbol, Y, which was originally given to it.[6] With increasing use, however, the American Standards Association has decreed that, in order to avoid certain conflicts, it shall be denoted by the symbol X rather than Y, and it is so designated in most recent publications. The symbol X is therefore adopted in this paper.

Use of Formula

The formula is given in terms of p_{1t} and T_{1t}, the total pressure and temperature, respectively, on the upstream side of the restriction. In most cases the reading of the usual thermometer or thermocouple is nearly enough equal to the total temperature, but for extremely high velocities the reading is usually intermediate between the true static and the true total temperature and a correction must be applied. This is true, of course, no matter what formula is used.

The total pressure is the pressure that would be shown by an impact tube pointing directly upstream. Sometimes a static rather than a total pressure is measured. The static pressure and temperature may be used in the formula if the usual correction for velocity of approach is made. This correction is often negligibly small.

In making flow measurements it is usually considered better practice to measure the differential

$$\Delta p_t = p_{1t} - p_2$$

directly, together with either one or both of the gage pressures, rather than to depend only on the latter. The reduction to common units and calculation of the pressure ratio is combined into one operation by the formula

$$\frac{p_{1t}}{p_2} = 1 + \frac{K'\Delta p_t}{p_2} = \frac{1}{1 - (K'\Delta p_t/p_{1t})}$$

Values of K' are given in Table 3 for the cases most likely to occur. The constants there given assume that, in accordance with usual practice, the readings of mercury columns have been reduced to equivalent heights at 32°F. and that the readings of water columns have been reduced to, or are considered closely enough equal to, equivalent heights at 60°F.

The formula gives what is called "gravimetric" flow. This term indicates merely a flow that the practical engineer is accustomed to express in pounds per second, pounds per minute, or the like and takes no stand on the controversial issue as to whether it should be denoted "mass" flow or "weight" flow. The corresponding volumetric flow at any specified pressure and temperature is obtained by multiplying by the specific volume at that pressure and temperature.

In certain problems the formula is used in the form

$$N = (\sqrt{T_1}w/A)/KCp_{1t}$$

as, for example, when checking the capacity of a restriction or duct for a specified flow. If the calculated value of N is greater than unity, it is impossible to pass the specified flow with the specified pressure and temperature. With N exactly equal to unity, the velocity is sonic. A value of N less than unity indicates the fraction of the total possible capacity being utilized.

Calculation of Tables

Most of the values of N have been calculated using seven-place logarithmic tables and a calculating machine. For the low-pressure ratios, where the number of significant figures given in seven-place logarithmic tables is rather small, the 16-place table of natural logarithms prepared by the Federal Works Agency under the sponsorship of the National Bureau of Standards[6] was used. In some cases the logarithms were themselves calculated directly from the appropriate infinite series.

Since the function N changes rapidly at low-pressure ratios, the increments of pressure ratio have been chosen with a view to making the differences between the tabulated values small enough for convenient interpolation throughout the entire table. However, interpolation should not be necessary in most practical cases. The table was originally prepared with the values of N carried out to the nearest fifth significant figure, which for the greater portion of the table is equivalent to five decimal places. However, it seemed that this number of places was greater than was needed in the great majority of practical cases and, in fact, would seldom be justifiable when the accuracy of the usual test and other data available are taken into consideration. The values here given have therefore been rounded off to the nearest fourth significant figure, with the incidental advantage of facilitating interpolation if this is required.

Table 3
Values of K' for Use in Calculating Pressure Ratio

$$p_{1t}/p_2 = 1 + (K'\Delta p_t/p_2) = \frac{1}{1 - (K'\Delta p_t/p_{1t})}$$

p_{1t}, p_2	Δp_t	K'
Inches Hg absolute*	Inches H_2O†	0.07347
	Inches Hg*	1.000
	Pounds per sq.in.	2.036
Pounds per sq.in. absolute	Inches H_2O†	0.03609
	Inches Hg*	0.4912
	Pounds per sq.in.	1.000

* At 32°F.
† At 60°F.

It is shown in reference 2 (formula D) that for low-pressure ratios the flow is closely proportional to

$$\sqrt{p_2\Delta p_t}$$

Equating this closely approximate formula to the formula here used and solving for N, it is found that for low-pressure ratios N is proportional to

$$\sqrt{p_2\Delta p_t}/p_{1t}$$

If all pressures are expressed in the same units, the constant of proportionality varies from 2.06806 at a pressure ratio of unity to 2.06416 at a ratio of 1.0500, with intermediate values nearly in direct proportion. Occasionally, this relation may be of use in calculating values of N not tabulated directly. Since N is a function of pressure ratio only, any convenient values of absolute pressure may be assumed in making the calculation.

References

[1] *Flow Measurement—1940*, A.S.M.E. Power Test Codes PTC 19.5.4-1940, Table 7, p. 30, and Sect. VIII, p. 59; American Society of Mechanical Engineers, New York, 1940.

[2] Moss, S. A., *Measurement of Flow of Air and Gas with Nozzles*, Trans. A.S.M.E., Applied Mechanics, Vol. 50, paper 3, 1928.

[3] Greenland, L. S., *Fluid Flow Through Restrictions*, Aircraft Engineering, Vol. XV, No. 172, p. 162, June, 1943.

[4] *Test Code for Centrifugal Compressors, Exhausters, and Fans*, A.S.M.E. Power Test Codes of 1935, pp. 12–29; American Society of Mechanical Engineers, New York, 1935.

[5] Moss, S. A., and Smith, C. W., *Engineering Computations for Air and Gases*, Trans. A.S.M.E., Applied Mechanics, Vol. 52, paper 8, 1930.

[6] *Table of Natural Logarithms*, Vol. III, prepared by Federal Works Agency, Work Projects Administration for the City of New York, sponsored by and obtainable from the National Bureau of Standards, Washington, D.C.

Coupled Surfaces

J. B. KENDRICK*

California Institute of Technology

Introduction

THE OBJECT OF THIS INVESTIGATION is to describe a new type of airplane control surface that is many times more powerful, as a stabilizing or damping means, than a fixed surface of equal area. This increase in effectiveness is accomplished in the following manner:

As shown in Fig. 1, the lateral force F (1) produced by angle of yaw ψ (2) causes the vertical surface to tip (3) about its base. Coupling link (4) between the rudder and a fixed point (preferably inside the fuselage) causes the rudder to deflect through angle β (5). The rudder deflection acts in the proper direction to reduce the angle of yaw ψ. This procedure has converted the control surface into an *automatic servo-control.*

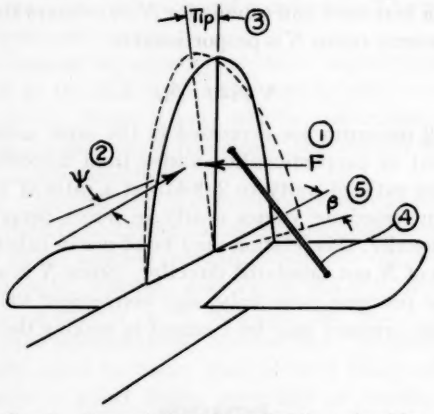

FIG. 1. General view of coupled fin and rudder.

Although Fig. 1 illustrates a vertical surface, this principle is not limited in usefulness to vertical tails alone. Any control surface that is hinged at the trailing edge of an airfoil may be adapted to an automatic servo-control in two steps, as follows:

(1) Hinge the forward portion of the airfoil upon a fore-and-aft axis. This provides the "error-smeller" element of the servo-control, because the forward part will tip whenever the surface is deflected from a trimmed position.

(2) Couple the rearward or flap portion to a fixed point on the airplane in such a manner that movement of the forward portion on *its* hinge will cause the flap to move in a direction to provide aerodynamic correction for the error in trim. In this way, the coupling linkage serves to actuate the flap and also to stabilize the forward part of the surface.

When the foregoing procedure is carried out according to certain rules that are to be given, the resulting control surface is sensitive to changes in angle of attack and acts automatically to reduce the error with a force proportional to the error.† (In this respect it functions in the same manner as an angle-of-attack-type autopilot.) As a free control, its effect upon the airplane is the same as a conventional surface of much larger area. It may be adapted to manual control in the normal manner, but one should note that the maximum lift or moment will be no greater than a conventional surface, even though the slope of the lift curve is many times as great.

Since any servomechanism is susceptible to a tendency to oscillate unless properly damped, this subject has been carefully studied, and stability criteria are provided for use in design. The resulting surface will return promptly to its original setting when deflected from a trimmed position in an airstream.

The static and dynamic stability will now be developed for the case of a vertical tail surface. This development will likewise serve for horizontal tails and, with slight modifications, may be adapted to the case of ailerons.

Definition of Terms

m_t = total mass of tail
m_r = mass of rudder
x_0 = c.g. A to rudder hinge
x = c.g. A to c.g. complete tail
x_r = rudder hinge to rudder c.g.
z_0 = c.g. A to tip hinge
z = tip hinge to c.g. complete tail
z_r = tip hinge to c.g. rudder

† Another arrangement of all-movable surfaces is described in reference 3, where the forward surface is hinged on an axis *parallel* to the rearward flap surface. Although this method of coupling provides a considerable increase in $dC_t/d\alpha$, the arrangement of perpendicular hinges described herein is even more powerful, as shown by the following comparison of the effectiveness factor $[1 + \tau(\beta/\psi)]$ for the two methods:

Method of Coupling		Static Condition	Dynamic Condition	Source of Data
Parallel hinges	theory	>2	...	....
	test	...	1.15[1]	Reference 3
Perpendicular hinges	theory	>8	>6	Figs. 3 and 4
	test	7.6	2.0[2]	Table 2

[1] Highest value reported. Larger values should be feasible.
[2] The dynamic stability theory was not completed when these tests were made. See "Correlation of Dynamic Stability Theory with Test."

Received September 6, 1945.
* Aeronautical Engineer.

R = coupling ratio = $\frac{x_l}{z_l} = \frac{\text{tip}}{\beta}$; $0 < R < 1$; $G = \frac{z}{x}R$

S = total tail area

S_r = rudder area

C = total tail chord

C_r = average rudder chord

$\bar{x}$ = c.g. A to $^1/_4c$ complete tail

$\bar{x}_r$ = $^1/_4c$ complete tail to c.p. rudder force due to β

$\bar{z}$ = tip hinge to c.p. complete tail

$C_{h\alpha} = \frac{dC_h{}^{(-)}}{d\alpha}$; $C_{h\beta} = \frac{dC_h{}^{(-)}}{d\beta}$; $C_{L\alpha} = \frac{dC_L{}^{(-)}}{d\alpha}$; $\tau = \frac{d\alpha'{}^{(+)}}{d\beta}$;

$\tau_1 = \tau\left(1 + \frac{\bar{x}_r}{\bar{x}}\right)$

$h_\alpha = \frac{C_{h\alpha}S_rC_r}{C_{L\alpha}S\bar{z}}$; $h_\beta = \frac{C_{h\beta}S_rC_r}{C_{L\alpha}S\bar{z}}$; $\tau_1 = \tau\left(1 + \frac{C_{m_{0\beta}}}{C_{L\alpha}\tau}\frac{C}{\bar{x}}\right)$

$M = \frac{m_r x_r}{m_l x}$; $(1 + f^*) = \frac{x_0 - x + x_r^*}{x}$; $C_{m_{0\beta}} = \frac{dC_{m_0}{}^{(-)}}{d\beta}$

a and b = radii of gyration of rudder (about a vertical axis) and the complete tail (about a horizontal axis), respectively, through their own c.g.'s

$H = \frac{\bar{z}}{\bar{x}}(h_\beta - \tau R) + \left[G^{*2} + M\left(\frac{x_r^*}{x} - 2G\frac{z_r}{z}\right)\right] + \left[G - M(1 + f^*)\right]\left[\tau_1 - \frac{\bar{z}}{\bar{x}}(R - h_\alpha)\right]$

$J = G^{*2} + M\left(\frac{x_r^*}{x} - 2G\frac{z_r}{z}\right) - \left[G - M(1 + f^*)\right]^2$

$K = \frac{\bar{z}}{\bar{x}}[\tau_1(R - h_\alpha) + (h_\beta - \tau R)]$; $L = \frac{-C_{L\alpha}qS\bar{x}}{m_l x^2}$

ψ = angle of yaw

β = rudder deflection

α = angle of attack of airfoil

q = dynamic pressure = $(\rho/2)U^2$

ρ = air density

U = air velocity

Static Stability of Coupled Fin and Rudder

The resistance to sideslip $dC_L/d\psi$ is equal to the sum of the lift-due-to-angle-of-attack $dC_L/d\alpha$ and lift-due-to-rudder-deflection $(dC_L/d\alpha)[(d\alpha'/d\beta)(d\beta/d\psi)]$, where $d\alpha'/d\beta$ is the change in effective angle of attack of the tail per degree of rudder deflection, normally denoted by τ; and $d\beta/d\psi$ is the rudder deflection per degree of yaw, which may be written β/ψ for small deflections. The sum of these effects is

$$\frac{dC_L}{d\psi} = \frac{dC_L}{d\alpha}\left(1 + \tau\frac{\beta}{\psi}\right) \tag{1}$$

The $dC_L/d\alpha$ of the normal tail is thus augmented by the factor $\tau(\beta/\psi)(dC_L/d\alpha)$ produced by the forced rudder deflection. *The coupled fin and rudder are therefore* $[1 + \tau(\beta/\psi)]$ *time as effective as a fixed vertical surface of the same area.* The value of β/ψ may now be derived in terms of the geometry. (The symbols are given above.)

As shown in Fig. 2, aerodynamic tipping moment = link restraining moment

$$(dC_L/d\alpha)(\psi + \tau\beta)qS\bar{z} = -F(y_l/l)z_l \tag{2}$$

and rudder hinge moment = link restraining moment

$$(C_{h\alpha}\psi + C_{h\beta}\beta)qS_rC_r = -F(y_l/l)x_l \tag{2a}$$

Dividing Eq. (2a) by Eq. (2) and solving for β/ψ,

$$\beta/\psi = (R - h_\alpha)/(h_\beta - \tau R) \tag{3}$$

As the coupling ratio R increases, the effectiveness $[1 + \tau(\beta/\psi)]$ likewise increases, until at some value R_s corresponding to $h_\beta - \tau R_s$, the denominator of Eq. (3) is equal to zero and $[1 + \tau(\beta/\psi)]$, approaches infinity. At larger values than R_s the coupled surface is unstable. R_s and its effect on stability are determined as follows:

$$1 + \tau\frac{\beta}{\psi} = 1 + \frac{\tau(R - h_\alpha)}{h_\beta - \tau R}; \quad h_\beta - \tau R_s = 0$$

therefore

$$R_s = h_\beta/\tau$$

$$1 + \tau\frac{\beta}{\psi} = 1 + \frac{\dfrac{R}{R_s} - \dfrac{h_\alpha}{h_\beta}\tau}{1 - (R/R_s)} = 1 + \frac{1 - \dfrac{R_s}{R}\dfrac{h_\alpha}{h_\beta}\tau}{(R_s/R) - 1} \tag{3a}$$

Optimum values of the effectiveness $[1 + \tau(\beta/\psi)]$ may be obtained in the following manner:

(A) Make the numerator as large as possible, and positive.

(1) Large τ indicates that a wide chord rudder should be used.

(2) Large R may be obtained with wide chord rudder on a low aspect ratio tail. However, R is really determined by B(2) below.

(3) h_α should be as small as consistent with large h_β under B(1).

(B) Make the denominator as small as feasible, and positive.

(1) Large $h_\beta = C_{h\beta}C_rS_r/C_{L\alpha}\bar{z}S$ indicates:

(a) Low aspect ratio, to give small $\bar{z}$ and, incidentally, low $C_{L\alpha}$.

(b) Large rudder chord C_r and area ratio S_r/S.

(c) High hinge moment coefficient slope, $C_{h\beta}$, suggests a rudder with small aerodynamic balance, and with cusp trailing edge. Surface contours should be carefully con-

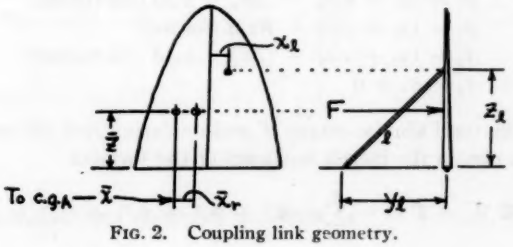

FIG. 2. Coupling link geometry.

trolled to avoid nonlinearity of $C_{h\beta}$ near neutral.

(2) τR should be adjusted to slightly less than h_β. Aerodynamic and manufacturing variations will prove the deciding factor in the minimum value to be used for $(h_\beta - \tau R)$, as shown in Eq. (3a).

Allowing a margin of say 10 per cent from R_s to cover aerodynamic and manufacturing variations, one obtains the following value of effectiveness for normal surface proportions, assuming $\tau = 0.65$ and $h_\alpha/h_\beta = 1/2$.

$$1 + \tau(\beta/\psi) = 1 + \{\tau[(0.9h_\beta/\tau) - h_\alpha]/0.10h_\beta\} = 1 + [0.9 - (0.65/2)]0.10 \doteq 6.8$$

A decided improvement in static stability may therefore be effected with surfaces coupled in this manner.

Excellent agreement is obtained between the static stability theory and test results, as shown in Fig. 3. The experimental points were obtained from free control wind-tunnel tests of the coupled tail at various angles of yaw, as shown by the solid curves of Fig. 4. Rudder deflection tests (as shown dotted in Fig. 4), when cross-plotted for various linkage ratios, gave the same results as the coupled tail.

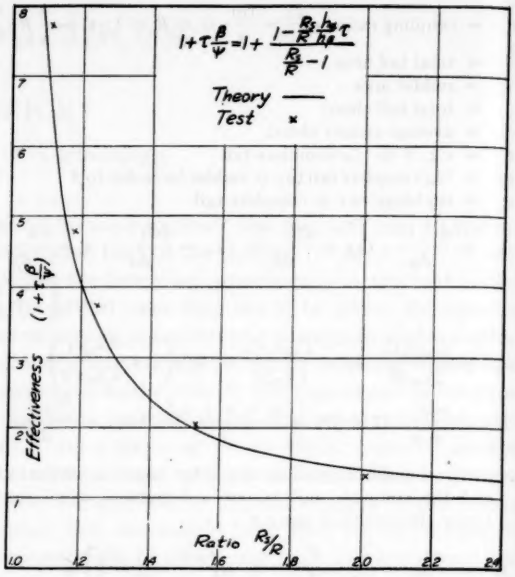

FIG. 3. Static stability characteristics of coupled fin and rudder.

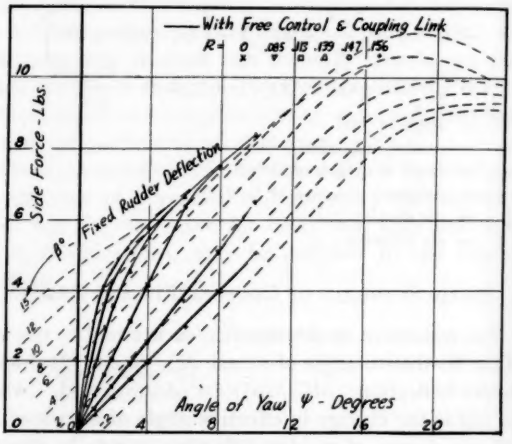

FIG. 4. Wind tunnel tests on coupled fin and rudder.

DYNAMIC STABILITY OF COUPLED SURFACES

Equations of Motion

The motion of the surfaces may be expressed in terms of the angle of yaw ψ and the rudder deflection β. It is now desired to express ψ and β in terms of equations of motion with respect to time, in order to indicate the dynamic behavior of the coupled surfaces. Furthermore, it is desired to develop a stability criterion that shows the relative importance of the various aerodynamic and mechanical factors, and their proper relationship to insure satisfactory stability. This may be done with the aid of Lagrange's equations of motion.[1]

$$(d/dt)(\partial T/\partial \dot{q}_k) - (\partial T/\partial q_k) = Q_k \qquad (4)$$

In Fig. 5, any small element P_i of mass m_i and Cartesian coordinates x_i, y_i, z_i may be expressed in terms of ψ and β, the generalized coordinates.

x_i and z_i will be constant for small values of ψ and β.

$$y_i = (x_0 + x_i)\psi - Rz_i\beta \text{ (for fin)}$$
$$y_i = (x_0 + x_i)\psi - (Rz_i - x_i)\beta \text{ (for rudder)}$$
$$\dot{y}_i = (x_0 + x_i)\dot{\psi} - Rz_i\dot{\beta} \text{ (for fin)}$$
$$\dot{y}_i = (x_0 + x_i)\dot{\psi} - (Rz_i - x_i)\dot{\beta} \text{ (for rudder)}$$
$$\dot{x}_i = \dot{z}_i = 0$$

The total kinetic energy T and its derivatives are used to obtain the inertia moments of the surfaces.

$$\text{K.E.} = T = {}^1/_2\sum_{i=1}^{n} m_i(\dot{x}_i^2 + \dot{y}_i^2 + \dot{z}_i^2) + {}^1/_2\sum_{i=1}^{n} m_i\dot{y}^2$$

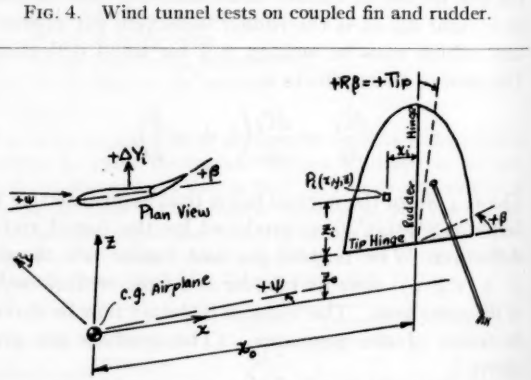

FIG. 5. Geometry of coupled fin and rudder.

$$T = {}^1/_2\sum_i m_i[(x_0 + x_i)\psi - Rz_i\dot{\beta}]^2 + {}^1/_2\sum m_i[(x_0 + x_i)\dot{\psi} - (Rz_i - x_i)\dot{\beta}]^2$$

$$\frac{\partial T}{\partial \dot{\psi}} = {}^1/_2\sum_i m_i[2(x_0 + x_i)^2\dot{\psi} - 2(x_0 + x_i)Rz_i\dot{\beta}] + \quad \text{(fin)}$$

$${}^1/_2\sum_i m_i[2(x_0 + x_i)^2\dot{\psi} - 2(x_0 + x_i)(Rz_i - x_i)\dot{\beta}] \quad \text{(rudder)}$$

$$\frac{\partial T}{\partial \dot{\beta}} = {}^1/_2\sum_i m_i[-2(x_0 + x_i)Rz_i\dot{\psi} + 2R^2z_i^2\dot{\beta}] + {}^1/_2\sum_i m_i[-2(x_0 + x_1)(Rz_i - x_i)\dot{\psi} + 2(Rz_i - x_i)^2\dot{\beta}]$$

$$\frac{d}{dt}\left(\frac{\partial T}{\partial \dot{\psi}}\right) = \sum_i m_i[(x_0 + x_i)^2\ddot{\psi} - (x_0 + x_i)Rz_i\ddot{\beta}] + \sum_i m_i[(x_0 + x_i)^2\ddot{\psi} - (x_0 + x_i)(Rz_i - x_i)\ddot{\beta}]$$

$$\frac{d}{dt}\left(\frac{\partial T}{\partial \dot{\beta}}\right) = \sum_i m_i[-(x_0 + x_i)Rz_i\ddot{\psi} + R^2z_i^2\ddot{\beta}] + \sum_i m_i[-(x_0 + x_i)(Rz_i - x_i)\ddot{\psi} + (Rz_i - x_i)^2\ddot{\beta}]$$

$$\left.\begin{aligned}\frac{d}{dt}\left(\frac{\partial T}{\partial \dot{\psi}}\right) &= m_fx^2\ddot{\psi} - m_fxzR\ddot{\beta} + m_rx_r(x_0 + x_r^*)\ddot{\beta}\\ \frac{d}{dt}\left(\frac{\partial T}{\partial \dot{\beta}}\right) &= -m_fxzR\ddot{\psi} + m_fz^{2*}R^2\ddot{\beta} + m_rx_r(x_0 + x_r^*)\ddot{\psi} - 2m_rx_rz_rR\ddot{\beta} + m_rx_r^{2*}\ddot{\beta}\end{aligned}\right\} \quad (4a)$$

Note that $\partial T/\partial\psi = \partial T/\partial\beta = 0$.

The potential energy terms Q_k are represented by the aerodynamic moments about the airplane c.g., and the rudder hinge:

$$\frac{d\text{P.E.}}{dq_k} = Q_k = \sum_{i=1}^{n}\left(X_i\frac{\partial x_i}{\partial q_k} + Y_i\frac{\partial y_i}{\partial q_k} + Z_i\frac{\partial z_i}{\partial q_k}\right) = \sum_i Y_i\frac{\partial y_i}{\partial q_k}$$

since $X_i = Z_i = 0$. Considering (i) as chordwise strips of the airfoil of width dz

$$\Delta Y_i = C_{L\alpha}\left[(\psi + \tau\beta) + (\dot{\psi} + \tau\dot{\beta})\frac{\bar{x}}{U}\right]qCdz \quad \text{(both)}$$

$$\Delta Y_i = \left[(C_{h\alpha}\psi + C_{h\beta}\beta) + (C_{h\alpha}\dot{\psi} + C_{h\beta}\dot{\beta})\frac{\bar{x}}{U}\right]qC_rdz \quad \text{(rudder)}$$

$$\partial y_i/\partial\psi = (x_0 + x_i) \quad \text{(both)}$$

$$\partial y_i/\partial\beta = -Rz_i \quad \text{(fin)}$$

$$(\partial y_i/\partial\beta = -(Rz_i - x_i) \quad \text{(rudder)}$$

Moments about the airplane c.g. and moments about the rudder hinge are, respectively,

$$\left.\begin{aligned}Q_\psi &= \sum_i C_{L\alpha}qC\left[(\psi + \tau\beta) + (\dot{\psi} + \tau\dot{\beta})\frac{\bar{x}}{U}\right]\times(x_0 + x_i)dz = C_{L\alpha}qS\bar{x}\left[(\psi + \tau_1\beta) + (\dot{\psi} + \tau_1\dot{\beta})\frac{\bar{x}}{U}\right]\\ Q_\beta &= \sum_i C_{L\alpha}\left[(\psi + \tau\beta) + (\dot{\psi} + \tau\dot{\beta})\frac{\bar{x}}{U}\right]\times qC(-Rz_i)dz + \sum_i\left[(C_{h\alpha}\psi + C_{h\beta}\beta) + (C_{h\alpha}\dot{\psi} + C_{h\beta}\dot{\beta})\frac{\bar{x}}{U}\right]qC_r^2dz\\ &= -C_{L\alpha}\left[(\psi + \tau\beta) + (\dot{\psi} + \tau\dot{\beta})\frac{\bar{x}}{U}\right]\times qSzR + \left[(C_{h\alpha}\psi + C_{h\beta}\beta) + (C_{h\alpha}\dot{\psi} + C_{h\beta}\dot{\beta})\frac{\bar{x}}{U}\right]\times qSC_r\end{aligned}\right\} \quad (4b)$$

Treatment of incremental terms, the values of which are often quite important to the final answer, will be:

(1) Terms marked ( )* are evolved from $\sum_i m_ix_i^2$ and $\sum_i m_iz^2$, the moments of inertia of the rudder about its hinge and of the complete tail about the tip axis, which become $m_rx_r^2[1 + (a^2/x_r^2)]$ and $m_iz^2[1 + (b^2/z^2)]$, respectively. For brevity these terms will be marked ( )* for identification.

(2) The centroid of β-produced aerodynamic forces is aft of the quarter-chord point, at $\bar{x} + \bar{x}_r$.[3] Let τ_1 designate the product $\tau[1 + (\bar{x}_r/\bar{x})] = \tau[1 + C_{m0\beta}(C/\bar{x})(1/C_{L\alpha}\tau)]$.

(3) The ratio $(x_0 + x_r^*)/x$ will be expressed as $(1 + f^*)$, where $f^* = (x_0 - x + x_r^*)/x$.

Substituting values from Eqs. (4a) and (4b) into Eq. (4), the equations of motion then become

$$\left.\begin{aligned}&m_fx^2\ddot{\psi} - C_{L\alpha}qS\bar{x}\left(\frac{\bar{x}}{U}\dot{\psi} + \psi\right) + m_fx^2[M(1 + f^*) - G]\ddot{\beta} - C_{L\alpha}qS\bar{x}\tau_1\left(\frac{\bar{x}}{U}\dot{\beta} + \beta\right) = 0\\ &m_fx^2[M(1 + f^*) - G]\ddot{\psi} - C_{L\alpha}qS\bar{z}(h_\alpha - R)\left(\frac{\bar{x}}{U}\dot{\psi} + \psi\right) + m_fx^2\left[G^{*2} - 2MG\frac{z_r}{z} + M\frac{x_r^*}{x}\right]\ddot{\beta} - C_{L\alpha}qS\bar{z}(h_\beta - \tau R)\left(\frac{\bar{x}}{U}\dot{\beta} + \beta\right) = 0\end{aligned}\right\} \quad (4c)$$

Denoting d/dt by the operator λ and the coefficients by a, b, c, and d, Eqs. (4c) have the form

$$(a_2\lambda^2 + a_1\lambda + a_0)\psi = -(b_2\lambda^2 + b_1\lambda + b_0)\beta \tag{4d}$$

$$(c_2\lambda^2 + c_1\lambda + c_0)\psi = -(d_2\lambda^2 + d_1\lambda + d_0)\beta \tag{4e}$$

Dividing Eq. (4d) by Eq. (4e) gives the following quartic equation in λ:

$$(a_2d_2 - b_2c_2)\lambda^4 + (a_2d_1 + a_1b_2 - b_2c_1 - b_1c_2)\lambda^3 + (a_2d_0 + a_0d_2 - b_2c_0 - b_0c_2 + a_1d_1 - b_1c_1)\lambda^2 + (a_1d_0 + a_0d_1 - b_1c_0 - b_0c_1)\lambda + (a_0d_0 - b_0c_0) = 0 \tag{5}$$

or

$$A\lambda^4 + B\lambda^3 + C\lambda^2 + D\lambda + E = 0 \tag{5a}$$

Solving for the coefficients A, B, C, D, and E

$$a_2 = m_i x^2 \qquad b_2 = m_i x^2[M(1 + f^*) - G] \qquad c_2 = m_i x^2[M(1 + f^*) - G] \qquad d_2 = m_i x^2\left[G^{*2} + M\left(\frac{x_r^*}{x} - 2G\frac{z_r}{z}\right)\right]$$

$$a_1 = \frac{-C_{L\alpha}qS\bar{x}}{U/\bar{x}} \qquad b_1 = \frac{-C_Lqs\bar{x}}{U/\bar{x}}\tau_1 \qquad c_1 = \frac{-C_{L\alpha}qS\bar{x}}{U/\bar{x}}(h_\alpha - R)\frac{\bar{z}}{\bar{x}} \qquad d_1 = \frac{-C_{L\alpha}qS\bar{x}}{U/\bar{x}}(h_\beta - \tau R)\frac{\bar{z}}{\bar{x}}$$

$$a_0 = -C_{L\alpha}qS\bar{x} \qquad b_0 = -C_{L\alpha}qS\bar{x}\tau_1 \qquad c_0 = -C_{L\alpha}qS\bar{x}(h_\alpha - R)\frac{\bar{z}}{\bar{x}} \qquad d_0 = -C_{L\alpha}qS\bar{x}(h\beta - \tau R)\frac{\bar{z}}{\bar{x}}$$

$$\left.\begin{aligned}
A &= (m_i x^2)^2\{G^{*2} + M[(x_r^*/x) - 2G(z_r/z)] - [G - M(1 + f^*)]^2\} = (m_i x^2)^2\{J\} \\
B &= \frac{-C_{L\alpha}qS\bar{x}(m_i x^2)}{U/\bar{x}}\left\{\frac{\bar{z}}{\bar{x}}(h_\beta - \tau R) + G^{*2} + M\left(\frac{x_r^*}{x} - 2G\frac{z_r}{z}\right) + \left[G - M(1 + f^*)\right]\left[\tau_1 - \frac{\bar{z}}{\bar{x}}(R - h_\alpha)\right]\right. = \\
&\qquad \left.\frac{-C_{L\alpha}qS\bar{x}}{U/\bar{x}}(m_i x^2)\{H\}\right. \\
C &= B(U/\bar{x}) + E(\bar{x}/U)^2 \doteq B(U/\bar{x}) \\
D &= 2E(\bar{x}/U) \\
E &= (C_{L\alpha}qS\bar{x})^2\{(\bar{z}/\bar{x})[\tau_1(R - h_\alpha) + (h_\beta - \tau R)]\} \\
E &= L^2(m_i x^2)^2\{(\bar{z}/\bar{x})(h_\beta - \tau R)[1 + \tau_1(R - h_\alpha)/(h_\beta - \tau R)]\} \\
E &= L^2(m_i x^2)^2\left\{\frac{\bar{z}}{\bar{x}}(h_\beta - \tau R)\left[\left(1 + \tau\frac{\beta}{\psi}\right) + \frac{C_{m_{0\beta}}}{C_{L\alpha}}\frac{C}{\bar{x}}\frac{\beta}{\psi}\right]\right\} = L^2(m_i x^2)^2K
\end{aligned}\right\} \tag{6}$$

$$\frac{B}{A} = \frac{-C_{L\alpha}qS\bar{x}}{m_i x^2(U/\bar{x})}\left\{\frac{\frac{\bar{z}}{\bar{x}}(h_\beta - \tau R) + G^{*2} + M\left(\frac{x_r^*}{x} - 2G\frac{z_r}{z}\right) + \left[G - M(1 + f^*)\right]\left[\tau_1 - \frac{\bar{z}}{\bar{x}}(R - h_\alpha)\right]}{G^{*2} + M[(x_r^*/x) - 2G(z_r/z)] - [G - M(1 + f^*)]^2}\right\} = \frac{L}{U/\bar{x}}\frac{H}{J} \tag{7}$$

$$C/A = L(H/J) + [L/(U/\bar{x})]^3(K/J) \doteq L(H/J) \tag{8}$$

$$D/C = [2/(U/\bar{x})](E/C) = [2L/(U/\bar{x})](K/H) \tag{9}$$

$$E/C = [(E/A)/(C/A)] = L(K/H) \tag{10}$$

Damping Criterion

The quartic Eq. (5a) represents stable motion, providing all the coefficients A, B, C, D, and E are positive and Routh's discriminant (cf. reference 1) $BCD - D^2 - B^2E > 0$. The latter condition may be reduced to the form

$$\left(\frac{B}{2A}\right)^2 - \frac{E}{A}\left(\frac{\bar{x}}{U}\right)^2 > 0, \text{ or } \frac{H}{J} - 4\left(\frac{K}{H}\right) > 0 \tag{11}$$

Eq. (5a) may be solved approximately by factoring into two quadratics.

$$[\lambda^2 + (B/A)\lambda + (C/A)][\lambda^2 + (D/C)\lambda + (E/C)] = 0 \tag{5b}$$

which represents the original equation accurately, providing $|\lambda_{1,2}| \gg |\lambda_{3,4}|$, where

$$\left|\lambda_{1,2}\right| \doteq \left| -\frac{L}{2U/\bar{x}}\frac{H}{J} \pm i\sqrt{L\frac{H}{J}}\right| \doteq \sqrt{L\frac{H}{J}}$$

and

$$\left|\lambda_{3,4}\right| \doteq \left| -\frac{L}{U/\bar{x}}\frac{K}{H} \pm i\sqrt{L\frac{K}{H}}\right| \doteq \sqrt{L\frac{K}{H}}$$

But according to Routh's discriminant, $H/J - 4(K/H) > 0$ (Eq. (11)), which means that $|\lambda_{1,2}| \geq 2|\lambda_{3,4}|$. Therefore $|\lambda_{1,2}| \gg |\lambda_{3,4}|$ and the factors of Eq. (5b) are satisfactory for the purpose of this investigation. Both of the above modes represent oscillatory motion, as indicated by the fact that $C/A > (B/2A)^2$ and $E/C > (D/2C)^2$.

The frequency and damping characteristics of the coupled tail may now be compared to those of a fixed tail of the same area, as shown in Table 1. It will be noted that both modes of the coupled tail may have greater damping and high frequency than the fixed tail. The degree of improvement depends upon the proper adjustment of the various terms comprising H, J, and K.

Optimum Proportions for Dynamic Stability

The damping criterion is represented by Routh's discriminant, which in this case reduces to $H/J - 4(K/H)$ (Eq. (11)). The ratios H/J and K/H are found to be the same as those that determine the damping and frequency of the 1st and 2nd modes, respectively, in Table 1. In order to attain the maximum damping and frequency of the 2nd or long mode, $H/J - 4(K/H)$ is made small but positive, by keeping the value of H small, J and K large.

The term H is made small in the following manner:

(1) Make $h_\beta - \tau R$ small but safely $+$, with allowance for variations.

(2) Make $[G - M(1 + f^*)][1 + (C_{m_0\beta}/C_{L_\alpha}\tau)(C/\bar{x})]$ small but safely $+$, with allowance for variations.

(3) Make $x_r^*/x \leq 2G(z_r/z)$, by adjusting z_r and x_r^*.

The term K is made large by the same rules as for static stability, see "Static Stability of Coupled Fin and Rudder." The term J is made large by adjusting the rudder mass balance and mass distribution, $M[(x_r^*/x) - 2G(z_r/z)]$. In this regard a compromise must be effected between this term in J and the same term in H, in order to obtain the desired small value of the ratio H/J.*

Summary of Damping Criteria

In the preceding section it was shown that certain terms within Eq. (6) are also of particular importance, because if these terms have the wrong sign the adverse effect on stability may be greater than the nominal value of the term. The overall stability may, therefore, be changed by any one of the following factors, which should be adjusted as specified, for proper stability:

(1) A, B, C, D and $E > 0$
(2) $(H/J) - 4(K/H) > 0$
(3) $(h_\beta - \tau R) > 0$
(4) $(R - h_\alpha) > 0$
(5) $\left[G - M(1 + f^*)\right]\left(1 + \dfrac{C_{m_0\beta}}{C_{L_\alpha}\tau}\dfrac{C}{\bar{x}}\right) > 0$

Correlation of Dynamic Stability Theory with Test

Before the stability theory was developed in its final form, dynamic wind-tunnel tests were conducted on two different model tail surfaces, with many different balance conditions. When the stability criteria were used to predict, by analysis, the behavior of these models in the dynamic tests, the results are as shown in Table 2. In eight out of nine cases, the above criteria gave the correct answer on stability.

* Typical relative values of the above factors for a vertical tail might be $H/J - 4(K/H) = 15/1 - 4(50/15) = 1.7$. In this case, the time to damp to $^1/_2$ amplitude for the 2nd mode would be $1/(2 \times 3.3) \doteq {}^1/_6$th as great as a fixed surface of equal area, and the natural frequency would be 1.8 times as great. The 1st mode would have a much higher damping and natural frequency than the 2nd mode.

TABLE 1
Coupled Tail vs. Fixed Tail

	Fixed Tail	Coupled Tail — 1st Mode short period	Coupled Tail — 2nd Mode long period
Equation of motion	$\ddot{\psi} + \frac{L}{U/\bar{x}}\dot{\psi} + L\psi = 0$	$\lambda^2 + \frac{B}{A}\lambda + \frac{C}{A} = 0$	$\lambda^2 + \frac{D}{C}\lambda + \frac{E}{C} = 0$
Damping ratio ξ	$\frac{L}{2U/\bar{x}}\frac{1}{\sqrt{L}} = \frac{\sqrt{L}}{2U/\bar{x}}$	$\frac{B}{2A}\sqrt{\frac{A}{C}} = \frac{\sqrt{L}}{2U/\bar{x}}\sqrt{\frac{H}{J}}$	$\frac{D}{2C}\sqrt{\frac{C}{E}} = \frac{\sqrt{L}}{U/\bar{x}}\sqrt{\frac{K}{H}}$
Undamped natural frequency ω_0	$\sqrt{L}$	$\sqrt{C/A} = \sqrt{L}\sqrt{H/J}$	$\sqrt{E/C} = \sqrt{L}\sqrt{K/H}$
Ratio $\frac{\xi \text{ coupled}}{\xi \text{ fixed}}$	.....	$\sqrt{H/J}$	$2\sqrt{K/H}$
Ratio $\frac{\omega_0 \text{ coupled}}{\omega_0 \text{ fixed}}$	.....	$\sqrt{H/J}$	$\sqrt{K/H}$
Ratio $\frac{\xi \text{ 1st mode}}{\xi \text{ 2nd mode}}$	$\sqrt{\frac{H}{J}\frac{H}{4K}} \geq 1$		
Ratio $\frac{\omega_0 \text{ 1st mode}}{\omega_0 \text{ 2nd mode}}$	$2\sqrt{\frac{H}{J}\frac{H}{4K}} \geq 2$		
Ratio time to damp to $^1/_2$ amplitude $\frac{\text{1st mode}}{\text{2nd mode}}$	$= \frac{0.693/(B/2A)}{0.693/(D/2C)} = \frac{1}{2}\left(\frac{4K}{H}\frac{J}{H}\right) \leq \frac{1}{2}$		
Ratio time to damp to $^1/_2$ amplitude $\frac{\text{2nd mode}}{\text{fixed tail}}$	$= \frac{L}{U/\bar{x}}\Big/\frac{2L}{U/\bar{x}}\frac{K}{H} = \frac{1}{2}\frac{H}{K}$		

TABLE 2
Dynamic Stability Correlation

Model → / Cond.	S_1	S_2	S_3	S_4	S_5	S_6	S_7	L_1	L_2	Prop. L_3
m_t, lbs.	1.98	1.95	1.54$_1$	1.54	1.54	1.54	1.62	2.68	2.68	2.9
m_r, lbs.	0.38	0.38	0.38	0.38	0.38	0.38	0.48	1.15	1.15	1.5
x, in.	36	36	36	36	36	36	36	84	84	84
x_r, in.	1.38	1.38	1.38	1.38	1.38	1.38	1.00	3.2	3.2	1.7
z, in.	7.75	6.06	3.75	3.75	3.75	3.75	3.75	8.4	8.4	8.4
z_r, in.	4.13	4.13	4.13	4.13	4.13	4.13	4.00	8.9	8.9	8.4
R,	0.115	0.0955	0.0722	0.0955	0.115	0.161	0.0722	0.167	0.143	0.235
S, sq.in.	84	84	84	84	84	84	84	2.64sq.ft	2.64	2.64
S_r, sq.in.	40	40	40	40	40	40	40	1.39	1.39	1.39
C, in.	8.4	8.4	8.4	8.4	8.4	8.4	8.4	...	...	...
$\bar{x}$, in.	34	34	34	34	34	34	34	82	82	82
$\bar{z}$, in.	4.0	4.0	4.0	4.0	4.0	4.0	4.0	6.0	6.0	6.0
$C_{h\alpha}$	− 0.004	− 0.004	− 0.004	− 0.004	− 0.004	− 0.004	− 0.004	− 0.004	− 0.004	− 0.004
$C_{h\beta}$	− 0.010	− 0.010	− 0.010	− 0.10	− 0.010	− 0.010	− 0.010	− 0.008	− 0.008	− 0.008
$C_{L\alpha}$	− 0.04	− 0.04	− 0.04	− 0.04	− 0.04	− 0.04	− 0.04	− 0.04	− 0.04	− 0.04
τ	0.65	0.65	0.65	0.65	0.65	0.65	0.65	0.67	0.67	0.67
h_α	0.047	0.047	0.047	0.047	0.047	0.047	0.047	0.088	0.088	0.088
h_β	0.118	0.118	0.118	0.118	0.118	0.118	0.118	0.175	0.175	0.175
M	0.00735	0.0075	0.0095	0.0095	0.0095	0.0095	0.0082	0.0164	0.0164	0.0164
z/x	0.215	0.169	0.104	0.104	0.104	0.104	0.104	0.100	0.100	0.100
x_r/x	0.0383	0.0383	0.0383	0.0383	0.0383	0.0383	0.0278	0.038	0.038	0.047
z_r/z	0.533	0.68	1.10	1.10	1.10	1.10	1.07	1.06	1.06	1.80
$\bar{z}/\bar{x}$	0.118	0.118	0.118	0.118	0.118	0.118	0.118	0.073	0.073	0.073
$1 + (a^2/x_r^2)$	2.33	2.33	2.33	2.33	2.33	2.33	3.6	2.33	2.33	2.33
$1 + (b^2/z^2)$	1.25	1.5	2.0	2.0	2.0	2.0	2.0	1.5	1.5	1.5
$1 + (\bar{x}_r/\bar{x})$	1.06	1.06	1.06	1.06	1.06	1.06	1.06	1.07	1.07	1.07
$1 + f^*$	1.09	1.09	1.09	1.09	1.09	1.09	1.10	1.09	1.09	1.09
(1) $(H/J) - 4(K/H)$	16.4	12.4	7.1	2.6	2.1	−45	6.4	− 3.4	− 4.5	6.6
	S	S	S	S	S	U	S	U	U	S
(2) $h_\beta - \tau R$	0.043	0.056	0.071	0.056	0.043	0.013	0.071	0.063	0.079	0.018
	S	S	S	S	S	S	S	S	S	S
(3) $R - h_\alpha$	0.068	0.048	0.025	0.048	0.068	0.114	0.025	0.079	0.055	0.147
	S	S	S	S	S	S	S	S	S	S
(4) $G - M(1 + f^*)$	0.0168	0.0080	− 0.0029	− 0.0004	0.0024	0.0063	− 0.0015	− 0.0012	− 0.0036	0.0017
	S	S	U	U	S	S	U	U	U	S
Stability prediction	S	S	$U_4^* = S$	$U_4^* = U$	S	U_1	$U_4^* = S$	U_1	U_1	S
Actual Test	$S\surd$	$S\surd$	$S\surd$	$U\surd$	$U\otimes$	$U\surd$	$S\surd$	$U\surd$	$U\surd$	...

S = stable; U = unstable; U^* = unstable unless (1) is large.

STABILIZING EFFECT OF COUPLED SURFACES

The purpose of a stabilizing surface on an airplane is to restore equilibrium conditions following a disturbance, in a minimum of time and without perceptible oscillations. The motion following a disturbance of a one-degree-of-freedom vibrating system represented by the equation $a\ddot{\psi} + b\dot{\psi} + c\psi = 0$ is:

$$\psi/\psi_0 = e^{-\xi\omega_0 t}\cos\omega_0 t = e^{-t/\tau}\cos(1/\xi)(t/\tau) \quad (12)$$

where $\tau = 2a/b$ represents a characteristic time;[4] $\xi = b/2a\omega_0$ represents the damping ratio as discussed in "Dynamic Stability of Coupled Surfaces"; and $\omega_0 = \sqrt{c/a}$ represents the undamped natural frequency of the coupled tail, when operating on its own moment of inertia, $m_t x^2$ *only*, as analyzed previously.

In "Dynamic Stability of Coupled Surfaces"; the coupled tail was found to have two modes of motion, represented by short and long period oscillations following a disturbance (cf. Table 1).

ratio of natural frequencies $\dfrac{\omega_0 \text{ short mode}}{\omega_0 \text{ long mode}} \geq \dfrac{2}{1}$

ratio of times-to-damp-to-$^1/_2$ amplitude

$$\frac{\text{short mode}}{\text{long mode}} \leq \tfrac{1}{2}$$

Each of these modes will respond to a disturbance in accordance with Eq. (12), as shown in Fig. 6.

The ratio of relative amplitudes of the long and short modes following a static displacement was found by numerical solutions to be approximately as the ratio of the frequencies, and independent of the forward veloc-

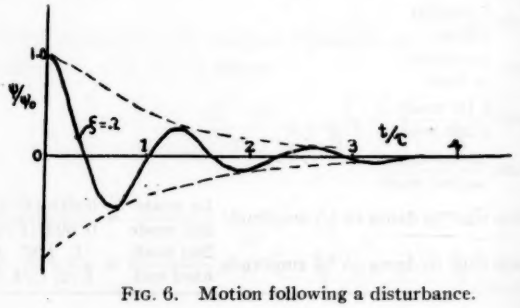

FIG. 6. Motion following a disturbance.

ity. These characteristics are believed to hold true in general because of the relative magnitude of terms resulting from "Optimum Proportions for Dynamic Stability," which insures that the frequency separation of the modes shall be great and that both modes shall have adequate damping. This causes the short mode to vanish quickly, leaving the long mode predominant. Conversely, since the long mode is predominant, the procedure was correctly stated to increase the damping and natural frequency of the coupled tail, and to insure that the long mode should predominate.

The damping ratio ξ for the long mode is

$$\sqrt{\frac{C_{L\alpha}qS\bar{x}}{(U^2/\bar{x}^2)m_i\bar{x}^2}}\sqrt{\frac{K}{H}} = \sqrt{\frac{C_{L\alpha}(\rho/2)S\bar{x}^3}{m_i\bar{x}^2}}\sqrt{\frac{K}{H}}$$

(see Table 1). The damping ratio is seen to be independent of the velocity. The natural frequency, however,

$$\omega_0 = \sqrt{\frac{C_{L\alpha}qS\bar{x}}{m_i\bar{x}^2}}\sqrt{\frac{K}{H}}$$

increases linearly with the velocity, since $q = (\rho/2)U^2$.

If the coupled tail is operated as described previously (i.e., without the remainder of the airplane), in an air stream of velocity U, and the rudder is subjected to a sinusoidal forcing function of frequency ω_f, the response of each mode is as shown in Fig. 7, point A. When the same tail is installed on an airplane, the natural frequencies ω_0 of the two modes remain the same but the natural frequency of the airplane becomes less than the long mode of the tail alone, because of increased inertia and other effects. The natural frequency of the airplane-plus-tail becomes the new forcing frequency ω_f for the tail, and as this frequency decreases with respect to the lowest ω_0 of the tail alone, the ratio ω_f/ω_0 decreases and the rudder action varies as shown in Fig. 7. The true stabilizing effect, measured by the time to damp to $1/2$ amplitude, then corresponds to point B, between the value determined for the dynamic condition as in "Dynamic Stability of Coupled Surfaces," and the static conditions, as in "Static Stability of Coupled Fin and Rudder," depending on the change in frequency from "tail alone" to "airplane-plus-tail." For extremely long period motion, the static stability takes charge and the improvement factor becomes $[1 + \tau(\beta/\psi)]$, corresponding to point C.

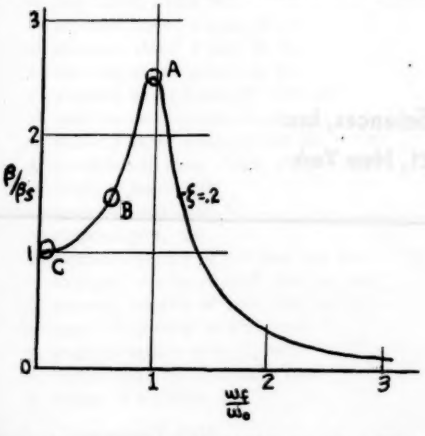

FIG. 7. Response of coupled tail to forced oscillation.

The above qualitative discussion shows the general trend of the dynamic stability. However, in order to determine accurately the dynamic behavior of airplane-plus-tail, the equations of motion of the airplane, including the effect of the coupled tail, should be solved. The general solutions for (1) longitudinal motion and (2) lateral and directional motion, provide subjects for further analysis and research.

The foregoing investigations assume no friction or free play in the control system. Friction and free play in the system will cause the rudder to lag behind the position it would have if these effects were absent. The result of this lag is a residual moment acting on the surface at all times and easily recognized whenever the lift passes through the zero lift condition. This lag is contradictory to the original hypothesis that β is proportional to ψ. Furthermore, the residual moment due to lag is an unstable effect, tending to extract energy from the air stream and create an undamped oscillation of the control, the amplitude of which increases as the lag angle increases. The effects of friction and free play may be corrected by reducing the linkage ratio, at the expense of control effectiveness $[1 + \tau(\beta/\psi)]$. The quantitative effect of these factors remains a subject for further investigation.

SUMMARY

In order to attain satisfactory results with the coupled tail, the surface geometry and airfoil contours, mass balance terms, coupling linkage, etc., must be in the correct proportions. Normal methods of construction are considered to be satisfactory in general, providing the design requirements for the coupled tail are met.

The adaptation of manual control to the surface may be done in several ways. The major requirement is to avoid excess friction and free play in the system. The same precautions are necessary in developing the coupling linkage mechanism, which should be housed within the fuselage if possible (for aerodynamic cleanness).

From the weight standpoint, the following comparison may be made:

(1) Weight increase due to additional hinges and coupling linkage.

(2) Weight decrease due to smaller surface and lower span.

Although no actual weight calculations have been made, it is believed that, for a given stabilizing effect, the coupled tail may be produced at a lower weight than a normal tail.

The procedure for obtaining maximum stabilizing effect is:

(1) Design for maximum static stability as in "Static Stability of Coupled Fin and Rudder."

(2) Check the damping criteria as in "Summary of Damping Criteria."

(3) Maximize the damping effect by the procedure of "Optimum Proportions for Dynamic Stability," by mass balances of fin and rudder, and proper selection of surface contours, linkage ratio, etc.

(4) Low friction and free play are necessary for satisfactory results.

By use of the above methods, it is possible to design stabilizing surfaces that are many times more effective than fixed surfaces of equal area. For example, the following results may be expected from a good design:

$$\text{ratio of static stability } \frac{\text{coupled tail}}{\text{fixed tail}} = \left(1 + \tau\frac{\beta}{\psi}\right) > 8$$

(cf. "Static Stability of Coupled Fin and Rudder")

$$\text{ratio of time to damp to } 1/2 \text{ amplitude } \frac{\text{coupled tail}}{\text{fixed tail}} = {}^1/_2(H/K) > 6$$

(cf. Table 1)

When compared to a normal free rudder, with its downstream floating tendency, these ratios will be somewhat larger. The coupling linkage, in fact, causes a considerable *upstream* floating tendency.

The advantages of coupled surfaces are shown by these comparisons. Whereas a normal surface may give static stability in the free condition, the coupled surface, with the additional margin of static stability and increased damping, will restore equilibrium conditions much more quickly after displacement. It will behave essentially like an automatic stabilizer. For this reason, properly designed coupled surfaces may be called "automatic control surfaces."

ACKNOWLEDGMENT

The author wishes to express his gratitude to Mr. Mac Short, of Lockheed Aircraft Corporation, whose foresight and confidence made this investigation possible; to Drs. H. J. Stewart, N. O. Myklestad, and C. C. Lin, as well as to Bernard Rasof, of California Institute of Technology, for helpful aid regarding some of the mathematical interpretations; and to Prof. O. C. Koppen and Ben Drisko, of Massachusetts Institute of Technology, for many useful suggestions and encouragement.

REFERENCES

[1] von Kármán, T., and Biot, M. A., *Mathematical Methods in Engineering;* McGraw-Hill Book Company, Inc., New York, 1940.

[2] Den Hartog, J. P., *Mechanical Vibrations;* McGraw-Hill Book Company, Inc., New York, 1940.

[3] Jones, R. T., and Kleckner, H. F., *Theory and Preliminary Flight Tests of an All-Movable Vertical Tail Surface,* N.A.C.A., A.R.R., January, 1943.

[4] Smith, E. S., *Automatic Control Engineering;* McGraw-Hill Book Company, Inc., New York, 1944.

Changes of Address

To facilitate the prompt receipt of copies of the JOURNAL OF THE AERONAUTICAL SCIENCES, members and subscribers are requested to give the Institute 30 days' notice of any change of address.

Notices should be sent directly to:

Institute of the Aeronautical Sciences, Inc.
2 East 64th Street, New York 21, New York

Airplane Maneuvering Loads

E. C. POSNER*

Lockheed Aircraft Corporation

ABSTRACT

The tend in Army, Navy, and C.A.A. structural loading requirements is leading more and more toward rationalization. This involves the solution of the equations of motion to determine the dynamic response to certain arbitrary control surface movements. For example, the Army maneuvering tail load criterion depends on the airplane's response to a given control movement applied in a fraction of a second, held there for a certain time interval, and then reversed to some percentage of the maximum value. The time interval involved is determined so that the maximum load factor reached is equal to the airplane limit factor. Likewise, the new rolling criterion consists of the application in a given time interval of an aileron angle of such a magnitude that a specified helical angle of roll is attained during the resulting airplane response. The proposed C.A.A. vertical surface loading requirement consists of a rapid neutralization of the rudder angle at some rationally determined angle of sideslip.

All these maneuvers have certain aspects in common: namely, they consist of a sequence of linearly varying control movement, followed by a constant deflection, and require the solution of the airplane's equations of motion to determine the resulting response. Generalized graphical methods of analysis are available, but the author has found that the analytical methods are in general easier to apply. The analytical solution of these equations is presented here in a manner that it is hoped will be understandable to those not well versed with the mathematical theory involved. Rigor may therefore be sacrificed for the sake of clarity.

NOTATION

The following notation is similar to that used in standardized works on dynamic stability, such as references 2 and 3. It is therefore considered outside of the scope of this paper to go into the development of these derivatives, except for the derivative $M_{\dot{w}}$, which has not been generally used and needs some clarification.

x	=	longitudinal body axis—positive forward
y	=	lateral body axis—positive to right
z	=	vertical body axis—positive down
Z	=	force along z-axis, lbs.
L	=	moment about x-axis, lb. ft.
M	=	moment about y-axis, lb. ft.
N	=	moment about z-axis, lb. ft.
U	=	velocity along x-axis, ft. per sec.
v	=	velocity along y-axis, ft. per sec.
w	=	velocity along z-azis, ft. per sec.
$\dot{w}$	=	acceleration along z-axis, ft. per sec.^{2}
ϕ	=	angle of bank, rad.
θ	=	angle of pitch, rad.
ψ	=	angle of yaw, rad.
$\dot{\phi}$	=	angular velocity of roll, rad. per sec.
$\dot{\theta}$	=	angular velocity of pitch, rad. per sec.
$\dot{\psi}$	=	angular velocity of yaw, rad. per sec.
β	=	angle of sideslip = v/U, rad.
α	=	angle of attack = w/U, rad.
δ	=	control surface deflection, rad.
W	=	weight of airplane, lbs.
m	=	mass of airplane = W/g, slugs
ρ	=	air density, slugs per cu.ft.
S	=	wing area, sq.ft.
b	=	wing span, ft.
S_t	=	tail area, sq.ft.
l_t	=	tail length, ft.
t	=	time, sec.
μ	=	$m/\rho Sb$ = mass factor
ν	=	$m/\rho SU$ = time factor, sec.
p	=	nondimensional velocity of roll = $\dot{\phi}\nu$
q	=	nondimensional velocity of pitch = $\dot{\theta}\nu$
r	=	nondimensional velocity of yaw = $\dot{\psi}\nu$
τ	=	t/ν = nondimensional time
k	=	radius of gyration, ft.
ϵ	=	angle of downwash, rad.
η_t	=	tail efficiency = ratio of dynamic pressure at tail to free stream
Δn	=	load factor increment
ΔP_t	=	maneuvering tail load increment

Subscripts

e	=	elevator
r	=	rudder
a	=	aileron
t	=	tail
m	=	maximum

ALL THE ANGLES, velocities, and forces of the above notations are incremental values from the balanced condition at the start of the time history. An exception to this is the forward velocity, U, which is taken equal to the air speed at the start of the maneuver.

$$Z_w, L_p, L_\delta, M_w, M_{\dot{w}}, M_q, M_\delta, N_v, N_r = \frac{dZ}{dw}, \frac{dL}{d\phi}, \frac{dL}{d\delta}, \text{ etc.}$$

$$z_w = Z_w/\rho US = Z_w\nu/m$$
$$m_w = M_w b/\rho USk_y^2 = M_w\nu^2 U/mk_y^2\mu$$
$$m_{\dot{w}} = M_{\dot{w}}/\rho Sk_y^2 = M_{\dot{w}}\nu U/mk_y^2$$
$$m_q = M_q/\rho USk_y^2 = M_q\nu/mk_y^2$$
$$m_\delta = M_\delta b/\rho U^2Sk_y^2 = M_\delta\nu^2/mk_y^2\mu$$
$$n_v = N_v b/\rho USk_z^2 = N_v\nu^2 U/mk_z^2\mu$$
$$n_r = N_r/\rho USk_z^2 = N_r\nu/mk_z^2$$
$$n_\delta = N_\delta b/\rho U^2Sk_z^2 = N_\delta\nu^2/mk_z^2\mu$$
$$l_p = L_p/\rho USk_x^2 = L_p\nu/mk_x^2$$
$$l_\delta = L_\delta b/\rho U^2Sk_x^2 = L_\delta\nu^2/mk_x^2\mu$$

Derivation of $M_{\dot{w}}$:

$$M_t = -{}^1/_2\rho U_t^2 S_t l_t C_{L_t}$$
$$M_{\dot{w}} = dM/d\dot{w} = (dM/d\alpha_t)(d\alpha_t/d\dot{w})$$

But

$$\Delta\alpha_t = t_\epsilon\frac{d\epsilon}{dt} = \frac{l_t}{U_t}\left(\frac{d\epsilon}{d\alpha}\right)\left(\frac{d\alpha}{dw}\right)\left(\frac{dw}{dt}\right)$$

Received December 3, 1945.

* Aerodynamic Analysis—Group Engineer.

where t_e is the time for the downwash from the wing to reach the tail. Then

$$d\alpha_t/d\dot{w} = (l_t/U_t)(d\epsilon/d\alpha)(1/U)$$

and

$$dM/d\alpha_t = -{}^1/_2\rho U_t^2 S_t l_t (dC_{L_t}/d\alpha_t)$$

Hence,

$$M_{\dot{w}} = -{}^1/_2\rho\sqrt{\eta_t} S_t l_t^3 (dC_{L_t}/d\alpha_t)(d\epsilon/d\alpha)$$

Maneuvering Horizontal Tail Loads

In the following derivation of the horizontal maneuvering tail loads, the development is accompanied by generalized formulas so that the solution can be made applicable to dynamic problems of a more involved nature.

As described in the abstract, the maneuvering horizontal tail loads depend on the dynamic response of the airplane to certain elevator movements. It is therefore necessary to set up the pertinent differential equations of motion and integrate these before the tail loads can be calculated.

The response of the airplane to elevator deflections occurs in the longitudinal plane of symmetry and involves three degrees of freedom, x, z, and θ. The corresponding velocities are U, w and $\dot{\theta}$. However, the time interval during the part of the maneuver of interest is short so that the forward speed, U, can be regarded as constant. There then remain only two degrees of freedom and, hence, two equations of motion.

Motion along z-axis:

$$\text{force} = \text{mass} \times \text{acceleration}$$
$$wZ_w = m(\dot{w} - \dot{\theta}U) \tag{1}$$

Motion about y-axis:

$$\text{moment} = \text{moment of inertia} \times \text{angular acceleration}$$
$$\delta_e M_\delta + wM_w + \dot{w}M_{\dot{w}} + \dot{\theta}M_q = mk_y^2(d\dot{\theta}/dt) \tag{2}$$

The term $\dot{\theta}U$ represents the centrifugal acceleration due to the angular velocity of pitch, $\dot{\theta}$, and acts along the z-axis.

It is convenient to convert into nondimensional form by multiplying the first equation by ν/mU and the second by ν^2/mk_y^2. The resulting equations become

$$\alpha z_w = (d\alpha/d\tau) - q \tag{3}$$

$$\mu\delta_e m_\delta + \mu\alpha m_w + m_{\dot{w}}(d\alpha/d\tau) + qm_q = dq/d\tau \tag{4}$$

These are now placed in operator form by substituting d to represent the operation $d/d\tau$. The equations then become

$$(d - z_w)\alpha - q = 0 \tag{5}$$

$$-(m_{\dot{w}}d + \mu m_w)\alpha + (d - m_q)q = \mu m_\delta \delta_e \tag{6}$$

where δ_e is a function of τ.

The solution of these two simultaneous differential equations is arrived at by operating on each by a factor that enables elimination of one variable. Operating on Eq. (5) by $d - m_q$ and Eq. (6) by 1, then adding,

$$d^2\alpha + (-z_w - m_q - m_{\dot{w}})d\alpha + (z_w m_q - \mu m_w)\alpha = \mu m_\delta \delta_e \tag{7}$$

This procedure is identical to that which would be followed if d were an algebraic multiplier instead of an operator. It is therefore possible to generalize by obtaining Eq. (7) directly by means of determinants. The general formula for solution of Eqs. (5) and (6) is:

$$\alpha = [f_1(d)/F(d)]\,\delta_e(\tau) \tag{8}$$

and

$$q = [f_2(d)/F(d)]\,\delta_e(\tau) \tag{9}$$

where $F(d)$ is the determinant made up of the operators of the variables on the left-hand side of Eqs. (5) and (6):

$$\begin{vmatrix} d - z_w & -1 \\ -m_{\dot{w}}d - \mu m_w & d - m_q \end{vmatrix} = d^2 + (-z_w - m_q - m_{\dot{w}})d + (z_w m_q - \mu m_w)$$

$f_1(d)$ is the determinant with the right-hand coefficients substituted for the operators of α:

$$\begin{vmatrix} 0 & -1 \\ \mu m_\delta & d - m_q \end{vmatrix} = \mu m_\delta$$

$f_2(d)$ is the determinant with the right-hand coefficients substituted for the operators of q:

$$\begin{vmatrix} d - z_w & 0 \\ -m_{\dot{w}}d - \mu m_w & \mu m_\delta \end{vmatrix} = \mu m_\delta(d - z_w)$$

The expansion of the general determinant

$$\begin{vmatrix} A_1 & A_2 & A_3 \\ B_1 & B_2 & B_3 \\ C_1 & C_2 & C_3 \end{vmatrix}$$

is

$$A_1B_2C_3 + B_1C_2A_3 + C_1B_3A_2 - A_3B_2C_1 - B_3C_2A_1 - C_3B_1A_2$$

The solution for α is, hence,

$$\frac{\mu m_\delta \delta(\tau)}{d^2 + (-z_w - m_q - m_{\dot{w}})d + (z_w m_q - \mu m_w)} \tag{10}$$

and for q is

$$\frac{\mu m_\delta (d - z_w)\delta(\tau)}{d^2 + (-z_w - m_q - m_{\dot{w}})d + (z_w m_q - \mu m_w)} \tag{11}$$

The interpretation of Eqs. (10) and (11) requires explanation. It is first necessary to split up into partial fractions. This is done by the following expansion: Let

$$\frac{f(d)}{F(d)} = \frac{A}{d - \lambda_1} + \frac{B}{d - \lambda_2} + \frac{C}{d - \lambda_3} + \cdots$$

where $\lambda_1, \lambda_2, \lambda_3, \ldots$ are roots of $F(d) = 0$ so that $F(d) = (d - \lambda_1)(d - \lambda_2)(d - \lambda_3) \ldots$.

Cross-multiplying,

$$f(d) = A(d - \lambda_2)(d - \lambda_3) \ldots + B(d - \lambda_1)(d - \lambda_3) \ldots + C(d - \lambda_1)(d - \lambda_2) \ldots$$

But

$$F'(d) = (d - \lambda_2)(d - \lambda_3) \ldots + (d - \lambda_1)(d - \lambda_3) \ldots + (d - \lambda_1)(d - \lambda_2) \ldots$$

and

$$F'(\lambda_1) = (d - \lambda_2)(d - \lambda_3) \ldots$$
$$F'(\lambda_2) = (d - \lambda_1)(d - \lambda_3) \ldots$$
$$F'(\lambda_3) = (d - \lambda_1)(d - \lambda_2) \ldots$$

Also

$$f(\lambda_1) = A(d - \lambda_2)(d - \lambda_3) \ldots$$
$$f(\lambda_2) = B(d - \lambda_1)(d - \lambda_3) \ldots$$
$$f(\lambda_3) = C(d - \lambda_1)(d - \lambda_2) \ldots$$

Hence,

$$A = \frac{f(\lambda_1)}{F'(\lambda_1)}, \quad B = \frac{f(\lambda_2)}{F'(\lambda_2)}, \quad C = \frac{f(\lambda_3)}{F'(\lambda_3)}, \text{ etc.}$$

Then

$$f(d)/F(d) = \sum_{\lambda_1}^{\lambda_n} f(\lambda)/F'(\lambda)(d - \lambda) \qquad (12)$$

This is known as Heaviside's expansion theorem. It should be noted that it breaks down when two roots of $F(d) = 0$ are equal, in which case other methods of approach must be used.

The integration of each term of this expansion is obtained as follows for each phase of the elevator movement. The first phase is assumed to consist of a linear variation of elevator angle with time until the time, τ_0, is reached, while the second phase consists of a constant deflection starting from time, τ_0.

Linear Elevator Deflection, $\delta(\tau) = K\tau$

Let

$$u = \tau/(d - \lambda)$$
$$(du/d\tau) - \lambda u = \tau$$
$$(d/d\tau)(e^{-\lambda\tau}u) = e^{-\lambda\tau}\tau$$
$$e^{-\lambda\tau}u\Big]_0^\tau = \int_0^\tau e^{-\lambda\tau}\tau d\tau = -(e^{-\lambda\tau}/\lambda^2)(\lambda\tau + 1)\Big]_0^\tau$$
$$e^{-\lambda\tau}u = (1/\lambda^2) - (e^{-\lambda\tau}/\lambda^2)(\lambda\tau + 1)$$
$$u = (e^{\lambda\tau} - \lambda\tau - 1)/\lambda^2$$

Hence,

$$\frac{f(d)}{F(d)} K\tau = K \sum_{\lambda_1}^{\lambda_n} \frac{f(\lambda)}{\lambda^2 F'(\lambda)} (e^{\lambda\tau} - \lambda\tau - 1) \qquad (13)$$

and

$$\alpha = K\mu m_\delta \left[\frac{e^{\lambda_1\tau} - \lambda_1\tau - 1}{\lambda_1^2(2\lambda_1 + B)} + \frac{e^{\lambda_2\tau} - \lambda_2\tau - 1}{\lambda_2^2(2\lambda_2 + B)} \right] \qquad (14)$$

where $F(d) = d^2 + Bd + C$, $F'(d) = 2d + B$, and $f_1(\lambda) = \mu m_\delta$.

It should be noted that the dependent variable u is assumed zero when the independent variable τ is zero. Where the boundary conditions of the problem are such that this is not true, then Eq. (13) does not apply.

Constant Elevator Deflection Starting from Time, τ_0, $\delta(\tau) = K\tau_0$

This phase of the motion can be considered to be made up of the difference between the linear motions $K\tau$ and $K(\tau - \tau_0)$. Hence,

$$f(d)/F(d)[K\tau - K(\tau - \tau_0)] = K \sum_{\lambda_1}^{\lambda_n} \frac{f(\lambda)}{\lambda^2 F'(\lambda)} \{ [e^{\lambda\tau} - \lambda\tau - 1] - [e^{\lambda(\tau - \tau_0)} - \lambda(\tau - \tau_0) - 1] \} = K \sum_{\lambda_1}^{\lambda_n} \frac{f(\lambda)}{\lambda^2 F'(\lambda)} \times [e^{\lambda\tau}(1 - e^{-\lambda\tau_0}) - \lambda\tau_0] \qquad (15)$$

and

$$\alpha = K\mu m_\delta \left[\frac{e^{\lambda_1\tau}(1 - e^{-\lambda_1\tau_0}) - \lambda_1\tau_0}{\lambda_1^2(2\lambda_1 + B)} + \frac{e^{\lambda_2\tau}(1 - e^{-\lambda_1\tau_0}) - \lambda_2\tau_0}{\lambda_2^2(2\lambda_2 + B)} \right] \qquad (16)$$

When the roots λ_1 to λ_n are real, the development of Eqs. (13) and (15) is straight forward. However if, a root is complex, there is another root that is its conjugate and the solutions must be converted into trigonometric form. This is done by converting all the complex terms into exponential form, combining, and then converting into trigonometric form. This can best be illustrated by going back to the original problem of Eq. (10). Here

$$F(d) = d^2 + Bd + C$$

where $B = -(z_w + m_q + m_{\dot{w}})$ and $C = z_w m_q - \mu m_w$. If the roots of $F(d) = 0$ are complex quantities, let

$$\lambda_1 = a + bi; \quad \lambda_2 = a - bi$$

But

$$\lambda = -(B/2) \pm \sqrt{(B/2)^2 - C}$$

Hence, $a = -B/2$ and $b = \sqrt{C - a^2}$ or $a^2 + b^2 = C$, and

$$F'(d) = 2d + B$$
$$F'(\lambda) = 2(a \pm bi) - 2a = \pm 2bi$$
$$f_1(d) = f_1(\lambda) = \mu m_\delta$$

Hence, for the elevator motion $\delta(\tau) = K\tau$, from Eq (14),

$$\alpha = K\mu m_\delta \left[\frac{e^{(a+bi)\tau} - (a + bi)\tau - 1}{(a + bi)^2 2bi} + \frac{e^{(a-bi)\tau} - (a - bi)\tau - 1}{-(a - bi)^2 2bi} \right] \qquad (17)$$

But the complex number $a + bi$ expressed in polar form is

$$\sqrt{a^2 + b^2}\,(\cos\gamma + i\sin\gamma)$$

where

$$\gamma = \tan^{-1}(b/a) = \sin^{-1}(b/\sqrt{C})$$

Also the trigonometric functions can be expressed in exponential form as follows:

$$\cos\gamma = (e^{i\gamma} + e^{-i\gamma})/2$$
$$\sin\gamma = (e^{i\gamma} - e^{-i\gamma})/2i$$

or $\cos\gamma + i\sin\gamma = e^{i\gamma}$, and $\cos\gamma - i\sin\gamma = e^{-i\gamma}$. Hence,

$$a + bi = \sqrt{C}e^{i\gamma}$$
$$a - bi = \sqrt{C}e^{-i\gamma}$$
$$(a + bi)^2 = Ce^{2i\gamma}$$
$$(a - bi)^2 = Ce^{-2i\gamma}$$

---

and

$$\alpha = K\mu m_\delta\left[\frac{e^{a\tau}e^{ib\tau} - \sqrt{C}\tau e^{i\gamma} - 1}{Ce^{2i\gamma}2bi} + \frac{e^{a\tau}e^{-ib\tau} - \sqrt{C}\tau e^{-i\gamma} - 1}{-Ce^{-2i\gamma}2bi}\right]$$

$$= K\mu m_\delta\left[\left(\frac{e^{a\tau}}{bC}\right)\left(\frac{e^{i(b\tau-2\gamma)} - e^{-i(b\tau-2\gamma)}}{2i}\right) - \left(\frac{\tau}{b\sqrt{C}}\right)\left(\frac{e^{-i\gamma} - e^{i\gamma}}{2i}\right) - \frac{e^{-2i\gamma} - e^{2i\gamma}}{bC2i}\right]$$

$$= K\mu m_\delta\left[\frac{e^{a\tau}}{bC}\sin(b\tau - 2\gamma) + \frac{\tau}{b\sqrt{C}}\sin\gamma + \frac{1}{bC}\sin 2\gamma\right]$$

$$= K\mu m_\delta\left[\frac{e^{a\tau}}{bC}\sin(b\tau - 2\gamma) + \frac{\tau}{C} + \frac{*2a}{C^2}\right] \tag{18}$$

For the elevator motion $\delta(\tau) = K\tau - K(\tau - \tau_0)$, from Eq. (16),

$$\alpha = K\mu m_\delta\left[\frac{e^{(a+bi)\tau}(1 - e^{-(a+bi)\tau_0}) - (a + bi)\tau_0}{(a + bi)^2\,2bi} + \frac{e^{(a-bi)\tau}(1 - e^{-(a-bi)\tau_0}) - (a - bi)\tau_0}{-(a - bi)^2\,2bi}\right] \tag{19}$$

$$= K\mu m_\delta\left[\left(\frac{e^{a\tau}}{Cb}\right)\left(\frac{e^{i(b\tau-2\gamma)} - e^{-i(b\tau-2\gamma)}}{2i}\right) - \left(\frac{e^{a(\tau-\tau_0)}}{Cb}\right)\left(\frac{e^{i[b(\tau-\tau_0)-2\gamma]} - e^{-i[b(\tau-\tau_0)-2\gamma]}}{2i}\right) - \left(\frac{\tau_0}{b\sqrt{C}}\right)\left(\frac{e^{-i\gamma} - e^{i\gamma}}{2i}\right)\right]$$

$$= K\mu m_\delta\left\{\frac{e^{a\tau}}{bC}\sin(b\tau - 2\gamma) - \frac{e^{a(\tau-\tau_0)}}{bC}\sin[b(\tau - \tau_0) - 2\gamma] + \frac{\tau_0}{C}\right\}$$

$$= K\mu m_\delta\frac{e^{a(\tau-\tau_0)}}{bC}[\sin(b\tau - 2\gamma)(e^{a\tau_0} - \cos b\tau_0) + \cos(b\tau - 2\gamma)\sin b\tau_0] + K\mu m_\delta\frac{\tau_0}{C}$$

$$= K\mu m_\delta[(Ee^{a(\tau-\tau_0)}/bC)\sin(b\tau - 2\gamma + \xi) + (\tau_0/C)] \tag{20}$$

where

$$\xi = \tan^{-1}[\sin b\tau_0/(e^{a\tau_0} - \cos b\tau_0)] = \sin^{-1}(\sin b\,\tau_0/E)$$

and

$$E = \sqrt{(e^{a\tau_0} - \cos b\tau_0)^2 + \sin^2 b\tau_0} = \sqrt{e^{2a\tau_0} - 2e^{a\tau_0}\cos b\tau_0 + 1}$$

The load factor increment Δn can be derived from the angle of attack increment α by the following relation:

$$\Delta n = (\rho/2)SU^2\left(\frac{dC_L}{d\alpha}\right)\left(\frac{\alpha}{W}\right) = \frac{1}{2}\left(\frac{dC_L}{d\alpha}\right)\left(\frac{\rho SU}{m}\right)\left(\frac{U}{g}\right)\alpha = -\frac{z_w U\alpha}{\nu g} \tag{21}$$

Knowing the angle of attack increment α as a function of nondimensional time τ from Eqs. (14) and (16) if roots are real or Eqs. (18) and (20) if roots are complex, it is possible to construct a load factor versus time curve and choose the time increment $\Delta\tau$ so that the limit load factor is just reached.

The curve 0-1-2-4-5 of Fig. 1 is obtained by adding the respective load factor curves corresponding to the elevator deflection 0-1-2-3 and the reversal motion 2-4-5.

Once the time interval $\Delta\tau$ is determined from the above plot, the tail loads can be easily obtained from the following relation:

$$\Delta P_t = \eta_t(dC_L/d\alpha)_t(\rho/2)U^2S_t\alpha_t \tag{22}$$

---

* $\sin 2\gamma = 2\sin\gamma\cos\gamma = 2ba/C$

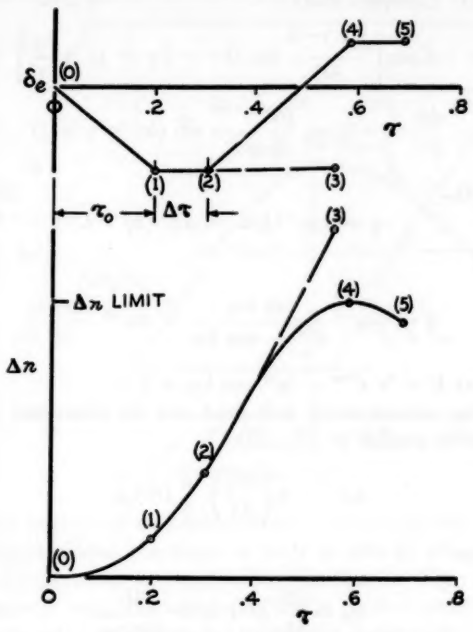

FIG. 1. Elevator and load factor time history.

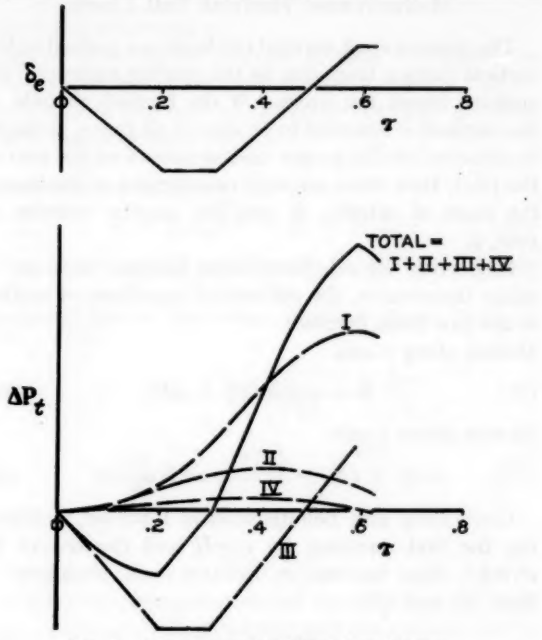

FIG. 2. Elevator and tail load time history.

where

$$\alpha_t = \left(\frac{d\alpha_t}{d\delta_e}\right)\delta_e + \left(1 - \frac{d\epsilon}{d\alpha}\right)\alpha + \frac{\dot{\theta} l_t}{U\sqrt{\eta_t}} + \left(\frac{d\epsilon}{d\alpha}\right)\left(\frac{d\alpha}{dt}\right)\left(\frac{l_t}{U}\right) \tag{23}$$

and $\dot{\theta} = q/v = (d\alpha/vd\tau) - (\alpha z_w/v)$ from Eq. (3).

The rate of change of angle of attack with time, $d\alpha/dt = d\alpha/vd\tau$, can be obtained by differentiation of the expression for α. From Eq. (14).

$$d\alpha/d\tau = K\mu m_\delta \textstyle\sum_{\lambda_1}^{\lambda_2} (e^{\lambda\tau} - 1)/\lambda(2\lambda + B) \tag{24}$$

From Eq. (16)

$$d\alpha/d\tau = K\mu m_\delta \textstyle\sum_{\lambda_1}^{\lambda_2} e^{\lambda\tau}(1 - e^{-\lambda\tau_0})/\lambda(2\lambda + B) \tag{25}$$

From Eq. (18)

$$\frac{d\alpha}{d\tau} = K\mu m_\delta\left[\frac{be^{a\tau}}{bC}\cos(b\tau - 2\gamma) + \frac{ae^{a\tau}}{bC}\sin(b\tau - 2\gamma) + \frac{1}{C}\right] = K\mu m_\delta\left[\frac{e^{a\tau}}{b\sqrt{C}}\sin(b\tau - \gamma) + \frac{1}{C}\right] \tag{26}$$

From Eq. (20)

$$\frac{d\alpha}{d\tau} = K\mu m_\delta\left[\frac{Eae^{a(\tau-\tau_0)}}{bC}\sin(b\tau - 2\gamma + \xi) + \frac{Ebe^{a(\tau-\tau_0)}}{bC}\cos(b\tau - 2\gamma + \xi)\right] =$$

$$K\mu m_\delta \frac{Ee^{a(\tau-\tau_0)}}{b\sqrt{C}}\sin(b\tau - \gamma + \xi) \tag{27}$$

The plot of Fig. 2 shows the tail load time history due to the elevator motion of Fig. 1. The tail load due to the respective components of Eq. (23) are shown. I is due to the airplane angle of attack corrected for down-wash at the tail; II is due to the angular velocity of pitch, or damping load; III is due to the elevator deflection; and IV is due to the time lag of the down-wash in reaching the tail.

It is evident that critical down tail load occurs at the start when the elevator is first fully deflected and the airplane has not had time to build up a positive angle of attack at the tail. The critical up load occurs when the elevator is reversed, since here, in addition to the load due down elevator, the angle of attack on the tail due to load factor is at its maximum and there is an appreciable damping load in the same direction.

Maneuvering Vertical Tail Loads

The maneuvering vertical tail loads are defined as the vertical surface loads due to the yawing motion of the airplane about the z-axis. If the banked altitude of the airplane is assumed to be zero at all times, as might be obtained by the proper aileron control on the part of the pilot, then there are only two degrees of freedom—the angle of sideslip, β, and the angular velocity of yaw, $\dot{\psi}$.

Neglecting the side-force terms because these are of minor importance, the differential equations of motion in the yaw plane becomes:

Motion along y-axis

$$0 = m[(dv/dt) + \dot{\psi}U] \tag{28}$$

Motion about z-axis

$$\delta_r N_\delta + vN_v + \dot{\psi}N_r = mk_z^2(d\dot{\psi}/dt) \tag{29}$$

Converting into nondimensional form by multiplying the first equation by v/mU and the second by v^2/mk_z^2, these become, in operator form, analogous to Eqs. (5) and (6)

$$d\beta + r = 0 \tag{30}$$

$$-(\mu n_v)\beta + (d - n_r)r = \mu n_\delta \delta_r \tag{31}$$

where δ_r is a function of τ.

It will be noted that these equations are similar to Eqs. (5) and (6) in that they are of second order with respect to β, and $f_1(d)$ is $-\mu n_\delta$ instead of μm_δ. Hence, the solution for β and $d\beta/d\tau$ can be written down directly by comparing with the solutions for α and $d\alpha/d\tau$ in Eqs. (14), (16), (18), and (20) and (24), (25), (26), and (27).

Linear Rudder Deflection, $\delta(\tau) = K\tau$

(a) Real roots

$$\beta = -K\mu n_\delta \sum_{\lambda_1}^{\lambda_2} \frac{e^{\lambda\tau} - \lambda\tau - 1}{\lambda^2(2\lambda + B)} \tag{32}$$

$$\frac{d\beta}{d\tau} = -K\mu n_\delta \sum_{\lambda_1}^{\lambda_2} \frac{e^{\lambda\tau} - 1}{\lambda(2\lambda + B)} \tag{33}$$

(b) Complex roots

$$\beta = -K\mu n_\delta \left[\frac{e^{a\tau}}{bC}\sin(b\tau - 2\gamma) + \frac{\tau}{C} + \frac{2a}{C^2}\right] \tag{34}$$

$$\frac{d\beta}{d\tau} = -K\mu n_\delta \left[\frac{e^{a\tau}}{b\sqrt{C}}\sin(b\tau - \gamma) + \frac{1}{C}\right] \tag{35}$$

Constant Rudder Deflection Starting from Time, τ_0, $\delta(\tau) = K\tau_0$

(a) Real roots

$$\beta = -K\mu n_\delta \sum_{\lambda_1}^{\lambda_2} \frac{e^{\lambda\tau}(1 - e^{-\lambda\tau_0}) - \lambda\tau_0}{\lambda^2(2\lambda + B)} \tag{36}$$

$$\frac{d\beta}{d\tau} = -K\mu n_\delta \sum_{\lambda_1}^{\lambda_2} \frac{e^{\lambda\tau}(1 - e^{-\lambda\tau_0})}{\lambda(2\lambda + B)} \tag{37}$$

(b) Complex roots

$$\beta = -K\mu n_\delta \left[\frac{Ee^{a(\tau-\tau_0)}}{bC}\sin(b\tau - 2\gamma + \xi) + \frac{\tau_0}{C}\right] \tag{38}$$

$$\frac{d\beta}{d\tau} = -K\mu n_\delta \frac{Ee^{a(\tau-\tau_0)}}{b\sqrt{C}}\sin(b\tau - \gamma + \xi) \tag{39}$$

where

$$\gamma = \tan^{-1} b/a = \sin^{-1} b/\sqrt{C}$$

and

$$\xi = \tan^{-1}\frac{\sin b\tau_0}{e^{a\tau_0} - \cos b\tau_0} = \sin^{-1}\frac{\sin b\tau_0}{E}$$

where $E = \sqrt{e^{2a\tau_0} - 2e^{a\tau_0}\cos b\tau_0 + 1}$.

The maneuvering tail load can be expressed in a manner similar to Eq. (22)

$$\Delta P_t = \eta_t\left(\frac{dC_L}{d\beta}\right)_t \frac{\rho}{2} U^2 S_t \beta_t \tag{40}$$

where

$$\beta_t = \frac{d\beta_t}{d\delta_r}\delta_r + \beta + \frac{\dot{\psi}l_t}{U\sqrt{\eta_t}} \tag{41}$$

and $\dot{\psi} = (r/v) - (d\beta/vd\tau)$ from Eq. (30).

It is desirable to derive an expression for the maximum angle of sideslip developed in the oscillation resulting from a given rudder deflection. This is done by equatin Eq. (39) to zero and substituting the resulting value for τ back in Eq. (38).

$$b\tau_m - \gamma + \xi = n\pi$$
$$\tau_m = (n\pi + \gamma - \xi)/b \tag{42}$$

where n is the lowest positive integer that makes τ_m greater than τ_0. Hence,

$$\beta_m = -K\mu n_\delta\left[\frac{Ee^{a(\tau_m-\tau_0)}}{bc}\sin(n\pi - \gamma) + \frac{\tau_0}{C}\right]$$
$$= -K\mu n_\delta\left(\frac{Ee^{a(\tau_m-\tau_0)}}{C\sqrt{C}} + \frac{\tau_0}{C}\right) \tag{43}$$

From Eq. (31) the value for the equilibrium angle

$$\beta_0 = -n_\delta K\tau_0/n_v \tag{44}$$

Hence,

$$\frac{\beta_m}{\beta_0} = \frac{\mu n_v}{\tau_0}\left[\frac{Ee^{a(\tau_m-\tau_0)}}{C\sqrt{C}} + \frac{\tau_0}{C}\right] = \frac{Ee^{a(\tau_m-\tau_0)}}{\tau_0\sqrt{C}} + 1 \tag{45}$$

A typical time history of β/β_0 is shown in Fig. 3 for a large conventional airplane. The locus of β_m/β_0 is also plotted for varying rudder deflection times, τ_0. It is interesting to note that the maximum angle of sideslip exceeds the equilibrium value by over 50 per cent for instantaneous rudder deflections and drops off slowly with increasing values of τ_0. It therefore appears necessary to consider the time history in strength calculations even in the case of slowly applied rudder.

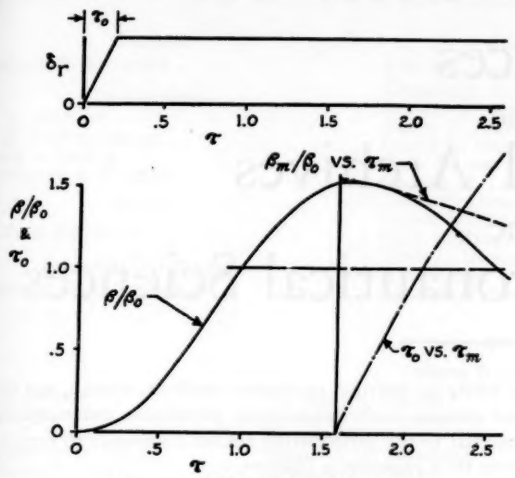

FIG. 3. Slideslip time history.

The neglect of side-force terms in Eq. (28) and the assumption that the angle of bank is zero at all times are conservative approximations as far as Fig. 3 is concerned, since the side force due to bank is restoring as well as the side force due to sideslip, both tending to reduce the maximum angle of sideslip.

MANEUVERING ROLLING LOADS

The maneuvering rolling loads are defined as the loads due to rolling motion about the x-axis. The rolling motion is produced by the application of a given aileron angle in a specified time, τ_0, and held constant thereafter. If the yawing moments induced by the aileron deflection and velocity of roll are considered balanced out by the rudder at all times, then there is only one degree of freedom involved, the angular velocity of roll, $\dot{\phi}$.

The corresponding differential equation in roll is:

Motion about x-axis

$$\delta_a L_\delta + \dot{\phi} L_p = m k_x^2 (d\dot{\phi}/dt) \tag{46}$$

Converting into nondimensional form by multiplying by v^2/mk_x^2, this becomes, in operator form, analogous to Eqs. (6) and (31).

$$(d - l_p)p = \mu l_\delta \delta_a \tag{47}$$

where δ_a is a function of τ.

By reference to the formulas already developed, the solution for p can be written down directly. Here, there is only one root of the complimentary equation and it therefore must be real.

Linear Aileron Deflection, $\delta(\tau) = K\tau$

$$p = K\mu l_\delta (e^{l_p \tau} - l_p \tau - 1)/l_p^2 \tag{48}$$

$$dp/d\tau = K\mu l_\delta (e^{l_p \tau} - 1)/l_p \tag{49}$$

Constant Aileron Deflection Starting From Time τ_0, $\delta(\tau) = K\tau_0$

$$p = K\mu l_\delta \frac{e^{l_p \tau}(1 - e^{-l_p \tau_0}) - l_p \tau_0}{l_p^2} \tag{50}$$

$$\frac{dp}{d\tau} = K\mu l_\delta \frac{e^{l_p \tau}(1 - e^{-l_p \tau_0})}{l_p} \tag{51}$$

CONCLUSION

It has been demonstrated that the maneuvering loads due to motions about all three axes of the airplane can be readily determined analytically for a sequence of control movement varying linearly with time up to a specified value and then held constant. The general formulas may be applied to any other type of motion that has a solution for the operation of Eq. (12). However, it will be found that, in general, the linear sequence is most adaptable to the limitations such as set up in the maneuvering horizontal tail load problem.

REFERENCES

[1] Jones, Robert T., *A Simplified Application of the Method of Operators to the Calculation of Disturbed Motions of an Airplane*, N.A.C.A. T. R. No. 560.

[2] Glauert, H., *A Non-Dimensional Form of Stability Equations for an Airplane*, British Air Ministry, R. & M. No. 1093.

[3] Bryant, T. W., and Gates, S. B., *Nomenclature for Stability Coefficients*, British Air Ministry, R. & M. No. 1803.

[4] Pearson, H. A., and Jones, P. T., *Theoretical Stability and Control Characteristics of Wings with Various Amounts of Taper and Twist*, N.A.C.A. T. R. No. 635.

Services of the Aeronautical Archives of the Institute of the Aeronautical Sciences

The services of the Aeronautical Archives are available to all members of the Institute, to Corporate Members, to advertisers in the AERONAUTICAL ENGINEERING REVIEW and, under usual library limitations, to the public. Four specialized services are available.

The Paul Kollsman Lending Library

This lending library service makes available, *without charge*, the latest and more important aeronautical books.

Members may request the loan of any aeronautical or technical book they wish to borrow. Through an exchange agreement with the Engineering Societies Library, any book on general engineering may be borrowed from its great collection of over 160,000 volumes.

A photostating service is available at usual library rates.

Applications for membership in the library and further information will be sent on request.

The W. A. M. Burden Reference Library

This reference library contains over 12,000 aeronautical books, magazines, pamphlets, and reports gathered from world-wide sources and is one of the most complete aeronautical libraries in the world. Material from this library is not available for loan but may be used for reference purposes at the Aeronautical Archives.

The Pacific Aeronautical Library

6715 Hollywood Boulevard
Hollywood 28, California

Established in cooperation with the aircraft companies the library serves. The leading aircraft companies in or near Los Angeles participate in its support and operation.

This service library for aeronautical research is available to the public for reading privileges. Source material includes aerodynamic and structural research reports, as well as books on drafting, production methods, history, and allied sciences. It furnishes books, periodicals, and pamphlet material to the participating aircraft companies to supplement their engineering libraries.

The Aeronautical Archives Technical Information Service

This service has experienced personnel under the supervision of trained aeronautical engineers to compile any information desired. The services range from listing specialized reference books to the preparation of exhaustive bibliographies, digesting of reports, and general surveys of any aeronautical subject. Some of the available services are:

Bibliographies on any aeronautical subject.
Reports on any aeronautical subject.
Digests of aeronautical books, papers, periodicals, and references.
Translations.
Engineering investigations of special aeronautical subjects.
Biographies of individuals engaged in aeronautics.
Photostats of any aeronautical or general engineering material.
Microfilms made on special order.
Photographs made from the Institute's photographic collection.
Drawings and tracings made.

In addition to the services mentioned any commission which comes within the scope of the Service will be accepted. Special arrangements may be made for work requiring several weeks or months.

Translators are available for accurate transcriptions of all foreign language data. Translations are carefully edited by trained engineers.

Reproductions of any material in the Aeronautical Archives of the Institute may be ordered at standard photostat rates.

INSTITUTE OF THE AERONAUTICAL SCIENCES, INC.
2 EAST 64TH STREET, NEW YORK 21, N.Y.

INSTITUTE of the AERONAUTICAL SCIENCES

President
ARTHUR E. RAYMOND

Vice-Presidents
P. R. BASSETT
J. H. KINDELBERGER
JOHN C. LESLIE
BURDETTE S. WRIGHT

Director
S. PAUL JOHNSTON

Executive Vice-President
BENNETT H. HORCHLER

Past-Presidents
J. C. HUNSAKER
CHARLES L. LAWRANCE
DONALD W. DOUGLAS
GLENN L. MARTIN
CLARK B. MILLIKAN
T. P. WRIGHT
GEORGE W. LEWIS
JAMES H. DOOLITTLE
FRANK W. CALDWELL
HALL L. HIBBARD
HUGH L. DRYDEN
R. H. FLEET
CHARLES H. COLVIN

Assistant to the President
GEORGE R. FORMAN

Secretary
ROBERT R. DEXTER

Treasurer
C. S. JONES

Controller
JOSEPH J. MAITAN

COUNCIL

LESTER D. GARDNER, *Chairman*

E. E. ALDRIN
PETER ALTMAN
REX B. BEISEL
LAWRENCE D. BELL
GEORGE W. BRADY
W. A. M. BURDEN
CHARLES H. COLVIN
JAMES H. DOOLITTLE
WILLIAM K. EBEL
SHERMAN M. FAIRCHILD
DONALD W. FINLAY
CHARLES FROESCH
LEROY R. GRUMMAN
R. PAUL HARRINGTON
W. WALLACE KELLETT
OTTO E. KIRCHNER
JEROME LEDERER
ROBERT J. MINSHALL
EARL D. OSBORN
ELMER A. SPERRY, JR.
ERNEST G. STOUT
FRED E. WEICK

ADVISORY COMMITTEE

W. M. ALLEN
WALTER BEECH
ERNEST R. BREECH
RALPH S. DAMON
DONALD W. DOUGLAS
R. H. FLEET
JACK FRYE
ROBERT E. GROSS
R. M. HAZEN
H. MANSFIELD HORNER
J. C. HUNSAKER
CROIL HUNTER
TH. VON KÁRMÁN
I. M. LADDON
P. W. LITCHFIELD
F. W. MAGIN
ALFRED MARCHEV
GLENN L. MARTIN
THOMAS A. MORGAN
R. C. MUIR
JOHN K. NORTHROP
W. A. PATTERSON
E. T. PRICE
F. W. REICHELDERFER
LAURANCE S. ROCKEFELLER
FRED H. ROHR
T. CLAUDE RYAN
GUY W. VAUGHAN
EDWARD P. WARNER

HONORARY MEMBERS

JOHN C. ADAMS
GRIFFITH BREWER
W. A. M. BURDEN
E. U. CONDON
L. C. CRAIGIE
IRA C. EAKER
HARRY F. GUGGENHEIM
HENRY G. HOUGHTON
GEORGE C. KENNEY
CURTIS E. LE MAY
GEORGE B. PEGRAM
E. M. POWERS
J. LAURENCE PRITCHARD
ARTHUR W. RADFORD
F. W. REICHELDERFER
L. B. RICHARDSON
H. B. SALLADA
CARL SPAATZ
L. C. STEVENS
NATHAN F. TWINING

HONORARY FELLOWS

H. H. ARNOLD
DONALD W. DOUGLAS
HUGH L. DRYDEN
W. F. DURAND
SIR RICHARD FAIREY
SIR ROY FEDDEN
J. C. HUNSAKER
SIR MELVILL JONES
GEORGE W. LEWIS
GLENN L. MARTIN
GEORGE J. MEAD
SIR FREDERICK HANDLEY PAGE
D. R. PYE
IGOR I. SIKORSKY
G. I. TAYLOR
TH. VON KÁRMÁN
EDWARD P. WARNER
ORVILLE WRIGHT
T. P. WRIGHT

BENEFACTORS

E. E. ALDRIN
HART O. BERG (Deceased)
W. A. M. BURDEN
E. L. CORD
DONALD W. DOUGLAS
SHERMAN M. FAIRCHILD
SIR RICHARD FAIREY
R. H. FLEET
FLORENCE GUGGENHEIM (Deceased)
C. D. HANSCOM
JOHN P. V. HEINMULLER
ALEXANDER KLEMIN
PAUL KOLLSMAN
BELLA C. LANDAUER
WILLIAM LANDAUER
GROVER LOENING
EDMUND C. LYNCH (Deceased)
F. W. MAGIN
GLENN L. MARTIN
GEORGE J. MEAD
S. A. REED (Deceased)
LAURANCE S. ROCKEFELLER
EDWARD P. WARNER

AMERICAN FELLOWS

JOHN D. ACKERMAN
E. E. ALDRIN
HARRY G. ARMSTRONG
KARL ARNSTEIN
J. L. ATWOOD
PAUL S. BAKER
RALPH S. BARNABY
P. R. BASSETT
WELLWOOD E. BEALL
REX B. BEISEL
G. M. BELLANCA
DON R. BERLIN
HENRY A. BERLINER
WILLIAM BOLLAY
B. C. BOULTON
GEORGE W. BRADY
LYMAN J. BRIGGS
W. G. BROMBACHER
CHARLES P. BURGESS
FRANK W. CALDWELL
KENNETH CAMPBELL
CHARLES H. CHATFIELD
ALLAN CHILTON
V. E. CLARK
FRANKLIN R. COLLBOHM
CHARLES H. COLVIN
KARL T. COMPTON
JOHN W. CROWLEY, JR.
RALPH S. DAMON
LUIS DE FLOREZ
SMITH J. DE FRANCE
J. P. DEN HARTOG
WALTER S. DIEHL
JAMES H. DOOLITTLE
C. S. DRAPER
IVAN H. DRIGGS
WILLIAM K. EBEL
C. L. EGTVEDT
FREDERIC FLADER
CHARLES FROESCH
JACK FRYE
GARLAND FULTON
LESTER D. GARDNER
RICHARD C. GAZLEY
MICHAEL E. GLUHAREFF
MELVIN N. GOUGH
LEROY R. GRUMMAN
HAROLD R. HARRIS
R. M. HAZEN
ALBERT F. HEGENBERGER
EDWARD H. HEINEMANN
S. D. HERON
HALL L. HIBBARD
L. S. HOBBS
PAUL E. HOVGAARD
WILLIAM HOVGAARD
ROBERT INSLEY
EASTMAN N. JACOBS
CLARENCE L. JOHNSON
ALEXANDER KARTVELI
PAUL H. KEMMER
J. H. KINDELBERGER
OTTO E. KIRCHNER
ARTHUR L. KLEIN
ALEXANDER KLEMIN
W. B. KLEMPERER
PAUL KOLLSMAN
OTTO C. KOPPEN
B. V. KORVIN-KROUKOVSKY
S. M. KRAUS
I. M. LADDON
B. S. LAND
CHARLES L. LAWRANCE
JOHN G. LEE
JOHN C. LESLIE
CHARLES A. LINDBERGH
WILLIAM LITTLEWOOD
GROVER LOENING
W. RANDOLPH LOVELACE, II
EUGENE E. LUNDQUIST
R. D. MACCART
JOHN R. MARKHAM
ERLE MARTIN
WM. H. MCAVOY
C. J. MCCARTHY
CLARK B. MILLIKAN
ROBERT J. MINSHALL
SANFORD A. MOSS
JOSEPH S. NEWELL
ALFRED S. NILES
JOHN K. NORTHROP
ARTHUR NUTT
SHATSWELL OBER
ROBERT R. OSBORN
W. BAILEY OSWALD
GEORGE A. PAGE, JR.
F. W. PAWLOWSKI
F. W. PENNOYER, JR.
A. A. PRIESTER
ARTHUR E. RAYMOND
F. W. REICHELDERFER
ELLIOTT G. REID
H. J. E. REID
H. C. RICHARDSON
LEONARD E. ROOT
C. E. ROSENDAHL
WILLIAM T. SCHWENDLER
JAMES M. SHOEMAKER
MAC SHORT
IGOR ALEXIS SIKORSKY
SELDEN B. SPANGLER
ELMER A. SPERRY, JR.
JOHN STACK
WILLIAM B. STOUT
HARRY A. SUTTON
C. FAYETTE TAYLOR
EDWARD S. TAYLOR
PHILIP B. TAYLOR
TH. THEODORSEN
T. E. TILLINGHAST
S. TIMOSHENKO
STARR TRUSCOTT
L. B. TUCKERMAN
RALPH H. UPSON
J. G. VINCENT
RICHARD VON MISES
FRANK L. WATTENDORF
P. V. H. WEEMS
FRED E. WEICK
R. D. WEYERBACHER
JOHN B. WHEATLEY
ANDREW V. WILLGOOS
DONALD H. WOOD
ROBERT J. WOODS
JOHN E. YOUNGER
ALBERT F. ZAHM
STEPHEN J. ZAND

An Appreciation

TO CORPORATE MEMBERS OF THE INSTITUTE OF THE AERONAUTICAL SCIENCES

Listed below are the leading aeronautical and industrial companies that make possible the publication of the *Journal of the Aeronautical Sciences*.

They enable the Institute to publish scientific and technical papers in the *Journal* and to devote its pages exclusively to editorial material.

Dues from individual members which would normally be used to publish this scientific and engineering monthly are thus released for additional services to the profession and industry.

The *Aeronautical Engineering Review* and the *Aeronautical Engineering Catalog*, together with the *Journal*, provide a comprehensive technical information service for the benefit of the aircraft and related industries.

ACADEMY OF AERONAUTICS, INC.
CASEY JONES SCHOOL OF AERONAUTICS
AERO INSURANCE UNDERWRITERS
AEROJET ENGINEERING CORPORATION
AEROQUIP CORPORATION
AGAWAM AIRCRAFT PRODUCTS, INC.
AIRBORNE INSTRUMENTS LABORATORY, INC.
AIRCHOX COMPANY DIVISION, JOYCE AVIATION, INC.
AIRCRAFT RADIO CORPORATION
AIRDON MANUFACTURING CORPORATION
AIRESEARCH MANUFACTURING COMPANY
AIRESEARCH MANUFACTURING COMPANY OF ARIZONA, INC.
AIREX MANUFACTURING COMPANY, INC.
ALLIS-CHALMERS MANUFACTURING COMPANY
ALLISON DIVISION, GENERAL MOTORS CORPORATION
ALUMINUM COMPANY OF AMERICA
AMERICAN AIRLINES SYSTEM
AMERICAN OVERSEAS AIRLINES, INC.
AMERICAN BOSCH CORPORATION
AMERICAN PHENOLIC CORPORATION
ASSOCIATED AVIATION UNDERWRITERS
ASSOCIATED FOUNDRIES & MANUFACTURERS, INC.
ATLAS SUPPLY COMPANY
BAKER STEEL & TUBE COMPANY
BEECH AIRCRAFT CORPORATION
BELL AIRCRAFT CORPORATION
BENDIX AVIATION CORPORATION
BENDIX PRODUCTS DIVISION
BENDIX RADIO CORPORATION
ECLIPSE-PIONEER DIVISION
EXPORT DIVISION
FRIEZ INSTRUMENT DIVISION
PACIFIC DIVISION
SCINTILLA MAGNETO COMPANY
THE BG CORPORATION
BOEING AIRCRAFT COMPANY
BOEING SCHOOL OF AERONAUTICS
BREEZE CORPORATIONS, INC.
ESSEX TOOL & DIE COMPANY
FEDERAL LABORATORIES, INC.
CAL-AERO TECHNICAL INSTITUTE, A DIVISION OF GRAND CENTRAL AIRPORT COMPANY
CARRIER CORPORATION
CESSNA AIRCRAFT COMPANY
CHANDLER-EVANS CORPORATION
CHASE NATIONAL BANK OF THE CITY OF NEW YORK
THE CLEVELAND GRAPHITE BRONZE COMPANY
THE CLEVELAND PNEUMATIC TOOL COMPANY
AUTOMOTIVE-AIRCRAFT DIVISION
CLIFFORD MANUFACTURING COMPANY
CONSOLIDATED VULTEE AIRCRAFT CORPORATION
NASHVILLE DIVISION
STINSON AIRCRAFT DIVISION
CONTINENTAL MOTORS CORPORATION
COX AND STEVENS AIRCRAFT CORPORATION
CULVER AIRCRAFT CORPORATION
CURTISS-WRIGHT CORPORATION
AIRPLANE DIVISION
DEVELOPMENT DIVISION
PROPELLER DIVISION
WRIGHT AERONAUTICAL CORPORATION
DOAK AIRCRAFT COMPANY, INC.
DOUGLAS AIRCRAFT COMPANY, INC.
EL SEGUNDO PLANT
LONG BEACH PLANT
THE DOW CHEMICAL COMPANY
DZUS FASTENER COMPANY, INC.
EASTERN AIR LINES, INC.
EATON MANUFACTURING COMPANY
THOMAS A. EDISON, INCORPORATED, INSTRUMENT DIVISION
EDO AIRCRAFT CORPORATION
THE ELECTRIC AUTO-LITE COMPANY
ELECTROL INCORPORATED
ENGINEERING AND RESEARCH CORPORATION
ETHYL CORPORATION
THE FAFNIR BEARING COMPANY
FAIRCHILD CAMERA & INSTRUMENT CORPORATION
FAIRCHILD AERIAL SURVEYS, INC.
FAIRCHILD ENGINE AND AIRPLANE CORPORATION
DURAMOLD DIVISION
FAIRCHILD AIRCRAFT DIVISION
RANGER AIRCRAFT ENGINES DIVISION
FEDERAL TELEPHONE AND RADIO CORPORATION
FIRESTONE AIRCRAFT COMPANY
FLEETWINGS DIVISION, KAISER CARGO, INC.
FLETCHER AVIATION CORPORATION
G & A AIRCRAFT, INC.
GENERAL AIRCRAFT EQUIPMENT, INC.
GENERAL AVIATION EQUIPMENT COMPANY, INC.
GENERAL ELECTRIC COMPANY
GENERAL INSTRUMENT CORPORATION
GENERAL MOTORS CORPORATION
AC SPARK PLUG DIVISION
AEROPRODUCTS DIVISION
BUICK MOTOR DIVISION
CADILLAC MOTOR CAR DIVISION
CHEVROLET MOTOR DIVISION
DELCO PRODUCTS DIVISION
DELCO-REMY DIVISION
EASTERN AIRCRAFT DIVISION
FISHER BODY DIVISION
FRIGIDAIRE DIVISION
HARRISON RADIATOR DIVISION
RESEARCH LABORATORIES DIVISION
ROCHESTER PRODUCTS DIVISION
THE B. F. GOODRICH COMPANY
THE GOODYEAR TIRE & RUBBER COMPANY
THE GRAY MANUFACTURING COMPANY
GRUMMAN AIRCRAFT ENGINEERING CORPORATION
GUIBERSON DIESEL ENGINE COMPANY
W. & L. E. GURLEY
HANNA ENGINEERING WORKS
HASKELITE MANUFACTURING CORPORATION
HAWAIIAN AIRLINES LIMITED
THE HILLIARD CORPORATION
THE INTERNATIONAL NICKEL COMPANY
JACK & HEINTZ, INC.
JOHNS-MANVILLE SALES CORPORATION
KELLETT AIRCRAFT CORPORATION
KENYON INSTRUMENT COMPANY, INC.
WALTER KIDDE & COMPANY, INC.
KOLLSMAN INSTRUMENT DIVISION, SQUARE D COMPANY
LANGLEY CORPORATION
LAVELLE AIRCRAFT CORPORATION
LEAR INCORPORATED
LIBERTY AIRCRAFT PRODUCTS CORPORATION
LINK AVIATION DEVICES, INC.
THE LIQUIDOMETER CORPORATION
LOCKHEED AIRCRAFT CORPORATION
LONGINES-WITTNAUER WATCH COMPANY, INC.
MAGNAFLUX CORPORATION
THE MARQUETTE METAL PRODUCTS COMPANY
THE GLENN L. MARTIN COMPANY
THE W. L. MAXSON CORPORATION
WARREN McARTHUR CORPORATION
McDONNELL AIRCRAFT CORPORATION
MENASCO MANUFACTURING COMPANY
MICROMATIC HONE CORPORATION
MINNEAPOLIS-HONEYWELL REGULATOR COMPANY
MOORE DROP FORGING COMPANY
NATIONAL CITY BANK OF NEW YORK
NATIONAL CREDIT OFFICE, INC.
THE NEW YORK AIR BRAKE COMPANY
NORMA-HOFFMANN BEARINGS CORPORATION
NORTH AMERICAN AVIATION, INC.
NORTH AMERICAN AVIATION, INC., OF TEXAS
NORTHROP AIRCRAFT, INC.
NORTHWEST AIRLINES, INC.
OWENS-CORNING FIBERGLAS CORPORATION
PAN AMERICAN WORLD AIRWAYS SYSTEM
THE PARKER APPLIANCE COMPANY
PENNSYLVANIA-CENTRAL AIRLINES CORPORATION
PESCO PRODUCTS COMPANY DIVISION, BORG-WARNER CORPORATION
PHILLIPS PETROLEUM COMPANY
PIONEER PARACHUTE COMPANY, INC.
THE PURE OIL COMPANY
REPUBLIC AVIATION CORPORATION
J. P. RIDDLE COMPANY
A. V. ROE CANADA LIMITED
JOHN A. ROEBLING'S SONS COMPANY
ROHR AIRCRAFT CORPORATION
ROOSEVELT FIELD, INC.
THE RYAN AERONAUTICAL COMPANY
SCIAKY BROTHERS
SCOTT AVIATION CORPORATION
SHELL OIL COMPANY, INC.
SIMMONDS AEROCESSORIES, INC.
SKYDYNE, INC.
SOCONY-VACUUM OIL COMPANY
SOLAR AIRCRAFT COMPANY
SPERRY GYROSCOPE COMPANY, INC.
SQUARE D COMPANY
STANDARD OIL COMPANY OF CALIFORNIA
STANDARD OIL COMPANY (INDIANA)
STANDARD OIL COMPANY OF NEW JERSEY
SWEDLOW AEROPLASTICS CORPORATION
THE TEXAS COMPANY
THOMPSON PRODUCTS, INC.
TINNERMAN PRODUCTS, INC.
TITEFLEX, INC.
TRANSCONTINENTAL & WESTERN AIR, INC.
TRIPLETT & BARTON, INC.
UNION CARBIDE AND CARBON CORPORATION
BAKELITE CORPORATION
HAYNES STELLITE COMPANY
LINDE AIR PRODUCTS COMPANY
NATIONAL CARBON COMPANY
UNITED AIRCRAFT CORPORATION
CHANCE VOUGHT AIRCRAFT DIVISION
HAMILTON STANDARD PROPELLERS DIVISION
PRATT & WHITNEY AIRCRAFT DIVISION
PRATT & WHITNEY AIRCRAFT CORPORATION OF MISSOURI
SIKORSKY AIRCRAFT DIVISION
UNITED AIR LINES, INC.
UNITED STATES AVIATION UNDERWRITERS, INC.
UNITED STATES RUBBER COMPANY
DOMINION RUBBER COMPANY, LTD.
THE VARIETY AIRCRAFT CORPORATION
VICKERS, INC.
VIDAL CORPORATION
THE WACO AIRCRAFT COMPANY
WARNER AIRCRAFT CORPORATION
THE WEATHERHEAD COMPANY
WESTERN AIR LINES, INC.
WESTINGHOUSE ELECTRIC CORPORATION
WESTON ELECTRICAL INSTRUMENT CORPORATION
WYMAN-GORDON COMPANY
YOUNG RADIATOR COMPANY